UNIVERSIDAD AUTÓNOMA DE NUEVO LEÓN
FACULTAD DE INGENIERÍA CIVIL

"EFFECT OF MINERALS ADMIXTURES ON HIGH-PERFORMANCE CONCRETE: C-S-H FORMATION AND PHYSICAL-MECHANICAL PROPERTIES"

POR

JORGE MAURILIO RIVERA TORRES

COMO REQUISITO PARCIAL PARA OBTENER EL GRADO DE DOCTOR EN INGENIERÍA DE MATERIALES DE CONSTRUCCIÓN Y ESTRUCTURAS

AGOSTO, 2018

UNIVERSIDAD AUTÓNOMA DE NUEVO LEÓN
FACULTAD DE INGENIERÍA CIVIL

"EFFECT OF MINERALS ADMIXTURES ON HIGH-PERFORMANCE CONCRETE: C-S-H FORMATION AND PHYSICAL-MECHANICAL PROPERTIES"

POR

JORGE MAURILIO RIVERA TORRES

COMO REQUISITO PARCIAL PARA OBTENER EL GRADO DE DOCTOR EN INGENIERÍA DE MATERIALES DE CONSTRUCCIÓN Y ESTRUCTURAS

DIRECTORES DE TESIS
Dr. ALEJANDRO DURÁN HERRERA
Dr. AREZKI TAGNIT-HAMOU

AGOSTO, 2018

UNIVERSITÉ DE SHERBROOKE

Faculté de génie
Département de génie civil

Effet des adjuvants minéraux sur le béton à haute performance: formation de C-S-H et propriétés physico-mécaniques.

Effect of minerals admixtures on high-performance concrete: C-S-H formation and physical-mechanical properties.

Thèse de doctorat
Spécialité: génie civil

Jorge Maurilio Rivera-Torres

Jury: Arezki TAGNIT-HAMOU (directeur)

Alejandro DURÁN-HERRERA (directeur)

Ammar Yahia (évaluateur)

Richard Gagné (évaluateur)

José Manuel Mendoza Rangel (évaluateur)

Sherbrooke (Québec), CANADA Août, 2018

Abstract

In order to improve the environmental impact of concrete, there is a global trend to replace Portland cement by minerals admixtures. In addition to the reduction in the environmental impact of the material, the incorporation of supplementary cementitious materials in concrete will densify the cementitious matrix and consequently improve its impermeability, a property associated with the durability and the service life of concrete. However, in most cases, the performance of a cementitious material is typically evaluated through the impact on the mechanical properties and the cost, leaving aside the durability and the effects at the microstructural level.

This work intends to study the effect of supplementary cementitious materials on formation of C-S-H and the development of the concrete microstructure. The effect of this development on mechanical properties and durability is evaluated. In this investigation, concretes with water/binder ratio of 0,45 and 0,35, where Portland cement is replaced by natural pozzolan or fly ash in dosage of 20% and 60% by mass of each material where used.

The experimental results indicate that the incorporation of natural pozzolan with a dosage of 60% leads to the production of concretes extremely resistant to the chloride ingress without a significant decrease in the compressive strength and modulus of elasticity (11% and 10% respectively at 90 days). The paste analysis by nanoindentation in joint with the qualitative Energy-Dispersive Spectroscopy (NI-EDS) reveal that the physical and mechanical properties of concrete with natural pozzolans are originated from an optimal combination of aluminum-containing hydrated products, a predominant phase of C-(A)-S-H and a well distributed small hard anhydrous inclusions. While the compressive strength and the modulus of elasticity in plain Portland cement concretes depend mainly on the formation of calcium silicate hydrates.

Keywords: Durability, natural pozzolan, chloride ingress, mechanical properties, nanoindentation, anhydrous inclusions, C-S-H, C-(A)-S-H.

Résumé

Afin d´améliorer l'impact environnemental du béton, il existe une tendance mondiale à remplacer le ciment Portland par des adjuvants minéraux, parce que en plus de réduir l'impact environnemental du matériau, l'incorporation de matériaux cimentaires supplémentaires dans le béton permet de densifier la matrice cimentaire et, par conséquent, améliorer son imperméabilité, propriété associée à la durabilité et à la vie utile du béton. Toutefois, dans la plupart des cas, la performance d'un matériau cimentaire est généralement évaluée par l´impact sur les propriétés mécaniques et le coût, en laissant de côté la durabilité et les effets au niveau microstructural.

Ce travail vise à étudier l'effet de ses propriétés mécaniques et de leur durabilité des matériaux cimentaires supplémentaire sur la formation des C-S-H et le développement de la microstructure du béton. Cet effet sur les propriétés mécaniques et la durabilité ont été évalués. Dans cette recherche, des bétons (avec un rapport eau/ciment de 0,45 et 0,35) ou 20% et 60% du ciment portland a été remplacé par des pouzzolanes naturelles ou des cendres volantes, ont été utilisés.

Les résultats obtenus expérimentalement indiquent que l'incorporation de la pouzzolane naturelle avec un dosage de 60% conduit à la production de bétons extrêmement résistants à la pénétration des chlorures sans diminution significative de la résistance à la compression et du module d'élasticité (11% et 10% respectivement à 90 jours). Les résultats des essais de nanoindentation copulé à la spectroscopie qualitative aux rayons X à dispersion d’énergie (NI-EDS) révèlent que les propriétés physiques et mécaniques des bétons avec des pouzzolanes proviennent d'une combinaison optimale de produits hydratés contenant de l'aluminium, une phase de prédominante C-(A)-S-H et des petites inclusions anhydres dures bien réparties; tandis que la résistance à la compression et le module d'élasticité des bétons avec seulement du ciment Portland dépendent principalement de la formation des silicates de calcium hydratés.

Mots-clés : Durabilité, pouzzolane naturelle, pénétration des chlorures, propriétés mécaniques, nanoindentation, inclusions anhydres, C-S-H, C-(A)-S-H.

Resumen

Para mejorar el impacto ambiental del concreto existe una tendencia global a sustituir el cemento Portland por adiciones minerales porque adicionalmente a la reducción del impacto ambiental del material, la incorporación de materiales cementantes suplementarios en el concreto densificará la matriz cementante y en consecuencia también mejorará su impermeabilidad, propiedad asociada con la durabilidad y vida útil del concreto. Sin embargo, en la mayoría de los casos, el desempeño de un material cementante se evalúa típicamente a través del impacto en las propiedades mecánicas y el costo, dejando de lado la durabilidad y los efectos a nivel microestructural.

Este trabajo pretende estudiar el efecto de los materiales cementantes suplementarios en la formación del C-S-H y la microestructura del concreto. Se evalúa el efecto de la microestructura en las propiedades mecánicas y la durabilidad. En esta investigación, fueron estudiados concretos con relaciones agua/aglutinante de 0,45 y 0,35, donde el cemento Portland es reemplazo por puzolana natural o ceniza volante en dosificaciones de 20% y 60% con respecto a la masa de cada material.

Los resultados experimentales de este trabajo indican que la incorporación de la puzolana natural con dosificaciones de 60% conducen a producir concretos extremadamente resistentes al ingreso de cloruros sin una disminución significativa de la resistencia a compresión y el módulo de elasticidad (11% y 10% respectivamente a 90 días). En este sentido, los resultados de los análisis estadísticos de pruebas de nanoindentación en conjunto con la Espectroscopía de Energía-Dispersiva cualitativa (NI-EDS), revelan que las propiedades físicas y mecánicas de concretos con puzolanas naturales, provienen de una combinación óptima de productos hidratados que contienen aluminio, una fase de predominante C-(A)-S-H y pequeñas inclusiones anhidras duras bien distribuidas. Mientras que la resistencia a compresión y el módulo de elasticidad de concretos con sólo cemento portland dependen principalmente de la formación de hidratos de silicato de calcio.

Palabras clave: Durabilidad, puzolana natural, ingreso de cloruros, propiedades mecánicas, nanoindentación, inclusiones anhidras, C-S-H, C-(A)-S-H.

Acknowledgments

First of all, I wish to thank my supervisor at Sherbrooke, **Professor Arezki Tagnit-Hamou**; who with his knowledge, experience, motivation, and patience helped me to enrich my research experience. Through his persistence, understanding and mainly his kindness that helped me to accomplish my Ph.D. study because during the most difficult times in my stay in Sherbrooke, he gave me the moral support to move on. In the same way, I would like to express my gratitude to my supervisor at Mexico, **Professor Alejandro Durán Herrera**; who encouraged me and motivated me to continue my Ph.D. studies both in Sherbrooke, QC, Canada and Monterrey, N.L., Mexico. He, like Prof. Tagnit-Hamou, provided me technical support in all the times and became more of a mentor and a friend than a professor.

I would like to thank the **professors Ammar Yahia, Richard Gagné and José M. Mendoza Rangel** for the time invested to read my thesis and for their wise comments to enrich the content of it. Special thanks to Professor Yahia for all the knowledge he shared during the Concrete Technology course during my stay in Sherbrooke.

I would like to express my special thanks to **William Wilson** since this work would not have been possible without the collaboration and help in the execution of the nanoindentation tests. **William** sincerely thank you for your patience and for your goodwill to help me interpret these results.

I would like to express my special thanks to **Professor Pedro L. Valdez Tamez** (Dean of the Civil Engineering School at UANL), because without his support it would not have been possible to carry out our stay at the Université de Sherbrooke. Likewise, I thank the **National Council for Science and Technology** (**CONACYT**) and **Professor César A. Juárez Alvarado** (Head of Graduate Department) for the opportunity to ingress to the doctoral program of Construction Materials and Structures offered at the Civil Engineering School of the UANL.

I also wish to thank **Mr. Jeff Sharman** for all the disinterested help and wise advice related to my experimental work. I also thank **Mrs. Irene Kelsey and Mr. Stephane Gutierrez** for Characterization of Materials in Université de Sherbrooke, for their patience and help during my experimental work.

I wish to express my sincere thanks to the laboratory technicians: **Mr. Rajko Vojnovic, Mr. Claude Faucher and Mr. Denis Bolduc**. It would not have been possible to conduct the experimental work without their invaluable support. In the same way, I greatly appreciate the generous and kind help received from **all the colleagues** of the concrete research group of Université de Sherbrooke. Special thanks to **Ana Balaguer Pascual, Josep Granero Aliques, Behrouz Esmaeilkhanian and Masoud Hosseinpoor** for all their unselfish support, mainly for their friendship given to me and my family during our stay in Sherbrooke.

My gratitude goes also to **Iliana M. Garza Gutiérre**z and **Francisco David Anguiano Pérez** for investing part of their valuable time in the review and translation of this thesis.

All **staff of the Department of Concrete Technology** of Institute of Civil Engineering of the UANL, infinitely I appreciate your support to carry out this research project.

Thanks to Prof. Leticia Torres and Prof. Isaías Juárez Ramírez for the help received.

Special thanks to José A. Rodríguez Campos from Holcim Mexico for his valuable support to carry out this work.

Last, but not least, I wish to thank my family, especially my wife **Adela Gutiérrez Gutiérrez** and my daughters **Adela C. Rivera Gutiérrez and Fernanda I. Rivera Gutiérrez** for all their support throughout this learning process; their encouragement and love helped me to move on and overcome the hard moments. Obviously I do not forget the support of my brother **José Antonio** and my sisters **Martha Alma and María de Lourd**es, thank you very much.

I dedicate this work to the memory of my parents **Mr. Maurilio Rivera Morales and Mrs. Martha Lilia Torres de Rivera**, mainly my mother who left this world during my stay in Sherbrooke.

Table of Contents

List of Figures

List of Tables

Chapter 1. Introduction.

The hydraulic cement based concrete is the most used building material in the world, from the beginning, this material showed a better performance from a durability point of view compared to other building materials. In addition, it is now relatively easy to get the necessary ingredients for its manufacture. Today, despite its wide application in the development of general infrastructure, concrete producers have not been able to boost its production in a sustainable way, especially in developing countries. Consequently, it is still difficult to extend in a more efficiently way the service life of concrete.

Nevertheless, in recent decades, important advances have been made in the production of concrete, starting from the simple concrete for general use, then high performance concretes, self-compacting concrete and ultra-high performance concretes.

In general, the use of mineral admixtures has been well accepted since it has been demonstrated to provide several enhancements to the physical and mechanical properties of the concrete. The majority of these materials are industrial byproducts. They are desirable from the point of view of the environment and energy care and conservation, for the benefits they can offer to concrete, such as increased durability, improvement of the impermeability of concrete, enhancement of resistance to alkali aggregate reactivity, resistance to sulfates attack, among others.

The optimum amount of these mineral admixtures, either in addition to or as partial replacement of cement used to make concrete, should be established through testing in order to determine if these materials improve certain properties. An overdose or under dose can be harmful and have unwanted effects because mineral admixtures react differently with different types of cement [PCA, 2008].

Fly ash, blast furnace slag, natural pozzolan and silica fume are the mineral admixtures most commonly used and are also known as supplementary cementitious materials. These materials have been widely used in producing concrete. Currently, due to their synergetic effect, concrete producers can combine two or more of these admixtures in order to optimize the physical and mechanical properties. Concrete mixtures using two cementitious materials are called binary blends whereas those with three mineral additions are called ternary blends.

However, while it is know that the use of mineral admixtures improves the physical and mechanical properties of concrete, there is still a lack of knowledge about the microstructure, and in recent decades, research work in this area has been made in order to produce efficient concretes from the durability viewpoint.

1.1 General context.

Nowadays, the challenge that civil engineering is facing is to create infrastructure in the context of sustainable development whit the use of construction materials at low cost and environmental impact. The Portland cement concrete is the construction material widely used in the world; unfortunately the Portland cement production releases to the atmosphere large amounts of CO_2, which is one of the main greenhouse and global warming overall contributors on our planet [Damtoft et al., 2008; Lothenbach et al., 2011]. Therefore, in modern concretes, it is indispensable to use supplementary cementitious material that help to reduce the dosage of Portland cement. The majority of mineral admixtures are byproducts of industrial processes which makes them even more desirable. Besides, most of them have proven to help improve the durability of concrete. On this point, last researches on the use these cementitious materials in the concrete have revealed that these cementitious materials increase the impermeability of concrete which has been attributed to a combined effect of microstructural densification and pozzolanic reaction leading to form secondary C-S-H; In other cases, increased formation of C-S-H was reported contributing to the increase of the durability of concrete. Regarding the C-S-H formation, which is the phase that has the greatest impact on the physical and mechanical properties of concrete, there have been large advances about it. However, most of the studies have been based only on Portland cement pastes or synthetic C-S-H [Richardson, 2004; Foley et al., 2012; Mendoza et al., 2015]. Few studies have been conducted in pastes with mineral admixtures and the results have been promising but contradictories. So, more studies are needed about the influence of mineral admixtures on C-S-H formation and the paste microstructure, themselves, in order to know their effect on the mechanical properties of this phase and finally to know how they improve the permeability and durability of concrete.

1.2 Definition and objectives.

Heretofore, the probable influence of the use of supplemental cementitious material on C-S-H formation has not been studied in great detail. So, in this project, the effect of mineral admixtures on the C-S-H formation will be studied in order to know how this material affect the physical and mechanical properties of this gel. In this will help us to know more and understand the mechanism of concrete microstructure densification. This study will give us guideline of having more control in the concrete mix design based on the microstructure in order to improve its permeability. This will result in concrete designs that are more efficient from the sustainability point of view because it will take advantage more efficiently of these types of supplementary materials leading to prolonged service life of the structures.

1.2.1 Objectives.

The main goal of this project is to study the C-S-H formation and evaluate the permeability of concretes produced with two mineral admixtures (MA). So, in order to fulfill this purpose, it is necessary to carry out the following specific objectives:

- Evaluate the permeability of concretes with two different dosages of minerals admixtures (20% and 60%) for each one.
- Evaluate the performance of mineral admixtures on the C-S-H formation with two different dosage (20% and 60%) for each one.
- Study the effect on concrete microstructure.
- Determine the physical and mechanical properties of the C-S-H.
- Study the impact of C-S-H and microstructure on physical and mechanicals properties on concrete with natural pozzolan and fly ash.
- Establish practical proportions to produce durable concrete incorporating natural pozzolan and/or fly ash under a scheme of sustainable development.

1.3 Thesis outline.

This research work was made with the collaboration between Universidad Autónoma de Nuevo León (UANL) and Université de Sherbrooke (UdeS) by means of an agreement of co-tutorship and dual-degree program.

The thesis is divided into five chapters. Following the introduction where the general context and the objectives are presented, chapter two is giving an overview of the literature review. The materials and experimental program are detailed in chapter three. The chapter four is presenting the results and discussions. Finally, the conclusions and recommendations are developed in chapter five.

Chapter 2. Literature review.

2.1 Role of mineral admixtures in high-performance concrete.

High-performance concrete was developed in the eighties; its name was proposed because in addition to its low water/binder ratio, it also has other enhanced features such as higher consistency, higher modulus of elasticity, greater strength bending, lower permeability, higher abrasion resistance and durability [Aïtcin, 1998].

High-performance concrete is that which meets special performance specifications and requirements of uniformity that cannot always be achieved routinely by using components, mixing practices, placement and traditional curing [ACI 318]. In general, it can be said that these concretes are developed to meet certain characteristics in particular applications and environments and have a lower water/binder ratio than 0.42, which approaches the theoretical value suggested by Powers to ensure complete hydration of the Portland cement [Aïtcin, 1998].

The role of mineral admixtures in high-performance concrete production may be the following: to produce delays in the time of setting, resulting in lower and less intensive early contractions; to achieve better concrete docility using less water; to reduce the production costs of concrete; to reduce the heat of hydration, and to increase durability of concrete. The disadvantages would be a slow initial strength development, and depending on its fineness, a greater shrinkage when drying.

2.2 Concrete durability.

The durability of reinforced concrete, due to the presence of agents promoting deterioration in the environment depend much on concrete permeability [Sabir et al., 1998; ASTM C1585, 2004]. Three mechanisms can be used to describe the transport of fluids within the concrete: permeability, diffusion and absorption. Permeability is the measure of water flow under a pressure gradient, diffusion is the movement of ions due to the concentration gradient and absorption can be described as the ability of the materials to take water through capillary suction [Nethalath, 2006; Bentz et al., 2001].

Corrosion of steel reinforcement in concrete is a serious problem that civil engineers are facing these days, trying to keep up the infrastructures that are in the process of aging. The main causes of this phenomenon are chloride attack and carbonation. These two mechanisms do not attack the integrity of concrete, but they do affect its permeability; so, in this manner, both attacks promote corrosion.

2.2.1 Electrical resistivity.

One parameter of durability measured in concrete is the electrical resistivity; with this measurement, it can be evaluated the following characteristics of concrete: fresh and hardened stage, degree of curing, resistance to chlorine ions penetration and corrosion rate of steel reinforcement [Andrade and D'Andrea, 2011]. The measurement of electrical resistivity is a simple, non-destructive, reliable and rapid test method, which can also be used for quality control of concrete during construction [Sengul and Gjorv, 2008].

The resistivity test is a low cost and repeatable method that allows testing several times, therefore, changes in concrete properties can be monitored using the same samples. The strength of the concrete can be measured in a few minutes as no special preparations of specimens are needed. Portable hand-held and battery-operated resistivity measurement devices commercially available can be used both in laboratory and on-site.

Resistivity testing has been standardized recently by ASTM C1760, in which the method for bulk resistivity is defined. The measurement of surface resistivity using the Wenner four-electrode method has also been implemented [AASHTO TP 95-11]. Relationships have been established between the two-electrode method (bulk resistivity) and the four-electrode Wenner method, showing results that are congruent with each other. However, Wenner's method proved to be a simpler and faster method to monitor concrete quality control during construction [Sengul and Gjorv, 2008].

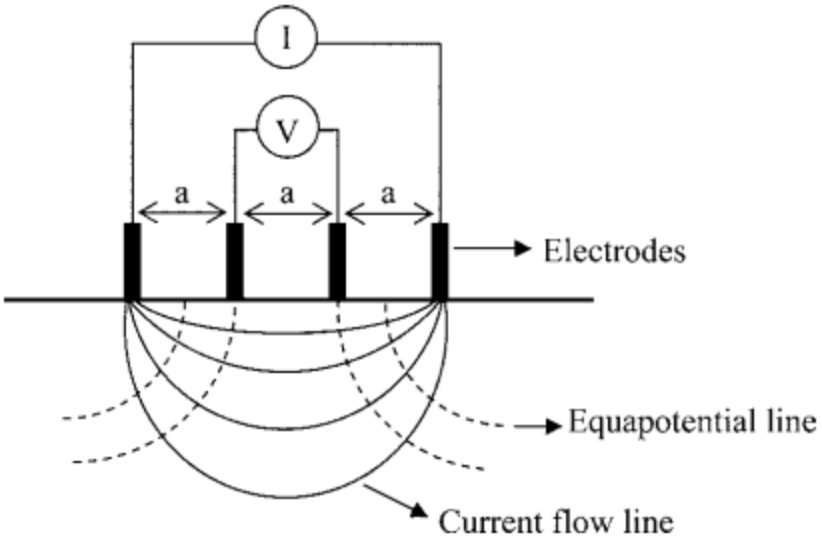

Figure 2.1 Schematic representation of four-electrode resistivity test (Wenner method) [Sengul and Gjorv, 2008]

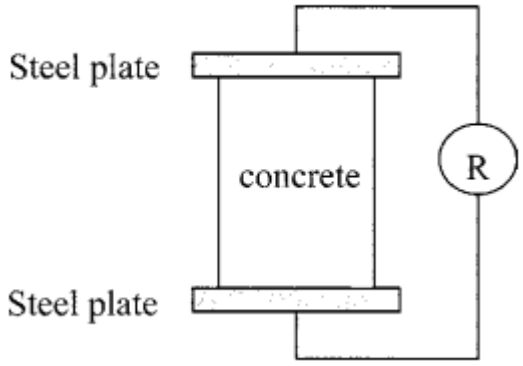

Figure 2.2 Two-electrode testing on concrete cylinders (ASTM C 1760) [Sengul and Gjorv, 2008]

2.2.2 Chloride ions permeability.

Reinforcing steel corrosion induced by chlorides is the most important degradation process in reinforced concrete structures, which has very important economic and social consequences. There are two main sources for the ingress of chloride into concrete structures: seawater and deicing agents used in the winter.

There are two ways in which chlorides are present in concrete: as free chlorides and bonded chlorides. The total amount of chlorides is the sum of these two but only free chlorides can move and contribute with a chemical potential or concentration [Tang and Zhu, 2007].

Chlorides penetrates concrete mostly by diffusion in the water-saturated pores and they are transported through the pores due to their permeability or by suction. Chloride ingress is generally accompanied by physical and chemical bonds.

The movement of chlorides through the solution generally causes bonds that can significantly delay the process of penetration. The ability of concrete to link chlorides depends on the type of cementitious material and of its hydration products. It is also affected by other factors such as temperature and alkalis concentration [Tang and Zhu, 2007].

Since durability of concrete structures is of great importance, several methods have been proposed for measuring the penetration of chlorides. However, due to the complexity of this process, it has been difficult to reach to a general agreement about the election of a single test method.

For years, in the United States two methods have been used [ASTM STP 169D, 2006]:

- ASTM C-1202 “Standard test method for electrical indication of concrete’s ability to resist chloride ion penetration”.
- AASHTO T-277 “Rapid chloride permeability test”

In the Nordic countries there are three test methods developed by NORDTEST [Gjorv, 2014]:

- NT BUILD 443 “Concrete, Hardened: Accelerated Chloride Penetration”, based on a non-stationary diffusion state under high chloride concentrations.

- NT BUILD 355 “Concrete, Mortar and Cement Based Repair Materials: Chloride Diffusion Coefficient from Migration Cell Experiments”, based on a stationary diffusion state.
- NT BUILD 492 “Concrete, Mortar and Cement Based Repair Materials: Chloride Diffusion Coefficient from Non-Steady Migration Experiments”, based on a non-stationary diffusion state.

2.2.3 Carbonation.

Carbonation is a process of gaseous carbon dioxide diffusion with carbonated ions. Diffusion of the gas is faster than ions. Therefore, the carbonation rate depends on the internal humidity of the concrete. In dry concretes, carbon dioxide can penetrate to great depth, but there is not enough water to carry out the carbonation reaction. Therefore, there is an optimum moisture condition in which the carbonation rate is at its peak.

The carbonation rate will depend on how fast the carbon dioxide and/or carbon ions moves into the concrete and react with the cement paste. Factors affecting the carbonation progress in concrete structures are:

Humidity

Carbonation rate diminishes in very dry environments, as well as very humid and saturated ones. The maximum carbonation rate appears when relative humidity of concrete is between 60 and 80% [Largerblad, 2006]. The wetting and drying cycles also seem to accelerate the carbonation process.

Temperature

The rate of diffusion and carbonation increase as temperature does.

Cementitious material content

Diffusion occurs inside the paste, and not in the aggregate. The amount of cementitious material does not affect the carbonation rate as long as the water/binder rate is maintained constant: that is, a larger amount of paste, but with the same porosity, will have the same carbonation depth, but with a larger volume of carbonated paste

Concrete quality

A higher water/binder ratio and a higher hydration grade produce a dense concrete with lower porosity. This will also result in dense carbonation products and consequently a reduction in carbonation. It is well known that a dab curing will result in a higher carbonation rate, possibly due to a diminished in the rate of hydration.

Type of cement and pozzolans effect

The use of blended cement is becoming more common every day. These cements are composed of Portland cement clinker, gypsum, limestone, blast furnace slag, fly ash, silica fume, etc.

As for fly ash, its pozzolanic reaction will cause a decrease in the content of calcium hydroxide and an increase in the content of C-S-H. A lower amount of calcium hydroxide will increase the rate of carbonation; however, the increase in the amount of C-S-H and its effect on the carbonated paste must be taken into account [Largerblad, 2006].

2.2.4 Drying shrinkage.

The shrinkage of concrete is a concern for its impact on its durability. The useful life of the structure can be significantly reduced to cause of the cracks induced by this effect (figures 2.3 and 2.4). Commonly the retraction is attributed to the drying of concrete over long periods of time, although recent studies have focused on problems at an early age or drying in a plastic state [Holt, 2001].

The most common solution to reduce volume changes at an early age is to avoid drying by proper handling of the concrete during the first hours after placement. It is imperative that the curing starts immediately after and for proper methods [Holt, 2000].

Figure 2.3 Early drying shrinkage on a slab roof. [a]

Figure 2.4 Reparation of shrinkage cracks in a wall. [b]

[a] http://opc.com.mx/boletines/grietas_plasticas.html

[b] http://www.xypexman.com/projects/proj-lagley.html

Shrinkage of concrete takes place in two different periods; at an early age and at a later age. Early age is understood as the first day (first 24 h after mixing) when the concrete is hardening and begins its hardening. Later or long-term age refers to an age greater than 24 hours. During the later age, the concrete is demolded and the retraction measures are carried out. The shrinkage at a later age is typically considered in structural design.

Long-term shrinkage has been measured in concrete practice for many years. In general, it is measured from 24 hours after mixing or at the time of demolding. It is measured in prismatic specimens of normalized dimensions registering the change in length over time, according to standards such as ASTM C157 or RILEM CPC 9.

The drying shrinkage refers to the reduction of the volume of concrete resulting from a loss of water. Initially, according to the aggregate particles more heavy settle free water escapes to the concrete surface as bleed water. This bleeding water can evaporate from the surface, causing the rise of more water inside the concrete by capillary suction.

The most common situation that results from drying shrinkage at an early age is the appearance of surface cracks. There can also be a cracking problem due to the water suction that can originate the form or material on which the concrete structure is displaced [Mindess and Young 2007]. On the other hand, if the rate of bleeding exceeds the rate of evaporation this excess water will act as a curing film. In this case, there will be no drying contraction at an early

age, since there is enough water on the surface that allows evaporation without extracting water from the capillary pores.

The mechanisms that cause retraction by drying are dependent on the size of the pores [Mehta and Monteiro, 2006]. The capillary pores are the spaces occupied by the excess of water, which are reduced during the hydration reactions of the cement; in this way, the existing relative humidity will be correlated with the size of the capillary pore inducing simultaneous stress and retraction [Janz, 2000].

2.3 C-S-H formation.

Concrete has a highly heterogeneous and complex microstructure made of three main components: hydrated cement paste, aggregates and interfacial transition zone between cement paste and aggregates. Due to this heterogeneity, each of these components has been individually studied in order to improve and control the physical and mechanical properties of this composite material [Mehta and Monteiro, 2006].

The main products of Portland cement hydration are calcium silicate hydrates (C-S-H) followed by calcium hydroxide or portlandite (CH). Other phases formed as a result of the hydration of the cement are hydrated aluminates and sulfo-aluminates AFm and AFt, whose formation depends on the composition of cement, the time and conditions of hydration.

C-S-H is a nearly amorphous material and forms up to about 60% of the paste. The hyphens in C-S-H indicate indefinite stoichiometry and the hydrate is sometimes referred to as "C-S-H gel". The C-S-H is produced along with calcium hydroxide in the chemical reaction of the silicate phases (β-C_2S and C_3S) with water.

The molar ratio of CaO to SiO (C/S ratio) in C-S-H is one of the main parameters in defining and controlling the properties of a calcium silicate hydrate system. This value varies from 1.2 to 2.3 in hydrates silicate phases and has an average of about 1.75. The C-S-H system may be divided into low and high lime content categories partitioned by the C/S ratio of about 1.1 where chemical and physical properties change noticeably [Raki et al., 2010].

It is widely believed that the fundamental properties of concrete such as strength, ductility, early rheology, creep and shrinkage, fracture behavior, durability, etc. are affected by

material properties at nano level [Corr and Shaha, 2005]. Thus, the nanostructure of C-S-H has been the subject of a lot of research. However, the exact structure of C-S-H is not known yet. So, several models have been proposed in order to understand and establish relationships between its structure and properties of concrete.

Among the models that have been developed to explain the above, we present two that we consider to have a watershed in the understanding of nanostructure and its effect on the properties of concrete (Figure 2.5). The Feldman and Sereda model suggests that the C-S-H is similar to clay particles, forms a three dimensional assemble of layer silicate sheets which locally tend to form parallel network groups with entrapped water and pore space [Feldman and Sereda, 1968 and 1970]. Jennings model suggests that the C-S-H structure is a colloidal network gel; the smallest distinct units of C-S-H are globules just under 5 nm in the smallest dimension, which pack together in two distinct structures called high density (HD) and low density (LD) of C-S-H. Furthermore, this model also tries to explain the implications of shrinkage and creep of the concrete [Jennings, 2003; Thomas and Jennings, 2006; Jennings, 2008 and Constantinides, 2013].

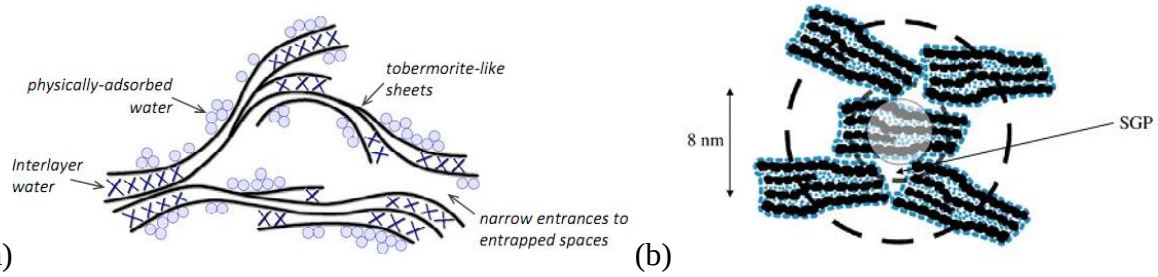

Figure 2.5 C-S-H models proposed by a) Feldman and Sereda and b) Jennings colloidal model.

Moreover, Richardson has detected the existence of two different structures in the C-S-H gel. Less dense morphology mainly in the space originally filled by water and other more dense morphology mainly in the space originally occupied by cement particles. He named the two morphologies of C-S-H gel as outer product (OP) and inner product (IP) respectively (Figure 2.6) [Richardson, 1999, 2000, 2004 and 2008].

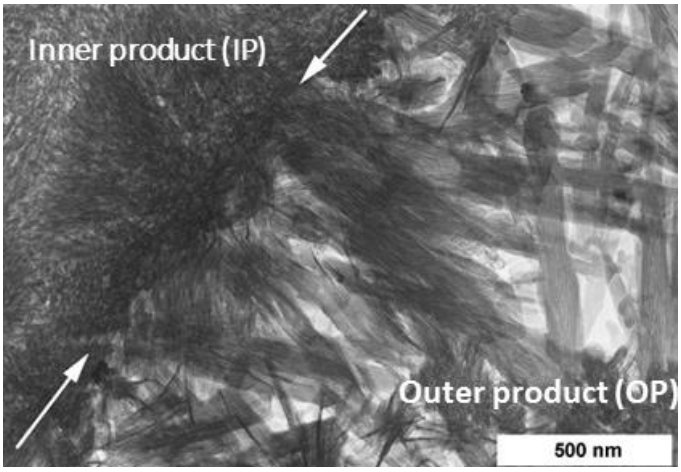

Figure 2.6 A TEM micrograph showing IP and OP C-S-H [Richardson, 2000].

Although, there has been many advances in the field of nanoscience, further investigation is required in order to develop more durable concretes that are friendly to the environment too. In this sense, this project we will study the effect of natural pozzolan on the C-S-H formation in order to know how these materials provide more impermeable concrete.

2.4 Physical and mechanical properties of C-S-H.

Typical concrete consist of ordinary Portland cement (OPC), fillers such as sand, coarse aggregates, admixtures and water. This combination of materials allows concrete to be produced in a fluid form that can be pumped and molded. The chemical reactions and resulting products produced when cement is mixed with water create a material that is highly complex [Davydov et al., 2011]. The principal component, C-S-H gel, has a local structure of a precipitate with nanoscale features that are difficult to model and understand. Over the last years, the mechanical properties of C-S-H gel have been determined by nanoindentation technique, and statistical analyses have been used to deconvolute these mechanical properties of individual phases in hardened cement pastes. Thus in this method, it is not necessary to know exactly the location or material phase where each nanoindentation test is performed [Ulm et al., 2007].

Velez et al., (2001) were among the first to determine the physical and mechanical properties on pure constituents of Portland cement clinker by nanoindentation having satisfactory and congruent results with Acker, (2001) (Table 2.1). Following their research, the possibility of studying the hydration products of the cement paste was opened.

Table 2.1. Indentation modulus of calcium silicates, calcium aluminate and calcium aluminoferrite present in Portland cement clinker [Acker, 2001].

Constituent	E (GPa)	Reference
C_3S	135 ± 7	Velez et al.
	135 ± 7	Acker
C_2S	130 ± 20	Velez et al.
	140 ± 10	Acker
C_3A	145 ± 10	Velez et al.
	160 ± 10	Acker
C_4AF	125 ± 125	Velez et al.

One of the first papers about the mechanical properties of C-S-H using nanoindentation technique was Constantinides and Ulm (2003 and 2004). They studied Portland cement pastes with water/cement ratio of 0,5. The average values of modulus of elasticity obtained were similar to those reported by Acker, (2001) who studied ultra-high performance concrete with very low water/cement ratio and with admixtures. For this reason, the results of Constantinides and Ulm suggested that mechanical properties of C-S-H were intrinsic (Table 2.2). Another important aspect of this research was that the volume fractions could be determined by nanoindentation corresponding to a percentage around 70% for LD C-S-H and 30% for HD C-S-H (see Figure 2.7), corroborating what was previously established by other authors about the existence of two different forms of C-S-H (Table 2.3).

Table 2.2. Elastic modulus of CH and C-S-H obtained by nanoindentation.

	Elastic modulus (GPa)	Reference
CH	38.0 ± 5.0	Constantinides and Ulm
	36.0 ± 3.0	Acker
HD C-S-H	29.4 ± 2.4	Constantinides and Ulm
	31.0 ± 4.0	Acker
LD C-S-H	21.7 ± 2.2	Constantinides and Ulm
	20.0 ± 2.0	Acker

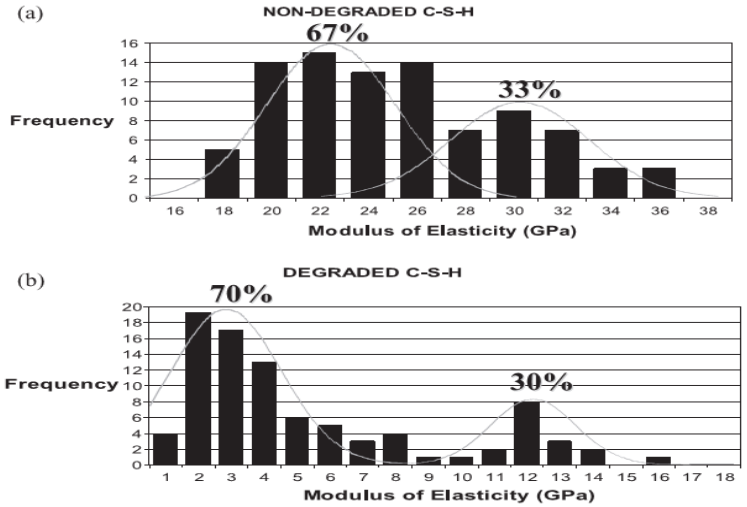

Figure 2.7. Results obtained by nanoindentation. Two types of C-S-H are identified: LD and HD. % indicates volumetric proportions by measuring the area under the curves [Constantinides and Ulm, 2004].

Table 2.3. Classification of the two morphological entities of C-S-H as found in the open literature [Constantinides and Ulm, 2004].

Classification	Reference
Inner product - Outer product	Taplin (1959), Groves (1987), Richardson (1999)
Middle product – Late product	Scrivener et al. (1985), Taylor (1997)
Phenograins – Groundmass	Diamond and Bonen (1993)
Low density – High density	Jennings (2000), Tennis and Jennings (2000)

Mondal et al., (2007) studied cement pastes (ordinary Type I Portland cement) manufactured with a water/cement ratio of 0,45. The age of the samples was 3 years. A Hysitron Triboindenter was used to determine the nano mechanical properties of C-S-H. They found that the elastic modulus could be divided in three different groups where values are decreasing with the distance from unhydrated particle (Figure. 2.8). The elastic properties were evaluated using the Oliver-Phar method, and the elastic modulus and hardness reported by them were similar to those reported previously (Table 2.4). They did not report result about the volume fraction, but they reported that the images by the AFM of C-S-H in hardened cement paste showed nearly spherical particles.

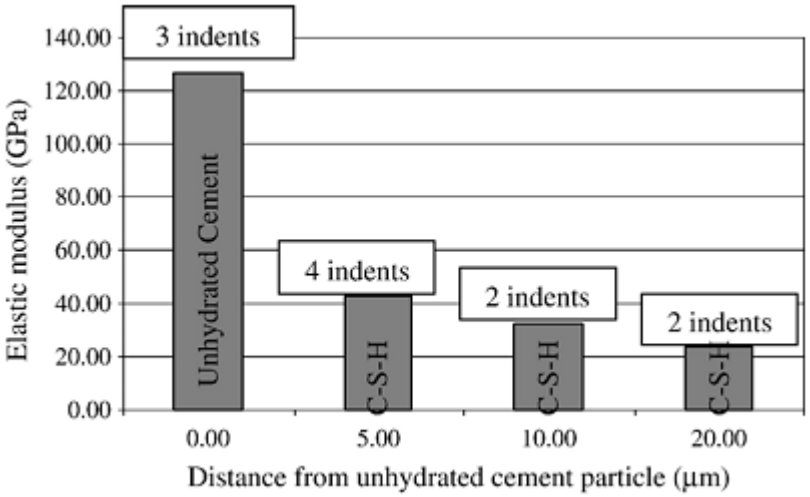

Figure. 2.8 Change in modulus of C-S-H with the distance from unhydrated particle [Mondal et al., 2007].

Table 2.4. Results of indentation where E is elastic modulus and H is hardness all in GPa [Monadal et al., 2007].

Unhydrated particle			High stiffness C–S–H		Medium stiffness C–S–H		Low stiffness C–S–H	
	E	*H*	*E*	*H*	*E*	*H*	*E*	*H*
Mean	122.20	6.67	41.45	1.43	31.16	1.22	22.89	0.93
S.D.	7.85	1.23	1.75	0.29	2.51	0.07	0.76	0.11

Constantinides and Ulm (2007) investigated the mechanical properties of C-S-H by using nanoindentation tests with the intention to validate this technique. For this purpose, they developed hundreds of nanoindentation tests in white cement pastes (same cement studied by Thomas and Jennings in 2002), with water/cement ratio of 0.5. The obtained values of Modulus of Elasticity of HD C-S-H and LD C-S-H were 29.1 ± 4.0 GPa and 18.2 ± 4.2 GPa respectively. According to the authors, both values were in excellent agreement with results of Acker and themselves in 2004 (Table 2.2). The hardness values obtained for HD and LD of C-S-H with the deconvolution technique were very much consistent with the results of Acker (Table 2.5).

Table 2.5 Hardness of CH and C-S-H obtained by nanoindentation.

	Hardness modulus (GPa)	Reference
CH	1.35 ± 0.5	Acker
	1.31 ± 0.23	Constantinides et al.
HD C-S-H	0.9 ± 0.3	Acker
	0.83 ± 0.18	Constantinides et al.
LD C-S-H	0.8 ± 0.2	Acker
	0.45 ± 0.14	Constantinides et al.

In regard to volume fraction of LD and HD C-S-H, they found that the LD C-S-H makes up around 65% of the total C-S-H, having a good agreement with previous results too (Fig. 2.1).

However, what seems to be the most important finding of this study was that both phases (LD C-S-H and HD C-S-H) exhibited a unique nanogranular behavior, which is driven by particle to particle contact forces rather than mineral properties. It is argued that during the hydration reactions, C-S-H nanoparticles are precipitated generating contact surfaces and contact points and creating in the course of this process a material which behavior is driven by contact forces. Thus, the estimated packing densities of the LD C-S-H of 0.63 and 0.76 for HD C-S-H almost coincide with limit packing densities of spheres. The LD C-S-H packing density almost coincide with the random packing density of spheres of 0.64 and HD C-S-H packing density almost coincide with the densest possible spherical packing in three dimensions of 0.74. Thus, it confirms that the morphology of the C-S-H has two characteristic packing modes one being an unstructured order (LD C-S-H) and other with a highly structured order (HD C-S-H) and its impact on the mechanical properties of LD C-S-H and HD C-S-H.

Due to advances in nanotechnology area, DeJong and Ulm (2007) studied the effect of elevated temperature on the nanogranular behavior of C-S-H in order to know what is causing the damage on Portland cement exposed to high temperatures. To achieve this, DeJon et al. conducted nanoindentation and thermogravimetric tests in Portland cement Type I pastes with w/c = 0.5. The temperatures employed in this study ranged from 20 to 1000 ^{o}C in three stages.

The results of DeJong and Ulm confirm the existence of two structurally distinct but compositionally similar C-S-H phases known as LD C-S-H and HD- C-S-H, but the principal thermal deterioration of C-S-H properties occurs above 200 ^{o}C (Figure. 2.9). Regarding the

volume fraction of the C-S-H, the relative volume proportion of the LD C-S-H and HD C-S-H practically do not change with exposure to high temperatures (Table 2.6).

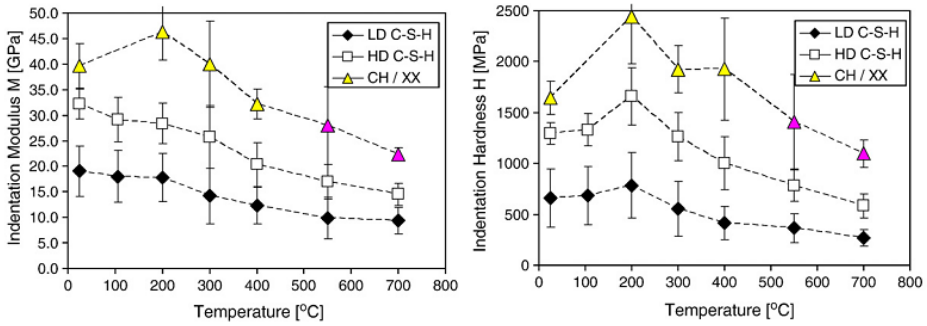

Figure 2.9 Summary of nanoindentation results. The bars at each point represent the standard deviation obtained with the deconvolution technique [DeJong and Ulm, 2007].

Table 2.6 Indentation modulus, hardness and C-S-H volume fraction [DeJong and Ulm, 2007].

Temp. [°C]	Indentation modulus *M* [GPa]			Indentation hardness *H* [GPa]			C-S-H [vol. %]	
	LD C-S-H	HD C-S-H	CH/XX	LD C-S-H	HD C-S-H	CH/XX	LD	HD
25	19.1±5.0	32.2±3.0	39.7±4.5	0.66±0.29	1.29±0.11	1.65±0.17	87	19
105	18.0±5.0	29.1±4.4	–	0.68±0.29	1.33±0.17	–	74	26
200	17.8±4.7	28.4±4.1	46.3±5.5	0.79±0.32	1.66±0.28	2.44±0.06	73	27
300	14.2±5.4	25.7±6.1	40.0±8.2	0.55±0.27	1.26±0.24	1.92±0.22	76	24
400	12.4±3.6	20.3±4.4	32.1±2.8	0.42±0.16	1.00±0.26	1.93±0.51	54	46
550	9.9±3.3	17.0±3.4	28.0±7.6	0.36±0.14	0.78±0.16	1.41±0.47	77	23
700	9.3±2.6	14.5±2.1	22.3±1.3	0.27±0.08	0.58±0.12	1.10±0.13	68	32
						Average:	72±10	28

Němeček (2009) studied the effect of load application on the evaluation of elastic properties of C-S-H using nanoindentation technique. For this purpose, he made pastes of white cement with water/cement ratio of 0,5, and cured the samples for two months. He prepared two series of experiments. The first was applied load with no dwell period, and the second one was applied load with dwell period. He found that the creep affect principally the hydrated phases. The final values of modulus at 20 mN were practically the same for both types of load (Figure 2.10). The elastic properties were obtained according to the Oliver-Phar methodology and were reported of 28.2 ± 4.4 GPa for "O" series and 26.9 ± 1.8 GPa for "C" series. These results were in good agreement with those reported by Constantinides and Ulm (2007).

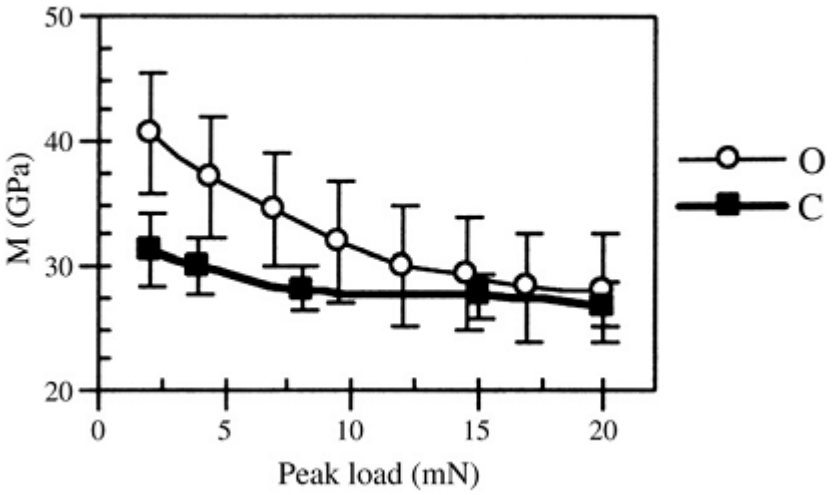

Figure 2.10. Indentation modulus for hydrated phases of cement paste. Thin lines represent "O" series with increasing loading cycles without a dwell period at the peak. Thick lines represent "C" series tested by cyclic loading to the same load with a 120 s dwell period at the peak [Němeček, 2009].

So far, the existence of LD C-S-H and HD C-S-H phases and their mechanical properties, as well as the relationship between these mechanical properties of C-S-H and packing density respectively was well established. Due to concerns to know if the packing densities, gel porosities and volume fraction of C-S-H can be modified by varying the substochiometric conditions, Vandamme et al. (2010) carried out a study on cement pastes with w/c ratios ranging from 0.15 to 0.4 with and without heat treatment. Cement pastes were prepared using an alite rich cement at w/c = 0,15, 0,20, 0,30, 0,35 and 0,4. The casting and curing temperatures were 20 ^{o}C. Five other samples were prepared at w/c = 0,15, 0,20, 0,25, 0,30 and 0,35, and at the age of 48 hours, they were subjected to a heat treatment at 90 ^{o}C for 48 hours.

Among the findings, it was shown that the values of Modulus of LD and HD of C-S-H of the pastes that did not receive heat treatment were consistent with previous results. In addition, a new phase was detected which they appointed Ultra-high-density (UHD). The results of modulus and hardness in pastes that were treated thermally were quite similar to pastes that did not receive this treatment, thus confirming that the mechanical properties of C-S-H are intrinsic and not dependent on mix proportion, heat treatment, etc. Furthermore, the difference in modulus and hardness values between LD C-S-H, HD C-S-H and UHD C-S-H are related to packing densities of these phases (Figure 2.11).

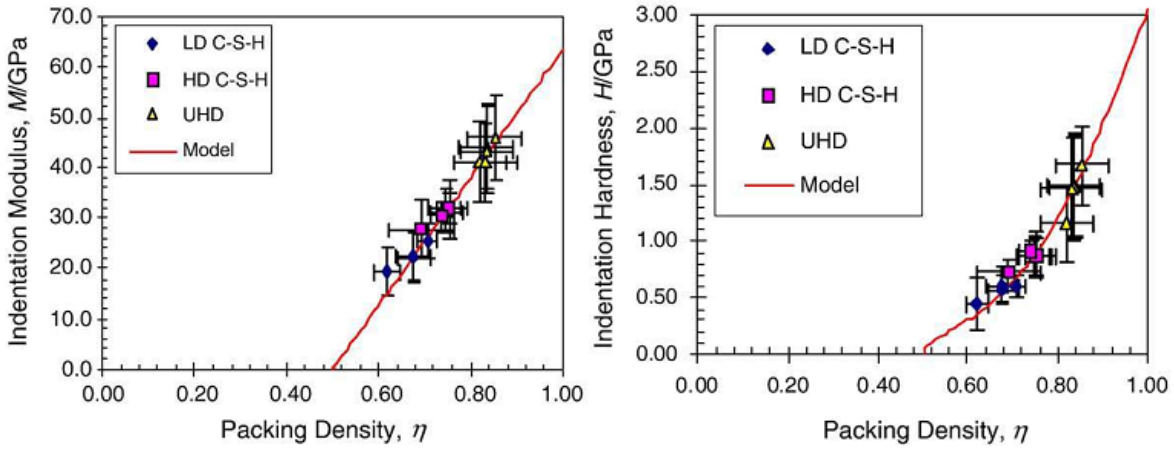

Figure 2.11 Results from deconvolution of five pastes without heat treatment [Vandamme et al., 2010].

Concerning to the volume fraction of C-S-H, they found that in the pastes that did not receive heat treatment, the volume fraction of LD C-S-H is raised by increasing the w/c ratio and HD C-S-H volume decreased. The volume fraction of UHD C-S-H remained nearly unchanged (Figure 2.12). Moreover, the heat treatment favored the increase in HD and UHD of C-S-H (Figure 2.13).

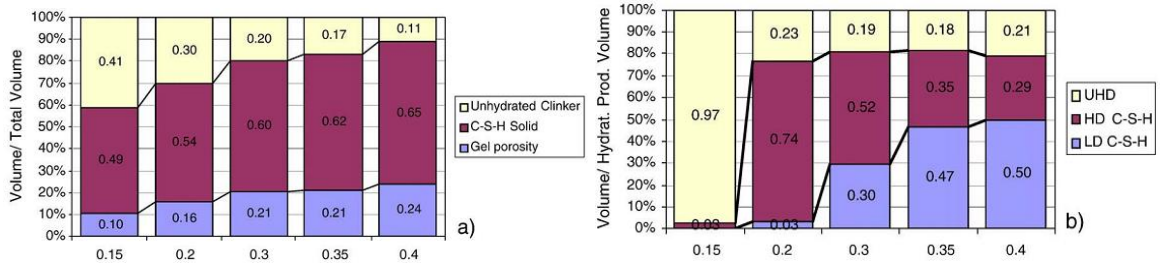

Figure 2.12 Volume fraction distribution without heat treatment: a) volume fractions of the cement paste composite, b) volume fraction of hydration phases. In x axis w/c ratio by mass [Vandamme et al., 2010].

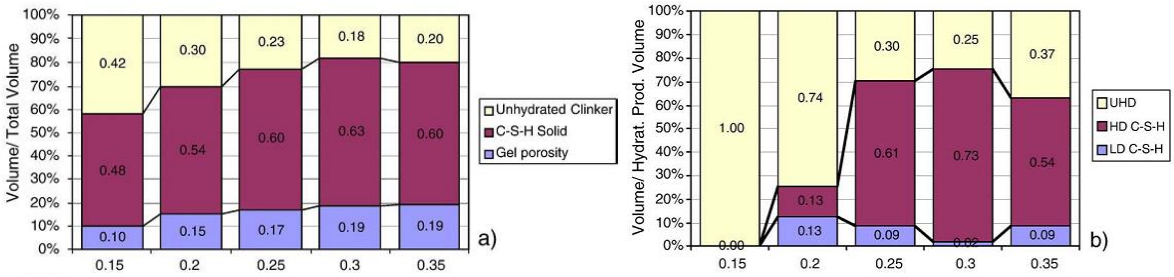

Figure 2.13 Effect of heat treatment on volume fraction distribution: a) volume fractions of the cement paste composite, b) volume fraction of hydration phases. In x axis w/c ratio by mass [Vandamme et al., 2010].

Sorelli et al. (2008) were among the first researchers to carry out a study on nanoindentation tests on samples of ultra-high performance concrete. They took samples from bridge plates for bending tests. The concrete was made with a water/binder ratio between 0.19 and 0.21. The ingredients used for manufacturing this concrete were cement CEM Type I, high-range water reducer admixture, silica fume, quartz powder, silica sand and steel fibers. At sixth day after casting, the material was heat treated for 48 h at temperature of 90 ^{o}C at relative humidity of 90 %. The age of nanoindentation tests were about 3 years.

The mean values of the indentation modulus of LD and HD C-S-H phases were 19.7 GPa and 34.2 GPa respectively, which were similar with respect to those reported in previous studies. Regarding the values of hardness, HD C-S-H was 1.36 GPa and slightly greater than the values reported previously. Finally, it was observed that the C-S-H matrix of ultra-high performance concrete is mainly composed of HD C-S-H, and its volume fraction was about 86%.

Sakulich and Li (2011) conducted nanoindentation tests on engineered cementitious composites. They prepared three different mixes; the used materials were Portland cement Type I, fine silica fume sand, fly ash Type F, high range water admixture, carbon black, single-walled nanotubes and polyvinyl alcohol fibers (PVA fibers). The water/binder ratio was 0,267 for all mixes. They did not detect any differences between LD and HD of C-S-H. They only reported the modulus value of Quartz, PVA fibers and unreacted fly ash whose value was 78.3 ± 14 GPa.

Having as antecedent that the concrete strength incorporating ultra-fine cementitious materials such metakaolin or silica fume is typically reported lower than normal concrete, while other supplementary cementitious materials (SCM), including fly ash and slag, result in similar or better behavior to high temperatures compared to normal concrete [Tylor, 1997; Herts, 1992; Poon et al., 2001]. Zadeh et al. (2013) studied concretes with different percentages of fly ash and slag exposed to fire-damage (300 ^{o}C) in order to investigate the changes on the C-S-H formation by using nanoindentation tests. The concretes studied were manufactured with Portland cement Type II and it replacement rates of 20 % fly ash class F, 60 % fly ash class F and 60 % slag cement grade 100 by mass. The water/binder ratio for the three concretes was 0,45.

With respect to undamaged concretes, the values for indentation modulus of LD C-S-H and HD C-S-H phases were similar to those reported in previous papers. However, the indentation hardness was higher compared to the values found in the literature. In regard to the volume fraction, there is no well-defined tendency, but it seems that the use of SCM decreases the volume of LD C-S-H (Table 2.7).

Table 2.7. Indentation modulus, hardness and volume of hydration products in undamaged concrete [Zadeh et al., 2013].

	LD C-S-H	HD C-S-H	UHD C-S-H or CH
Indentation modulus, M			
OPC (w/c = 0.4), Vandamme et al.	22.5 ± 5.0	30.4 ± 2.9	40.9 ± 7.7
OPC (w/c = 0.5), DeJong and Ulm	19.1 ± 5.0	32.2 ± 3.0	39.7 ± 4.5
OPC with 21% silica fume (w/b = 0.4), Vandamme	23.64 ± 4.07	30.59 ± 2.87	42.18 ± 5.87
OPC with 20% fly ash (w/b = 0.45)	18.72 ± 7.1	35.00 ± 6.5	-
OPC with 60% fly ash (w/b = 0.45)	15.82 ± 5.12	32.88 ± 8.0	-
OPC with 60% slag (w/b = 0.45)	21.63 ± 6.68	33.66 ± 7.59	-
Indentation hardness, H			
OPC (w/c = 0.4), Vandamme et al.	0.61 ± 0.17	0.92 ± 0.1	1.46 ± 0.45
OPC (w/c = 0.5), DeJong and Ulm	0.66 ± 0.29	1.29 ± 0.11	1.65 ± 0.17
OPC with 21% silica fume (w/b = 0.4), Vandamme	0.62 ± 0.13	0.91 ± 0.11	1.42 ± 0.40
OPC with 20% fly ash (w/b = 0.45)	0.93 ± 0.38	3.68 ± 1.98	-
OPC with 60% fly ash (w/b = 0.45)	0.87 ± 0.34	3.14 ± 0.89	-
OPC with 60% slag (w/b = 0.45)	0.97 ± 0.41	2.55 ± 1.13	-
Volume fraction, f			
OPC (w/c = 0.4), Vandamme et al.	0.57	0.21	0.22
OPC (w/c = 0.5), DeJong and Ulm	0.77	0.12	0.11
OPC with 21% silica fume (w/b = 0.4), Vandamme	0.60	0.21	0.19
OPC with 20% fly ash (w/b = 0.45)	0.65	0.35	-
OPC with 60% fly ash (w/b = 0.45)	0.57	0.43	-
OPC with 60% slag (w/b = 0.45)	0.65	0.35	-

The modulus values of HD C-S-H phase in damaged concrete samples seems not be affected. However, the results on LD C-S-H phase indicate that these were affected by fire because they showed lower values. The same pattern was presented in hardness as volume fraction of LD C-S-H and HD C-S-H (Table 2.8).

Table 2.8. Indentation modulus, hardness and volume of hydration products in damaged concrete [Zadeh et al., 2013].

	LD C-S-H	HD C-S-H	UHD C-S-H or CH
Indentation modulus, M			
OPC (w/c = 0.5), DeJong and Ulm	14.2 ± 5.4	25.7 ± 6.1	40.0 ± 8.2
OPC with 20% fly ash (w/b = 0.45)	12.31 ± 5.14	25.73 ± 12.74	-
OPC with 60% fly ash (w/b = 0.45)	12.82 ± 5.54	30.08 ± 13.45	-
OPC with 60% slag (w/b = 0.45)	13.84 ± 5.22	27.98 ± 11.38	-
Indentation hardness, H			
OPC (w/c = 0.5), DeJong and Ulm	0.55 ± 0.27	1.26 ± 0.24	1.92 ± 0.22
OPC with 20% fly ash (w/b = 0.45)	0.64 ± 0.34	2.31 ± 1.26	-
OPC with 60% fly ash (w/b = 0.45)	0.57 ± 0.38	2.21 ± 1.42	-
OPC with 60% slag (w/b = 0.45)	0.46 ± 0.22	1.59 ± 0.83	-
Volume fraction, f			
OPC (w/c = 0.5), DeJong and Ulm	0.76	0.24	Unknown
OPC with 20% fly ash (w/b = 0.45)	0.61	0.39	-
OPC with 60% fly ash (w/b = 0.45)	0.53	0.47	-
OPC with 60% slag (w/b = 0.45)	0.60	0.40	-

Liu et al. (2013) studied Portland cement pastes blended with ground granulated blast furnace slag. The cement was replaced by 30 % and 70 % of this slag by mass and the w/c ratio of the pastes was 0.4. Nanoindentation tests for 3 days, 90 days and one year were conducted. Once again, the elastic modulus values of LD C-S-H and HD C-S-H were similar to those reported in previous studies.

About the volume fraction results, the volume of LD C-S-H was gradually reduced and the volume fraction of HD C-S-H increased with the prolongation of hydration age. Likewise, the volume of LD C-S-H decreased and HD volume raised as slag consumption increased. According to the results of this paper, the micromechanical properties of C-S-H were not affected by their Ca/Si ratios. The hardness results were not reported.

In order to improve the understanding of the microstructures of C-S-H in cementitious composites through studying their physical and mechanical properties, Hu and collaborators (2014) studied the mechanical properties of C-S-H gel present in cementitious composites using the nanoindentation technique. They manufactured five mixtures with different mix proportions: two pastes mix with water/cement ratios of 0.23 and 0.40 and three mortar mix with water/ cement ratios of 0,23, 0,35 and 0,53.

In this study, they detected four distinct phases, which they named 1) Very porous C-S-H gel (VP C-S-H), 2) Outer product C-S-H gel (OP C-S-H), 3) Inner product C-S-H gel (IP C-S-H), and 4) Crystalline phase (Figure 2.14).

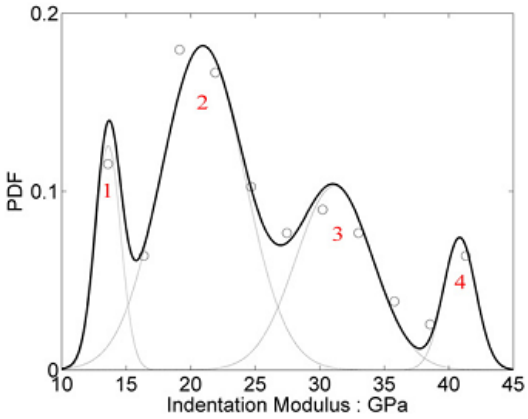

Figure 2.14. Probability distribution of indentation modulus of C-S-H/CH composites present in cement paste matrix [Hu et al., 2014).

With respect to indentation modulus, they used a deconvolution method with maximum likelihood estimation of multiple Gaussians model and they found that a higher water/cement ratio leads IP and OP C-S-H to have lower elastic moduli (Table 2.9). Concerning SEM/EDX analysis on C-S-H gel, they found that a higher water/cement ratio leads to C-S-H gel with lower Ca/Si ratio. Finally, they reported that the average porosity of inner product is significantly lower than outer product.

Table 2.9. Summary of indentation modulus of inner product and outer product in GPa [Hu et al., 2014].

C–S–H		CP0.23	CP0.4	M0.35	M0.53
OP	Mean	28.9	25.2	26.5	20.8
	S.D.	6.1	2.8	2.9	3.2
IP	Mean	39.8	31.6	34.7	31.0
	S.D.	6.7	2.9	2.4	3.0

Hu and Li (2014) carried out an investigation in Portland cement pastes with the main objective to predict their elastic modulus. For it, they conducted nanoindentation tests in Portland cement pastes (Type I) with water/cement ratio of 0.4. They named both different C-S-H structures as outer product and inner product; by reporting indentation modulus and hardness of outer product of 25.2 ± 2.8 GPa and 0.75 ± 0.26 GPa respectively. This result was higher than those reported of low density C-S-H above. In relation to inner product, they reported 31.6 ± 2.9 GPa for modulus and 1.14 ± 0.17 GPa for hardness (Figure 2.15).

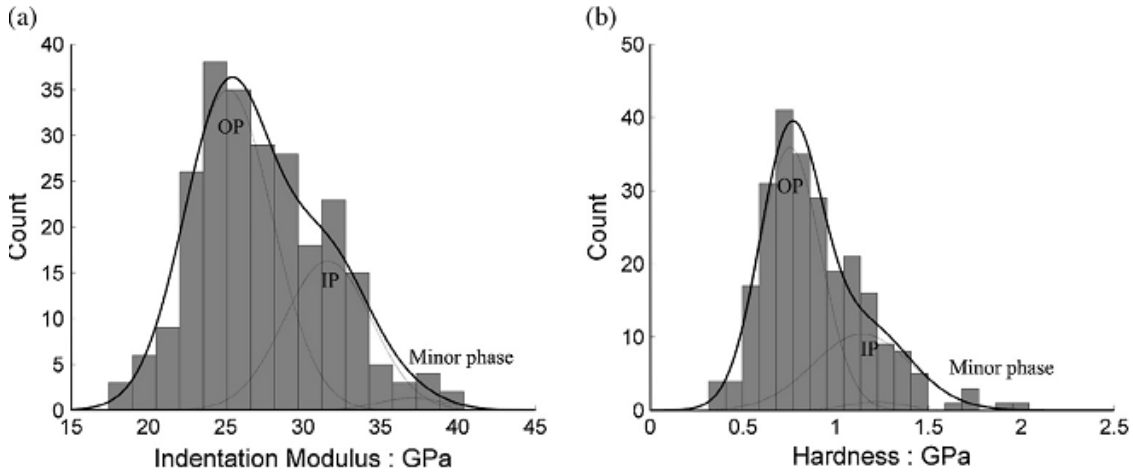

Figure 2.15. Histograms of indentation modulus (a) and hardness (b) of the C-S-H phase in Portland cement paste [Hu and Li, 2014].

Thereafter, in order to study the microstructure and mechanical properties of fly ash blended cement paste, Hu (2015) manufactured four cement paste mix with water/cement ratios of 0,23 and 0,4. Two cement paste were manufactured with just Type I Portland cement as reference, the other two were manufactured with 30% of fly ash replaced (in mass percentage) of Portland cement holding a constant water/binder ratio as that of the references.

Between the findings from nanoindentation tests on residual fly ash, he detected two types of fly ash with different mechanical properties and chemical composition (Table 2.10). On the other hand, he reported that the incorporation of fly ash decreases the Ca/Si ratio, indentation modulus and hardness of C-S-H gels at the same water/binder ratio (Table 2.11).

Table 2.10. Mechanical parameters of fly ash present in fly ash blended cement pastes [Hu, 2014].

	w/b = 0.4			*w/b* = 0.23		
	M (GPa)	*H* (GPa)	*f*	*M* (GPa)	*H* (GPa)	*f*
Fly ash (I)	51.7 ± 6.8	2.47 ± 0.70	0.39	48.2 ± 12.9	2.24 ± 0.79	0.23
Fly ash (II)	75.1 ± 8.8	8.47 ± 1.91	0.61	76.9 ± 10.6	8.33 ± 1.62	0.77

Table 2.11. Summary of mechanical parameters of C-S-H gel [Hu, 2014].

	Cement paste		Fly ash blended cement paste	
	w/b = 0.4	*w/b* = 0.23	*w/b* = 0.4	*w/b* = 0.23
Outer product				
M (GPa)	25.2 ± 2.8	28.9 ± 6.1	22.9 ± 3.2	26.7 ± 4.3
H (GPa)	0.75 ± 0.26	0.87 ± 0.25	0.58 ± 0.16	0.75 ± 0.21
Inner product				
M (GPa)	31.6 ± 2.9	39.8 ± 6.7	32.5 ± 5.4	35.5 ± 7.1
H (GPa)	1.14 ± 0.17	1.51 ± 0.38	1.16 ± 0.35	1.21 ± 0.40

After working with Portland cement pastes, Hu and Li (2015) studied Portland cement pastes containing silica fume and fly ash and their results were contradictory (Table 2.12) with respect to those reported before [Hu, 2014].

To carry out this study, they produced three pastes with the same water/binder ratio of 0,4; the first one with only Portland cement (Type I), the second one Portland cement replaced by 10% of silica fume and the last one contained a 30% of Portland cement substitution by fly ash. About fly ash particles, they detected through nanoindentation tests two types of fly ash (Figure 2.16). Besides, they also reported that the relative amount of inner product increased significantly with the incorporation of silica fume and increased slightly with the incorporation of fly ash. Finally, they showed that incorporation of silica fume and fly ash lead to a significant change in chemical composition of outer products and inner product (Table 2.13).

Table 2.12. Deconvolution results of the C-S-H phase [Hu and Li, 2015].

Sample	OP 'C–S–H'			IP 'C–S–H'		
	M (GPa)	*H* (GPa)	*f*	*M* (GPa)	*H* (GPa)	*f*
CP	25.2 ± 2.8	0.75 ± 0.26	0.67	31.6 ± 2.9	1.14 ± 0.17	0.31
CP10%SF	25.1 ± 1.9	0.75 ± 0.09	0.37	29.2 ± 4.1	0.93 ± 0.22	0.61
CP30%FA	22.9 ± 3.2	0.58 ± 0.16	0.58	32.5 ± 5.4	1.16 ± 0.35	0.39

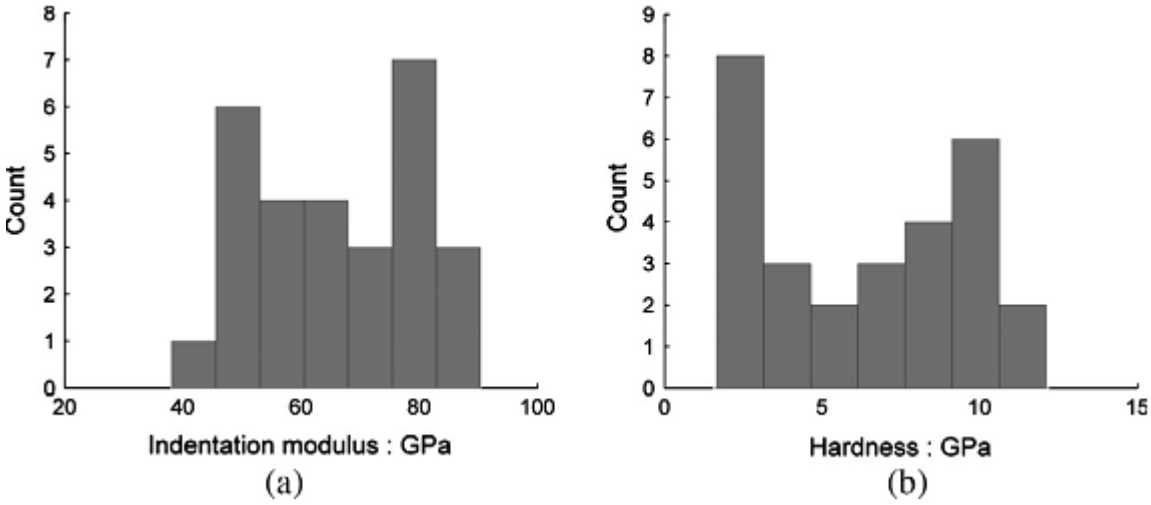

Figure 2.16. Histograms of indentation modulus (a) and hardness (b) of the residual fly ash particles [Hu and Li, 2015].

Table 2.13. Average Ca/Si, Ca/(Si+Al), Al/Si ratios of the C-S-H phase using SEM-EDS [Hu and Li, 2015].

		CP		CP10%SF		CP30%FA	
		Mean	SD	Mean	SD	Mean	SD
OP 'C–S–H'	Ca/Si	2.34	0.30	2.13	0.64	2.00	0.72
	Ca(Si + Al)	2.08	0.17	1.91	0.55	1.51	0.49
	Al/Si	0.12	0.04	0.11	0.04	0.35	0.19
	N	24		36		23	
IP 'C–S–H'	Ca/Si	2.17	0.19	1.98	0.21	1.77	0.28
	Ca(Si + Al)	2.03	0.17	1.77	0.19	1.47	0.23
	Al/Si	0.07	0.02	0.12	0.03	0.21	0.04
	N	34		53		27	
All	Ca/Si	2.25	0.26	2.04	0.44	1.88	0.54
	Ca(Si + Al)	2.05	0.20	1.83	0.38	1.48	0.37
	Al/Si	0.09	0.04	0.11	0.04	0.27	0.15
	N	58		89		50	

Xu et al. (2015) evaluated the elastic modulus and hardness of cement paste by using nanoindentation technique with addition of modulus mapping. In this study, the nanoindentation was performed in two distinctive phases: unhydrated cement grain and hydration products (C-S-H) (Figure 2.17). The modulus and hardness of C-S-H gel were between 20 - 40 GPa and 1 - 2 GPa respectively (Figure 2.18). Regarding modulus mapping, it allow evaluating the storage and loss moduli for small areas with high resolution (Figure 2.19), and seems that by using this technique, it is possible to detect that the gel behavior is more viscoelastic than the cement grain. Finally, the results obtained by this technique were similar with respect to those obtained by nanoindentation (Table 2.14).

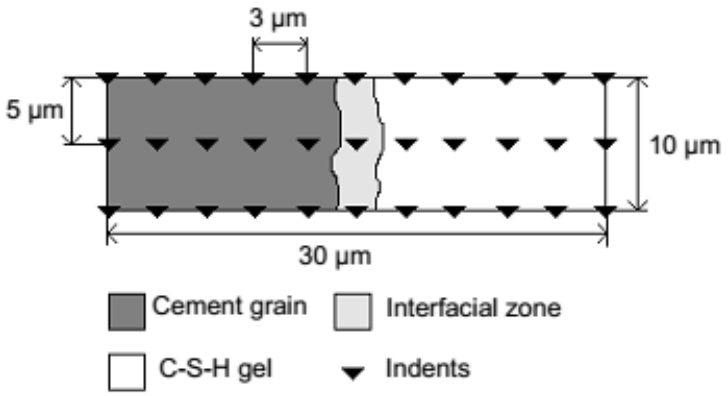

Figure 2.17. Grid nanoindentation across the interface between C-S-H gel and cement grain [Xu et al., 2015].

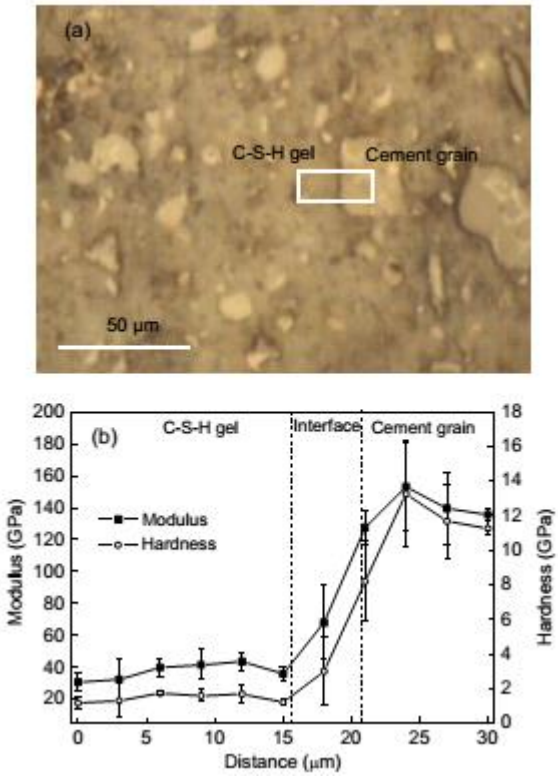

Figure 2.18 Gird nanoindentation results on interface between C-S-H gel and cement grain. (a) Optical image, (b) Modulus and hardness vs. position [Xu et al., 2015].

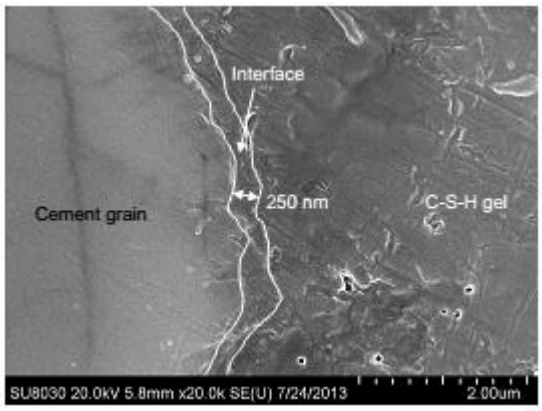

Figure 2.19 SEM image of interface between C-S-H gel and cement grain [Xu et al., 2015].

Table 2.14. Results modulus mapping.

Test location	Modulus (GPa)
C-S-H gel	20 – 50
Cement grain	90 – 110
Interface zone	61.5 – 68.3

2.5 Concrete permeability.

Since its inception, the hydraulic concrete has been a construction material par excellence due to its easy production and availability of ingredients that practically can be found all around the world. However, despite the easy production, it is necessary to pay attention to the dosage of the components for achieving prolonged service life of this material. The majority of concrete deterioration cases is connected to corrosion of reinforcement due to carbonation or chloride penetration. In urban and industrial areas where environmental pollution results in significant concentration of carbon dioxide, the carbonation process is initiated, and it promotes corrosion of reinforcement. Numerous surveys have indicated that chloride ions, originating from deicing salts or seawater, are the primary cause of reinforcing steel corrosion in highways and marine or coastal structures [Damtoft et al., 2008].

Mineral admixtures such as fly ash, blast furnace slag, natural pozzolan and silica fume also known as supplementary cementitious materials (SCM), have been used in the production of concrete in order to densify the cementitious matrix and thereby improve the physical and mechanical properties [Ahmaruzzaman, 2010; Ganesh and Kumar, 2000] by particularly reducing the permeability of concrete. Unfortunately, it is not still possible to do more efficient concrete mixture design with these cementitious materials in order to extend the useful life of concrete structures.

Bouzoubaâ et al. (2001) investigated the effect on mechanical properties and durability in concretes using high consumption of fly ash in blended cements, the total consumption of Portland cement was 379 kg/m^3, With w/b = 0,32. The Portland cement represented 45 % of total cementitious materials and the remaining 55 % was fly ash. The fly ash in this study did not meet the requirements of fineness indicated in ASTM C-618, but met the chemical requirements of ASTM Class F fly ash. The compressive strength reached at 28 days was 30.5 MPa, and the modulus of elasticity was 22.4 GPa.

The resistance to the chloride-ion penetration was determined according to ASTM C 1202 and was significantly higher for the concrete with fly ash than for the control concrete. At 91 days, the total charge passed was less than 400 Coulombs for concretes with fly ash and for concrete control was higher to 2000 Coulombs.

Malhotra et al. (2000) studied the long-term effects (10 years) with respect to the mechanical and durability properties of concrete with supplementary cementitious materials. Supplementary materials studied were fly ash, blast furnace slag and condensed silica fume. For concrete manufactured with fly ash, the total cementitious consumption was 350 kg/m^3, which corresponded to 57% fly ash and the remaining 43% was Portland cement with w/b ratio of 0.29. All concretes showed good performance in mechanical properties (compression resistance and modulus of elasticity). Regarding durability tests, the fly ash concrete turned out to have the best performance about the resistance penetration of chloride ions, but had lower performance in penetration of CO_2, by presenting an advance profile of 5 mm during 10 years. This result was superior to the concretes with silica fume and blast furnace slag that presented penetrations under 1 mm. Despite this, the authors think that the results of fly ash concretes are extremely low.

Papadakis (2000) manufactured mortars using different supplementary cementitious materials which were silica fume, low-calcium fly ash and high calcium fly ash in order to study the resistance against carbonation and chloride ingress. The w/c ratio of the control mix was 0,5. For consumption of these supplementary cementitious materials (SCM), he used two criteria: aggregate replaced by SCM and cement replaced by SCM.

In the case of aggregate replaced by SCM, three different amounts were selected according to SCM type: silica fume 5, 10 and 15 % addition to cement mass; low-calcium fly ash 10, 20 and 30 % addition to cement mass, and high-calcium fly ash 10, 20 and 30 % addition to cement mass too. In the case of cement replaced by SCM, the same amounts were also selected: silica fume 5, 10 and 15 % replacement the control cement mass; low-calcium fly ash 10, 20 and 30 % replacement of the control cement mass and high-calcium fly ash 10, 20 and 30 % replacement of the control cement mass.

In this paper it was established that for all mortars with supplementary cementitious materials, the carbonation depth decreases as aggregate replaced by SCM increases and increases as cement replaced by SCM increases. The lowest carbonation depth was for high-calcium fly ash, then for low-calcium fly ash and the highest for silica fume.

Regarding the chloride tests, the specimens incorporating a SCM, whether it substitutes aggregates or cement, exhibited significantly lower total chloride content for all depths from the

surface. Silica fume exhibited the lowest degree of chloride penetration, then low-calcium fly ash and high-calcium fly ash the highest.

Hosam El-Dim H. Seleem and collaborators et al., (2010) worked with concretes incorporating silica fume, ground granulated blast furnace slag and metakaolin in order to study the seawater resistance of concrete; for this they conducted water permeability (Figure 2.20) and chloride penetration resistance tests. For the latter the concrete was exposed to synthetic sea water.

All concrete mixtures produced in this work had a w/b ratio of 0.32, the ordinary Portland cement content was 400 kg/m^3, the supplemental materials were employed as an addition to cement with a ratio of 20 % by mass.

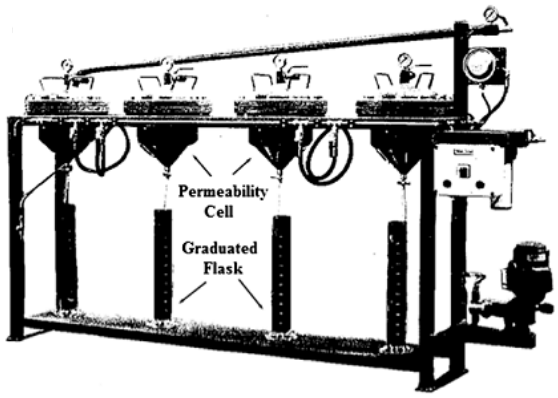

Figure 2.20. Water permeability apparatus [Seleem et al., 2010].

The compressive strength of all concretes with supplementary materials were higher than the control mixture. All mixes with supplementary materials were efficient in reducing the permeability of concrete for below the control mix. The ternary blend Portland cement-metakaolin-silica fume was superior to all other mixtures in producing impermeable concrete. Ground granulated slag was less efficient than the other employed materials regarding chloride penetration resistance (Table 2.15).

Table 2.15. Results of permeability and chloride penetration [Seleem et al., 2010].

Mix designation		Permeability ($K \times 10^{-10}$), cm/s	Chloride Cl^- concentration (%)			
			6 months		12 months	
			Surface layer	Inside specimen	Surface layer	Inside specimen
Mc	Control	2.36	0.1	0.09	0.5	0.48
Mk	First group	1.16	0.08	0.01	0.37	0.1
Mf		0.884	0.04	0.01	0.06	0.03
Mgs		1.47	0.1	0.06	0.5	0.16
Mk-f	Second group	0.78	0.08	0.03	0.14	0.04
Mk-gs		1.31	0.08	0.04	0.35	0.12
Mf-gs		0.92	0.04	0.01	0.2	0.04

Mc.- Control mix, Mk.- Metakaolin mix, Mf.- Silica fume mix, Mgs.- Slag mix. Mk-f.- Metakaolin silica fume mix, Mk-gs.- Metakaolin slag mix, Mf-gs.- Silica fume-slag mix.

Uysal et al. (2012) studied the effectiveness of mineral admixtures and fillers on mechanical properties, chloride ion permeability and impermeability of self-compacting concrete (SCC). The mineral admixtures studied were flay ash class C (FA) and granulated blast furnace slag (GBFS); the fillers studied were limestone powder (LP), basalt powder (BP) and marble powder (MP).

The Portland cement was replaced in 15%, 25% and 35% by fly ash and was replaced in 20%, 40% and 60% by granulated blast furnace slag. The total cementitious content for all mixtures was 550 kg/m^3 and the w/b ratio was selected in 0,33. The rapid chloride ion permeability was conducted in accordance with ASTM C-1202, and water impermeability was determined by using water impermeability test equipment (Figure 2.21) according to DIN 1048 standard. Both tests were carried out at 28 days.

Figure 2.21. Water permeability test equipment [Uysal et al., 2012].

The compressive strength in mixes with mineral admixtures decreased as the mineral admixtures consumption increased, however the mix with 15% of slag developed higher strength than control mix. Regarding durability tests, the chloride ion permeability decreased when mineral admixtures increased regardless of mineral admixture type (Figure 2.22). The results of water permeability depth indicated that the mix with 20% of slag showed the best performance (Figure 2.23). Despite the fact that water penetration increased when the consumption of mineral admixtures increased, the mixes with mineral admixtures had better performance than mixes with fillers.

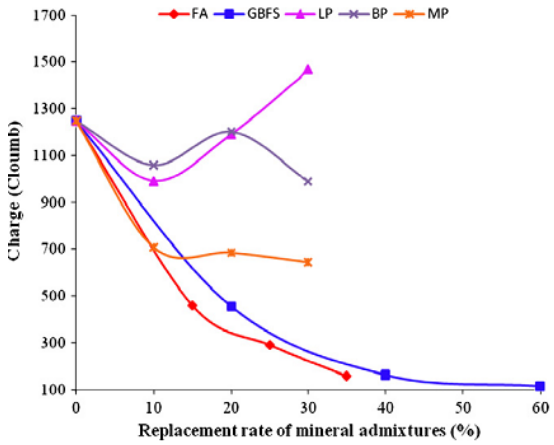

Figure 2.22. Chloride ion permeability versus mineral admixture type at different replacement rates [Uysal et al., 2012].

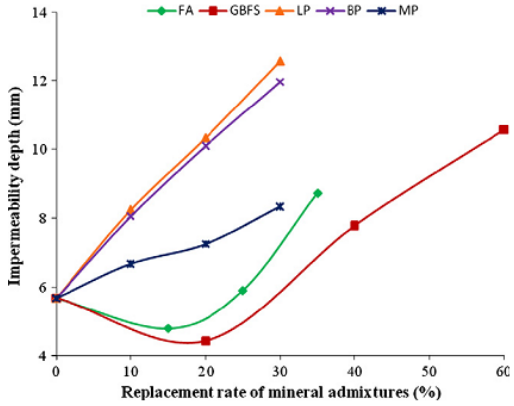

Figure 2.23. Water impermeability depths versus mineral admixture type at different replacement rates [Uysal et al., 2012].

A. Elahi et al. (2010) evaluated the mechanical and durability properties of high performance concretes containing supplementary cementitious materials in both binary and ternary systems. The mechanical property assessed was the compressive strength, while the durability characteristics were investigated in terms of chloride diffusion, electrical resistivity, air permeability and water absorption.

The minerals admixtures studied in this paper were fly ash (FA), ground granulated blast-furnace slag (BS) and silica fume (SF), Portland cement was replaced with fly ash up to 40%, and ground granulated blast-furnace slag up to 70% and silica fume up to 15%. All concretes mixes studies had a water/binder of 0,3 and the total binder content was 485 kg/m^3.

The silica fume performs better than other mineral admixtures for the strength development (Table 2.16) and bulk resistivity (Figure 2.24). In general, it was found that all mixes with mineral admixtures turned out greater bulk resistivity than the control mix, being attributed to the combined effect of microstructural densification and more C-S-H formation. Regarding water absorption tests, there was a decrease in sorptivity with age for all the mixes, the mixture with silica fume was less pronounced in improving the sorptivity.

Table 2.16. Strength of mixes relative to the control at each test age [Elahi et al., 2010].

Mix ID	Compressive strength at different ages relative to control (%)			
	3 days	7 days	28 days	91 days
HP-CC	100	100	100	100
HP-SF7.5	102.1	109.7	117.3	109.9
HP-SF15	86.7	98.8	120.8	115.6
HP-BS50	74.0	95.2	98.6	96.8
HP-BS70	38.1	61.7	74.3	77.9
HP-SF + BS50	60.5	89.4	105.8	101.3
HP-FA20	80.6	81.1	79.5	87.5
HP-FA40	49.5	54.0	58.0	75.8
HP-SF + FA20	61.0	71.2	94.3	97.5
HP-SF + FA40	46.0	57.5	76.0	88.7

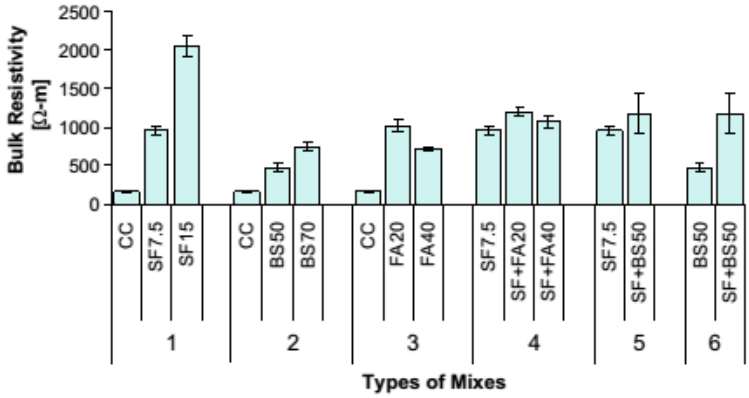

Figure 2.24. Bulk resistivity results [Elahi, et al., 2010].

The ternary mixes containing ground granulated blast-furnace/fly ash and silica fume performed the best among all mixtures to resist the chloride diffusion (Figure 2.25), and the mix containing fly ash showed favorable permeation results.

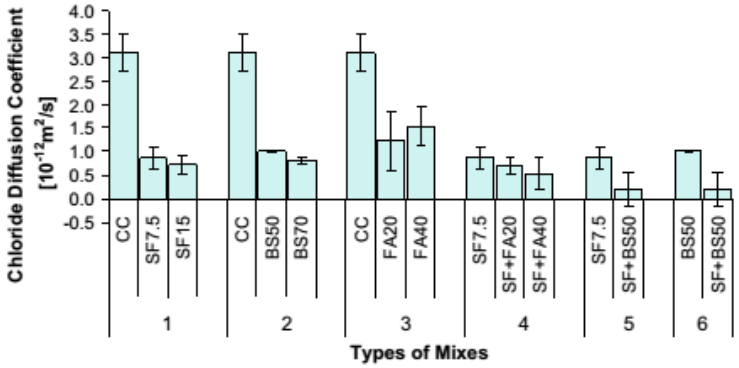

Figure 2.25 Results of chloride diffusion coefficient [Elahi et al., 2010].

Ali Reza Bagheri and collaborators (2012) studied the mechanical and durability properties of binary and ternary concretes containing silica fume and low reactivity blast furnace slag. Replacement levels of cement with slag were 15%, 30% and 50% with respect to the cement mass. Replacements levels of SF were 2.5%, 5%, 7.5%, and 10%. The water/binder ratio and total cementitious materials content were kept constant for all mixes at 0,38 and 420 kg/m^3 respectively. Concrete mixes were evaluated for compressive strength, electrical resistance, chloride permeability (ASTM C1-202 RCPT test) and chloride migration (AASHTO TP64 RCMT test), at various ages up to 180 days.

The binary mix with low reactivity slag did not increase the strength with respect to the reference mixture. However, it provided considerable durability improvement in the long term. The appropriate combination (ternary mix) to reach a similar control mixture strength and simultaneously increasing the electric resistance and reducing penetration of chlorides (long term) was 15% slag with 5% SF. A study about the microstructure was not reported.

Lee et al. (2012) studied cement-based mortars with additions of fly ash and silica fume in order to establish durability indices. They made binary and ternary mixes with water/binder ratios of 0.45 and 0.65. The findings were that the fly ash and SF improved the compressive strength, porosity, absorption, chloride penetration and corrosion resistance. The most material was silica fume followed by the combination of silica fume and fly ash, and then fly ash. The researchers reported that the microstructure of mortars with silica fume or fly ash had fewer pores, more lane structure and more C-S-H particles (Figures 2.26 and 2.27).

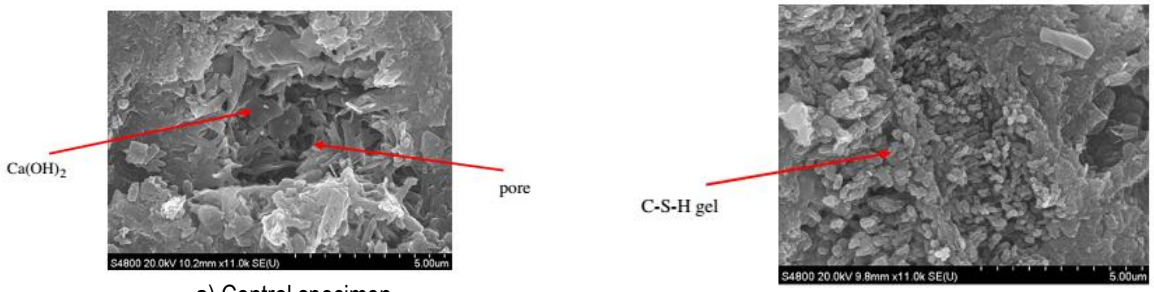

a) Control specimen.

b) 10 % silica fume specimen.

Figure 2.26. SEM observations of silica fume specimens (w/b = 0,45, 11000x) [Lee et al., 2012].

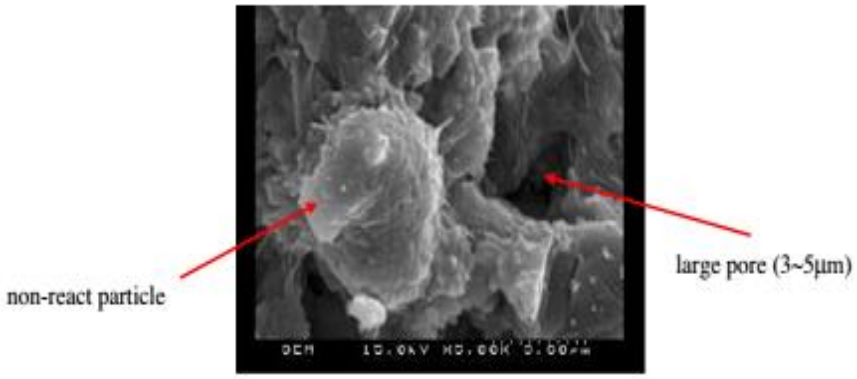

Figure 2.27. SEM observations of 15 % fly ash specimens (w/b = 0,45, 5000x) [Lee et al., 2012].

Chapter 3. Materials and experimental program.

The experimental program is divided on three stages. The stage 1, is called selection of mineral admixtures and is presented in section 3.2.1. In this stage two MA are selected among four materials presented in section 3.1. The chosen MA were those who showed the greatest and lowest reactivity when added to Portland cement paste and mortar mixtures. The used dosages were of 20% and 60% replacement of the mass of the Portland cement, these dosages are among the typically studied in order to evaluate the effect of high and low MA contents. The stage 2, correspond to the microstructural analysis in binary cementitious pastes (using the two mineral additions chosen from stage 1) by nanoindentation tests in conjunction with chemical analysis (NI-EDS) and the stage 3 which consist of analyzing the physical and mechanical properties of concretes produced with the same mineral additions chosen from the stage 1.

The Stages 1 and 2 were carried out in UdeS; in which, the microstructural analyzes (stage 2) were developed by William Wilson under the supervision of the Prof. Arezki Tagnit-Hamou and Luca Sorelli. The stage 3, was developed in UANL under the supervision of the Prof. Alejandro Durán-Herrera. The description of the materials used in this work is presented below.

3.1 Materials.

For the present study, the following minerals admixtures, from different parts of Mexico, were considered for this project: fly ash (FA), ground granulated blast furnace slag (S) and natural pozzolan (NP). For each of these materials, as well as the Portland cement used, the following properties were determined: density according to ASTM C 188, fineness according to the procedure described in ASTM C 204, particle size distribution by a laser particle analyzer, strength activity index based on ASTM C 190, ASTM C 311 and ASTM C 989. Finally, the main chemical and mineralogical compositions of the cementitious materials was determined by X-ray fluorescence, as well as X-ray diffraction analysis. The description of the test methods are presented in section 3.3.

3.1.1 Fly Ashes

Two different kinds of fly ash were used, one, from the Thermoelectric Central "José López Portillo" at Nava, Coahuila, identified as FA1, and another one, from the Thermoelectric Central "Plutarco Elías Calles" at La Unión de Isidro Montes de Oca, Guerrero, identified as FA2. The strength activity index (SAI) of the FA1 was of 67% and 71% at 7 and 28 days of age, respectively; as well, the results for the FA2 were of 76% and 85% at the same ages. The SAI of FA1 (71%) is under the minimal requirement of ASTM; while FA2, present SAI at 28 days (85%) higher than ASTM requirement. Table 3.1 show that the fly ash (FA1) has more SiO_2 content (60,7%) than FA2 (53,8%).

As it can be seen in the Figure 3.1, the results of X-ray diffraction analysis exhibit the presence of vitreous phases (an amorphous hump between 18° and 25° of 2θ in the X-ray diffraction spectrum). As well, in both the Table 3.1 and Figure 3.2, it can be seen that the fly ashes had coarser particles than the slag or natural pozzolan. The Blaine fineness of FA2 is significantly higher (464 m^2/kg) than fineness of FA1 (330 m^2/kg).

3.1.2 Slag

A ground granulated blast furnace slag from the Steel plant “Lázaro Cárdenas Las Truchas”, Port of Lázaro Cárdenas, Michoacán., was used, and identified as S. The strength activity index of the S was of 64% and 85% at 7 and 28 days of age, respectively. The chemical composition of slag (Table 3.1) present significantly low SiO_2 content (18,7%) and very high CaO (50,1%) and SO_3 contents (8,4%).

As it can be seen in the Figure 3.1, the results of X-ray diffraction analysis exhibit the presence of vitreous phases (an amorphous hump between 28° and 35° of 2θ in the X-ray diffraction spectrum), along with crystalline phases of merwinite, potassium aluminum oxide, calcium carbonate and metal oxides. As well, in both the Table 3.1 and Figure 3.2, it can be seen that the slag had finer particles than the fly ashes.

3.1.3 Natural Pozzolan

The natural pozzolan used was extracted from the city of Orizaba, Veracruz, México, and identified as NP. The strength activity index of the NP was of 87% and 98% at 7 and 28 days of age, respectively. The SAI at 7 and 28 days are significantly higher tha ASTM requirement. The chemical composition of NP show the highest content of SiO_2 (65.2%) and Na_2O equiv (6,23%) compared to the others.

As it can be seen in the Figure 3.1, the results of X-ray diffraction analysis exhibit the presence of vitreous phases (an amorphous hump between 18° and 35° of 2θ in the X-ray diffraction spectrum), along with crystalline phases consisting mainly of plagioclase and feldspars (such as albite and anorthite). The NP is the finest (836 m^2/kg) among the cementitious materials used in this project with average diameter of 7,6 πm, as it can be seen in Table 3.1 and Figure 3.2.

3.1.4 Portland Cement

A Portland cement of general use (OPC), complying with Canadian standards was selected for this project. Its chemical and physical properties are shown in the Table 3.1and Figure 3.2. The average particle size of this cement is 15,6 µm.

Table 3.1. Chemical composition and Physical properties of the Portland cement and mineral admixtures.

Materials	Chemical composition									Physical properties		
	SiO_2	Al_2O_3	Fe_2O_3	CaO	MgO	SO_3	K_2O	Na_2O	Na_2O* equiv	Density g/cm^3	Blaine fineness m^2/kg	Average diameter µm
Portland cement	20,2	4,7	2,6	62,0	1,9	3,5	0,9	0,2	0,79	3,1	420	15,6
Fly ash (FA1)	60,7	24,0	3,4	2,6	0,7	0,02	0,9	0,6	1,19	2,06	330	46,0
Fly ash (FA2)	53,8	21,1	5,6	7,7	0	0,6	1,3	0	0,85	2,38	464	26,3
Slag (S)	18,7	11,3	2,1	50,1	2,1	8,4	0,4	0,3	0,56	2,83	369	18,9
Natural Pozzolan (NP)	65,2	14,9	3,5	3,2	2,1	0,03	3,7	3,8	6,23	2,5	836	7,6

* Na_2O equiv = $\%Na_2O + 0,658\ \%K_2O$

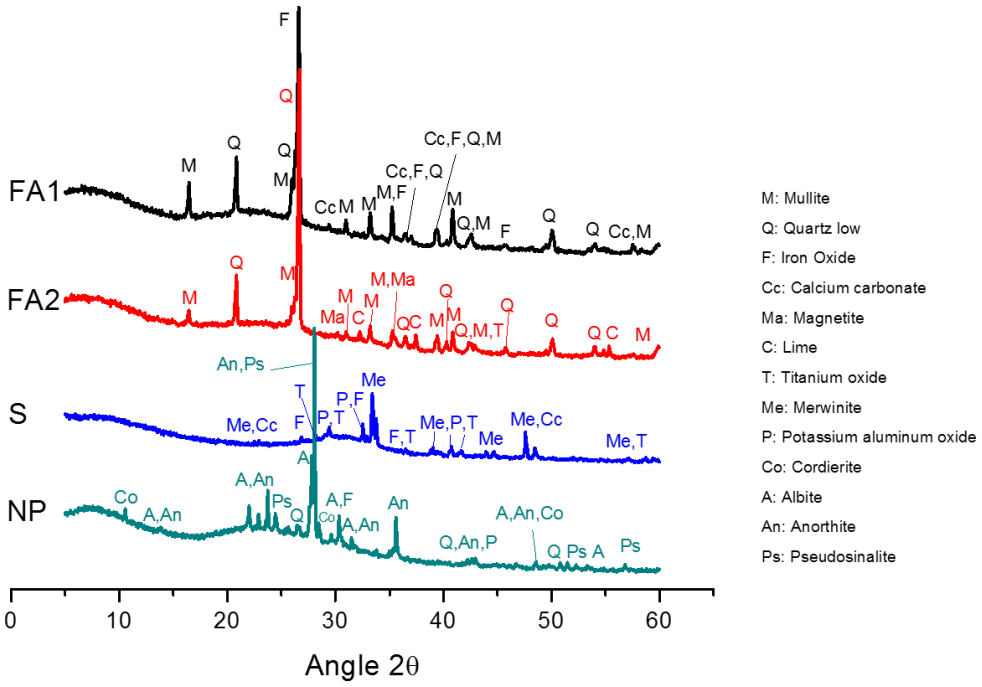

Figure 3.1. XRD patterns of minerals admixtures.

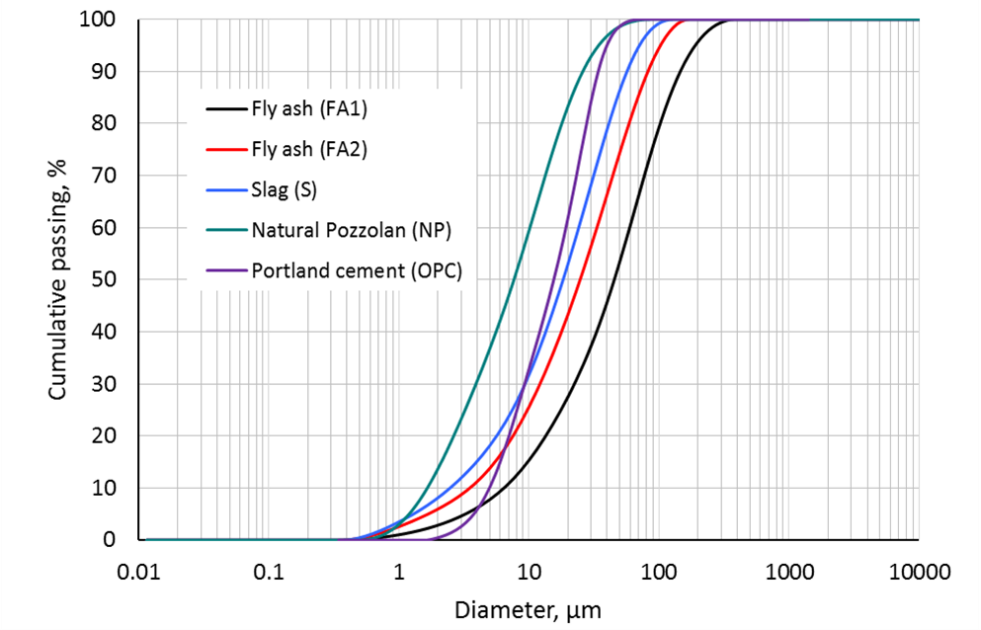

Figure 3.2. Particle size distribution of minerals admixtures.

3.1.5 Aggregates

The aggregates used in the present study for the production of the concrete mixtures consist of typical crushed limestones from the metropolitan area of Monterrey, Nuevo León, México, which had their densities and absorptions determined according to the procedure indicated in ASTM C 127 for the coarse aggregate (density of 2,72 g/cm^3 and absorption of 0,86%) and ASTM C 128 for the sand (density of 2,64 g/cm^3 and absorption of 2,04%). For both aggregates (sand and coarse), their particle size distribution by sieving was determined according to the procedures described in ASTM C 136 and its results are shown in the Figures 3.3 and 3.4. In Figure 3.4, it can be seen that the sand exceeded the maximum amount allowable according to ASTM C 33 for the sieves #100 and #200 by an average of 8% in each sieve.

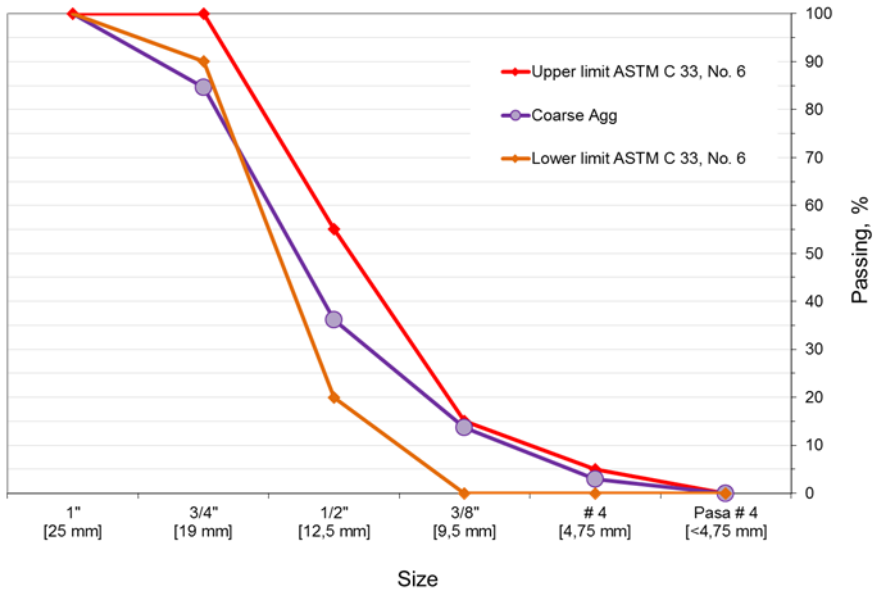

Figure 3.3. Particle size distribution of coarse aggregate.

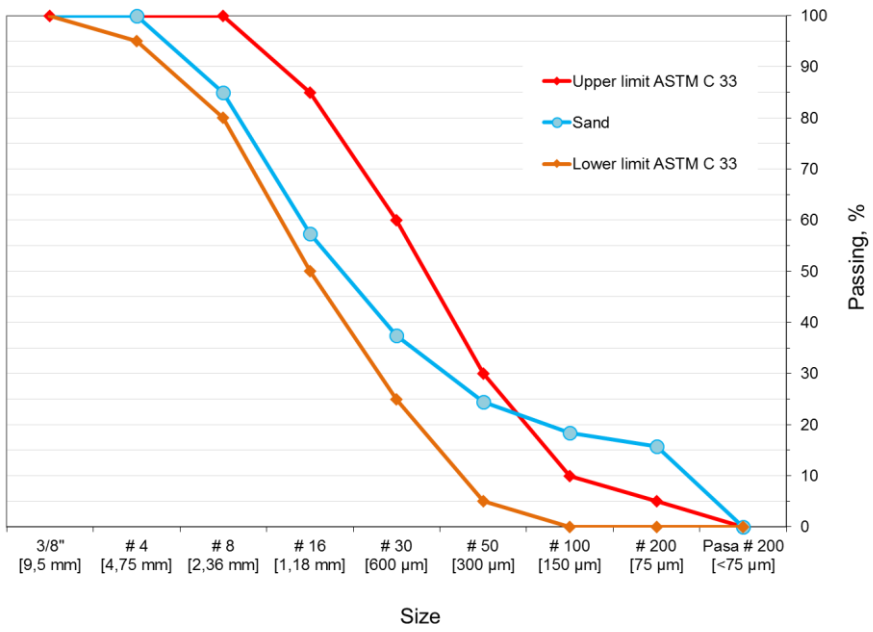

Figure 3.4. Particle size distribution of sand.

3.1.6 Chemical admixture.

For the stage of concrete mixture elaboration, a high range water reducer admixture (superplasticizer) was used, Plastol Precast Plus, type A and F according to ASTM C 494, manufactured by Euclid. The density of this admixture was of 1,12 g/cm^3 and it was determined using a Le Chatelier flask, recording to the displaced volume in the graduated scale in the flask, and its mass in an electronic Ohaus scale, Model Explorer E04130, with 1 mg of precision. The solids content of this admixture is of 51%, and it was obtained by placing a sample of approximately 190 g of admixture in a recipient, which was placed in an oven at 110°C until a constant mass was reached; the weight of the remaining residue in the recipient from the original sample, expressed in percentage of the original mass, represents the amount of solids content in the admixture sample.

3.2 Experimental program.

3.2.1 Stage 1. Selection of mineral admixtures.

The objective of this stage of the study was to choose two of the four minerals admixtures described in section 3.1. For this purpose, two water/binder ratios were used (0,35 and 0,45) to produce pastes and mortars only with Portland cement as a reference. Once the references were defined, the aforementioned mineral admixtures were used to produce pastes and mortars with binary cementitious systems.

Both the pastes as well as the mortars were made with Portland cement replacements of 20% and 60% in mass by each of the selected cementitious materials. The paste mixtures were produced according to the procedure described in ASTM C 1738. Pastes with a W/B ratio of 0,45 were identified as the series AP, and pastes with a W/B ratio of 0,35 were identified as the series BP. In the Table 3.2 the complete identifications for each series are shown.

The hydration level of the different paste mixtures produced in this stage were evaluated by X-ray diffraction and thermogravimetric analyses at the ages of 28 and 90 days. During that time, the paste mixtures were kept submerged in limewater.

The main advantage of a mineral admixture, when it is used as a replacement of Portland cement, is to consume the lime produced during the cement hydration to form additional C-S-H, providing a long-term strengthening of the paste. Therefore, the X-ray diffraction is a technique for monitoring the pozzolanic reaction of mineral admixtures, it allows to determine the consumption of lime by means of comparing the decrease of the characteristic peaks of portlandite in the paste containing the addition compared to the reference mixture (plain Portland cement paste). This technic, is not very efficient in the case of lime quantification, because the cement hydration product is not always crystalline. Because of this problem, the thermogravimetric analysis is used for the portlandite consumption. Through the thermogravimetric analysis the portlandite content in the pastes with mineral admixtures can also be known in order to determine the effect of the pozzolanic reaction by means of the lime consumption, and therefore know their hydration level. These analytic techniques are described in the section 3.3.

The objective of producing mortars with binary cementitious systems was to know the effect of each of the mineral admixtures in the compressive strength development. For this purpose, 50-mm cube specimens were produced according to the procedure described in ASTM C 109. The compressive strength was determined at the ages of 7, 28, 56 and 90 days. The mortars with a W/B ratio of 0,45 were identified as the series AM and the mortars with a W/B ratio of 0,35 were identified as the series BM. In Table 3.3 the complete identifications for each mortar series are shown, and in the Figure 3.5 presents a flow chart of this stage. The mineral admixtures elected in this stage were FA1 and NP; so, in stages 1 and 2, FA1 will be referred to only as FA for simplification purposes. The results are shown in Chapter 4 (section 4.1).

Table 3.2. Pastes identification.

Series	W/B	Pastes ID
AP	0,45	APR
		AFA1-20 and AFA1-60
		AFA2-20 and AFA2-60
		AS-20 and AS-60
		ANP-20 and ANP-60
BP	0,35	BPR
		BFA1-20 and BFA1-60
		BFA2-20 and BFA2-60
		BS-20 and BS-60
		BNP-20 and BNP-60

Notes: APR and BPR are plain Portland cement pastes (references), "-20" means a replacement of 20% of the Portland cement mass for each mineral admixture and "-60" means a replacement of 60% .

Table 3.3. Mortars identification.

Series	W/B	Pastes ID
AM	0,45	AMR
		AMFA1-20 and AMFA1-60
		AMFA2-20 and AMFA2-60
		AMS-20 and AMS-60
		AMNP-20 and AMNP-60
BM	0,35	BMR
		BMFA1-20 and BMFA1-60
		BMFA2-20 and BMFA2-60
		BMS-20 and BMS-60
		BMNP-20 and BMNP-60

Notes: AMR and BMR are plain Portland cement mortars (references), "-20" means a replacement of 20% of the Portland cement mass for each mineral admixture and "-60" means a replacement of 60%.

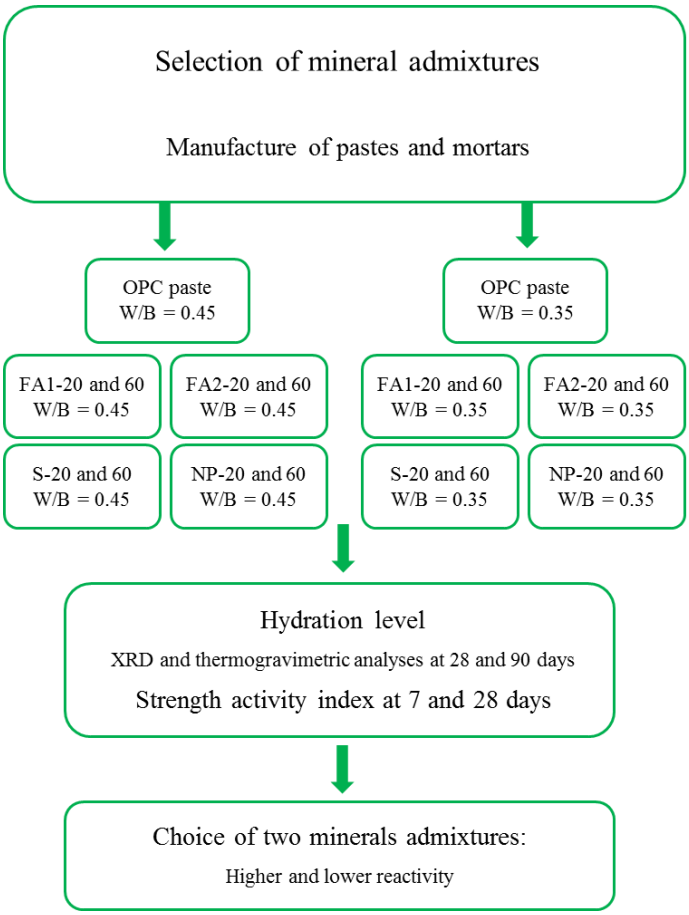

Figure 3.5. Scheme of experimental program for stage 1.

3.2.2 Stage 2. Microstructural analysis of OPC pastes containing NP.

The objective of this stage is to study the effect of the minerals admixtures in the C-S-H formation, in order to determine if these additions influence the increase in the formation of high density C-S-H and their effect on the mechanical properties and durability of concrete. For this, the microstructural analysis of the pastes with FA as well as NP will be performed by means of nanoindentation tests in joint with optical and scanning microscopy (SEM) including energy dispersive analyses (EDS); these methods are described further in the section 3.3.3. These analyses were made at the ages of 90 days of curing, and during that time the paste specimens were immersed in limewater. According to the experimental program, it was originally intended

to study a total of 10 pastes with a binary cementitious system, with the W/B ratios of 0,35 and 0,45. Since the academic stay for this project was limited to only 18 months, it was only possible to perform the tests on the pastes with NP and a W/B ratio of 0,35 (BR, B20NP and B60NP). This part of the study was conducted by William Wilson while simultaneously in México the respective tests in concrete mixtures were being carried out, corresponding to the stage 3 of this project, which is described further. The figure 3.6 show a flow chart for stage 2.

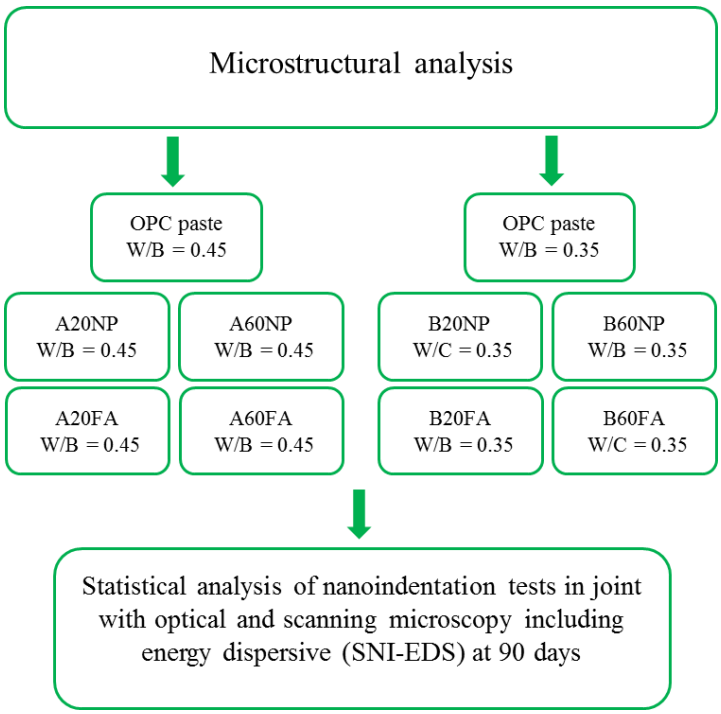

Figure 3.6. Scheme of experimental program for stage 2.

3.2.3 Stage 3. Concrete production containing FA and NP.

Since one of the main objectives was to evaluate the permeability of the concrete mixtures based on the study about the C-S-H formation; in this stage, concrete mixtures were made, maintaining the same W/B ratios (0,35 and 0,45) and the same substitutions of Portland cement for NP and FA than those planned in the paste mixtures produced in the Stage 2 of this study. The concrete mixture proportions were optimized in order to obtain a target slump of 200 ± 20 mm as shown in the Table 3.4.

The permeability of the concrete mixtures was evaluated by means of tests considered as durability indicators: chloride migration coefficient and electrical surface resistivity. These tests, their conditions and considerations are further described in the sections 3.3.4.2.3 and 3.3.4.2.4.

Table 3.4. Concrete Mixtures composition; dry materials and the water include the absorption of the aggregates, kg/m^3.

Series	W/B	Mixture	Water	PC	Fly Ash	Natural Pozzolan	SP Admixture	Coarse Aggregate	Sand Aggregate
A	0.45	AR	217	425	-	-	1,2	791	938
		A20NP	217	340	-	85	1,2	797	929
		A60NP	216	170	-	255	1,2	780	910
		A20FA	216	340	85	-	1,2	788	918
		A60FA	215	170	255	-	1,0	748	878
B	0.35	BR	184	450	-	-	2,3	827	980
		B20NP	183	360	-	90	2,3	830	965
		B60NP	183	180	-	270	2,5	826	944
		B20FA	183	360	90	-	2,3	818	954
		B20FA	182	180	270	-	2,5	776	911

The mechanical properties evaluated were the Young's modulus of elasticity and the compressive strength. The modulus of elasticity was determined at the ages of 28 and 90 days, and the compressive was monitored up to 90 days of curing. The details of these tests are described in the sections 3.3.4.2.1 and 3.3.4.2.2. A flow chart is presented in Figure 3.7.

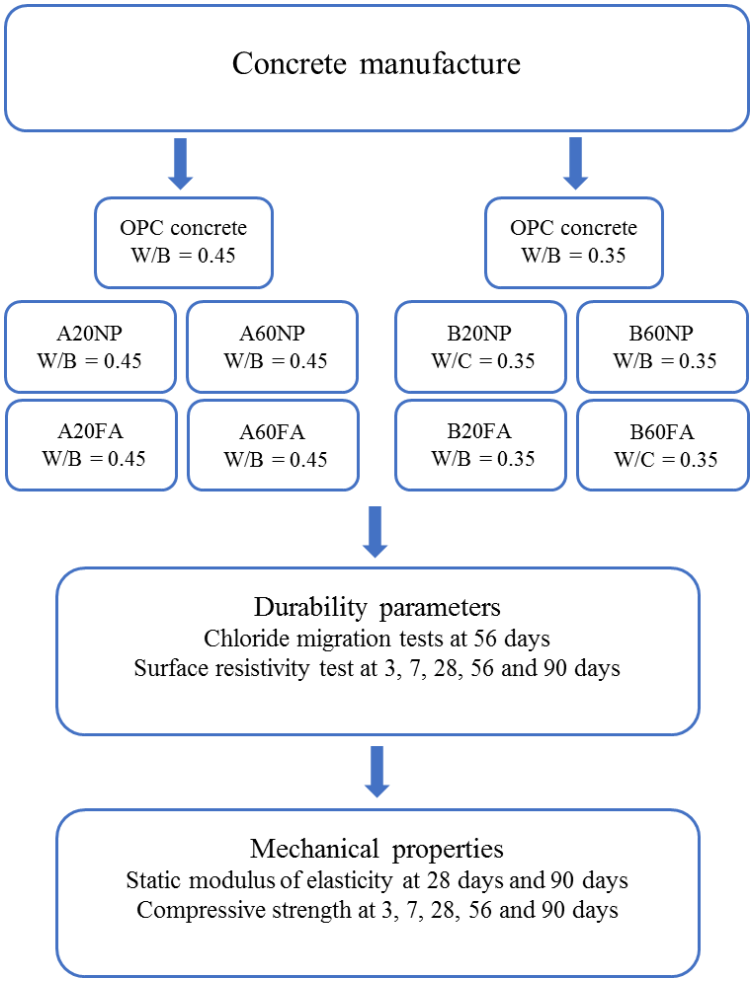

Figure 3.7. Scheme of experimental program for stage 3.

3.3 Test methods.

3.3.1 Characterization of cementitious materials.

The characterization of the cementitious materials was made by means of X-ray diffraction, X-ray fluorescence, as well as particle size analysis by laser diffraction. In addition, the density and fineness of the materials were determined. The details of the test methods are presented below.

3.3.1.1. X-ray diffraction

This technique provides a simple and practical method for identifying crystalline and non-crystalline compounds (amorphous) qualitatively. It is also possible to perform a semi-quantitative analysis through this method. This technique examines the crystalline structure of a solid material by deflecting a beam of primary or monochromatic X-rays which strikes a sample. The deflexion angles are related to the distance between the plane networks of a crystal. According to the Bragg's Law:

$$N\lambda = 2d\sin\theta$$

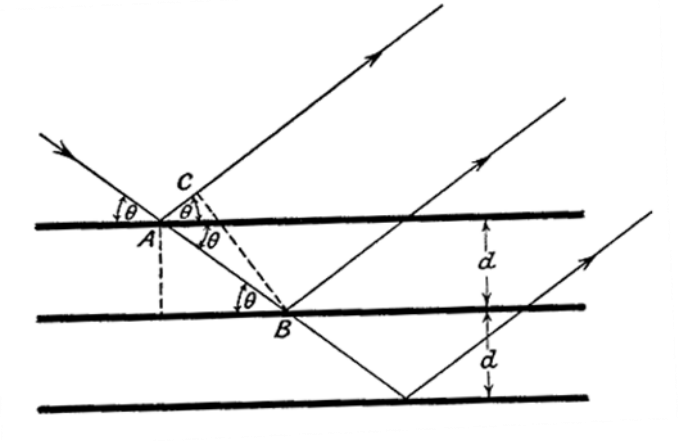

Figure 3.8. Bragg's Law scheme

"n" is an absolute number called order of reflection, *"λ"* is the wavelength of the X-rays, *"d"* is the characteristic separation between crystal planes of a given specimen, *"θ"* is the angle between the incidental beam and the reflected reticulated planes.

By measuring the angles (θ), under which the X-rays left by the crystal constructively interfere, the inter-planar separation of each crystallographic phase can be determined.

In order to identify an unknown compound, the diffraction pattern of the simple is registered using a diffractometer. A list of *d* values and the relative intensities of the diffraction lines are compiled, these data are compared with the standard line patterns with the JADE software. With the appearance of intense peaks it becomes evident the existence of a crystalline phase.

The apparatus used in the CCM laboratory was a PANalytical diffractometer with a copper cathode (CU Kα). The X-ray tube operated at 45 kV and 40 mA. The X-ray tube operated at 45 kV and 40 mA. The test was performed in the angle ranges 2θ from 5 to 70° at a scan rate of 0.18°/s.

3.3.1.2. X-ray fluorescence spectrometer (XRF)

Spectrometry by XRF is a non-destructive qualitative and quantitative elemental analysis method based on the measurement of wavelengths or X-ray energy emitted by the sample after being bombarded by a primary radiation. The equipment used in the CCM laboratory was a PANanalytical Axios-Advanced X-ray Fluorescence spectorometer (XRF). The study sample is oven-dry at a temperature of 1000 °C for a 5-hour period. The weight difference is measured to determine the loss of ignition (LOI). Next, the sample is mixed with a bonding admixture (lithium borate and lithium bromide) to melt (1000-1200° C) in a vitreous-grained sample. The sample is then measured by XRF with parameters of 60kV and 66mA. The results are presented in the form of oxides.

Figure 3.9. Look of X-ray fluorescence spectrometer (UdeS).

3.3.1.3. Particle size analysis by laser diffraction

This method is based on the principle of diffraction of light by small particles and provides knowledge of the classification curves for samples containing particles ranging from 0.3 μm to 300 μm, but may cover different size ranges according to the model used.

There are particle analyzers that employ both dry and wet processes. The particle analyzers using dry processes analyze dry powders, but in the wet process, it is necessary that the powder be dispersed in a solvent with ultrasound.

The suspension is pumped to a test cell and is subjected to a laser beam. The beam is diffracted by the suspended particles according to a pattern that is dependent of the particle diameter and the wavelength of the laser

The unit counts the particles by their diameter to show the particle size curve of the suspension. In this way, it is possible to obtain the key parameters de studied powder: mean particle size and the Cumulative slope size, which led a more precise estimation of the cement reactivity, water demand and workability. The used equipment was a Malvern Mastersizer 2000 particle size analyzer.

Figure 3.10. Aspect of Particle size analyzer by laser diffraction (UdeS).

3.3.1.4 Density

Density is defined as the ratio of the mass per unit volume of a solid or particle, excluding voids between particles. This property was determined using a helium pycnometer according to ASTM C 188. The result is usually reported in grams per cubic centimeter (g/cm^3). However, for the design of concrete mixtures it may be more useful to express it as a relative density (also known as specific density). The relative density is a dimensionless value calculated by dividing the density of the sample between the density of the water at 4 °C (1.0 g/cm^3).

Figure 3.11. Appearance of Helium pycnometer (UdeS).

3.3.1.5. Blaine fineness

Fineness determination of the cementitious materials was made following the procedure described in ASTM C 204. This test was carried out by measuring the time it takes to pass a certain volume of air through a sample that is compacted in a cell. Then, the resulting time is compared to the time used to pass a given sample which includes the area of the specific surface known. By checking the density and porosity of these two samples the specific surface area of the target simple is determined.

Figure 3.12. Look of Blaine apparatus (UdeS).

3.3.2 Stage 1. Selection of mineral admixtures.

In this stage the pozzolanic activity of the 4 mineral admixtures options was evaluated by means of the analytic techniques of XRD and thermogravimetric analysis. The XRD technique was described previously in the section 3.3.1.1.

3.3.2.1. Thermogravimetric analysis.

The thermogravimetric analysis (TGA) is a thermal analysis technique which consists of measuring the mass change of a sample as a function of time for a given temperature or temperature profile. From a given cementing material, the hydration water, portlandite content and calcium carbonates of the carbonation or initially contained in the aggregates are quantified.

The equipment used for the thermogravimetric analysis was a TA Instruments SDT Q600 (Figure 3.13). The principle is based on the measurement on the change of mass of the sample as a function of time and temperature. The analysis is performed on hardened pastes previously pulverized by grinding. The pastes are subjected to a temperature rise from 50 °C to 1000 °C at a rate of 10 °C/min under a nitrogen purge (100 ml/min). The data is processed using universal analysis software TA 2000.

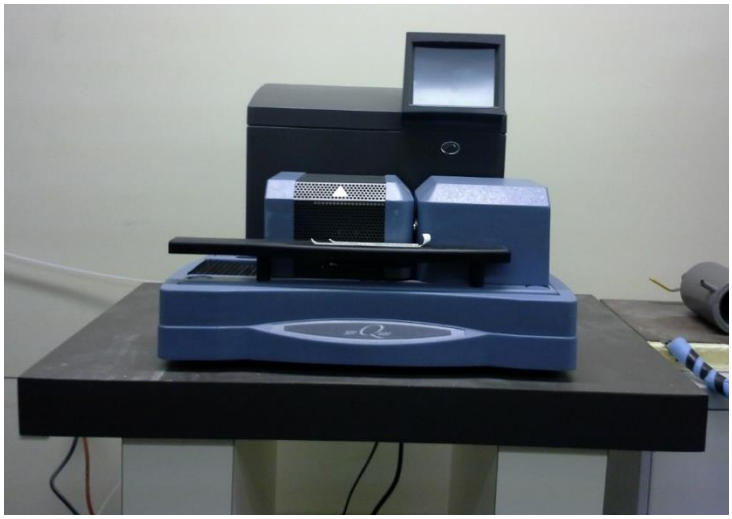

Figure 3.13. Appearance of thermogravimetric Analyzer SDT Q600 (UdeS).

3.3.3 Stage 2. Microstructural analysis.

In order to study the effect of the mineral admixtures on both the microstructure and the physic-mechanical properties of concrete, the three pastes mentioned in Section 3.2.2 were made taking care that the temperature of these pastes was oscillating between 19 and 23 °C according to the procedure described in ASTM C 1738. The following analytical techniques were used: optical and scanning electron microscopy (SEM/EDS) and nanoindentation tests. Details of the test methods are presented below.

3.3.3.1 Scanning Electron Microscope (SEM/EDS).

Scanning Electron Microscopy (SEM) is an electron microscope technique capable of producing high resolution images of a sample surface using the principle of electron-matter interactions.

A very thin electron beam scans the surface sampling point by point, where interactions occur and are detected by a sensor (Figure 3.14). After bombardment, the interactions between the electrons and the atoms composing the material cause several types of emissions, such as: secondary electrons, retro-dispersed electrons and X-rays.

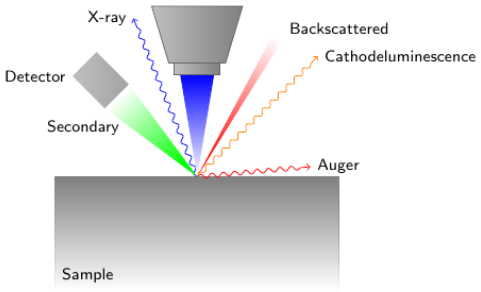

Figure 3.14. Types of emissions associated with the electron beam

The low energy secondary electrons are accelerated to a secondary electron detector that amplifies the signal (in some types of SEM, scattered retro electrons are detected) for each impact point of an electrical signal. The intensity of the electrical signal, which is proportional to the number of electrons detected, depends both on the nature of the sample at the point of impact that determines the performance of secondary electrons and on the topography of the sample at the point considered. In this way, by scanning beam onto the sample a mapping of the scanned area is obtained.

A Hitachi S-3400N scanning electron microscope (Figure 3.15) equipped with an Oxford Inca Energy 250 Energy-Dispersive Spectrometer (EDS) was used for chemical mapping of the regions of interest including nanoindentation grids. The accelerating voltage was set to 12 kV and a magnification of 370X was used to comprise a surface of 300 µm x 210 µm in a single view (the size of a nanoindentation grid). High-quality chemical maps were obtained by averaging 15 frames obtained using a map dwell time of 1024 seconds.

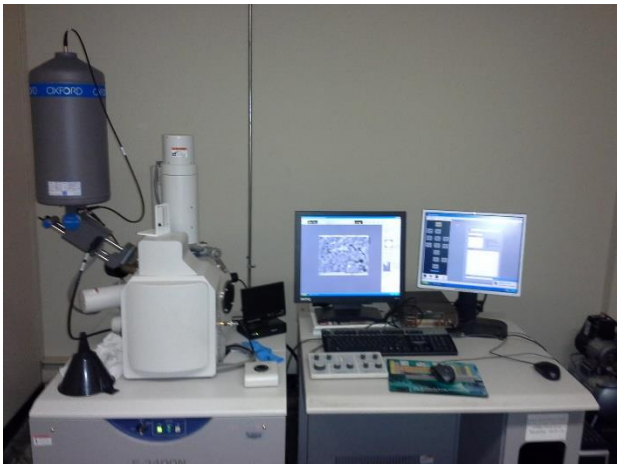

Figure 3.15. Aspect of Hitachi S-3400N scanning electron microscope (UdeS).

3.3.3.2 Nanoindentation test.

The nanoindentation test consists of establishing contact between an indenter and a sample. This test provides a load-depth penetration curve (P-h). From this curve it is obtained the necessary information to determine the indentation modulus M and the indentation hardness H. Figure 3.16 shows a typical load-depth graph of a nanoindentation test, which is initially generated by a constant load increase, followed by a constant fixed load for a given time and finally a constant discharge. M and H are defined as:

$$M = \frac{1}{2}\left(\frac{dp}{dh}\sqrt{\frac{\pi}{A}}\right)\Big|_{h=h_{max}} \quad (1) \qquad M = \frac{1}{2}\left(\frac{dp}{dh}\sqrt{\frac{\pi}{A}}\right)\Big|_{h=h_{max}}$$

$$H = \left(\frac{p}{A}\right)\Big|_{h=h_{max}} \quad (2) \qquad H = \left(\frac{p}{A}\right)\Big|_{h=h_{max}}$$

Where p is the load of indentation, h is the depth of indentation y h_{max} is the maximum depth of indentation. A is the projected contact area and can be extrapolated from the depth h of indentation through the method of Oliver and Pharr (1992 and 2004).

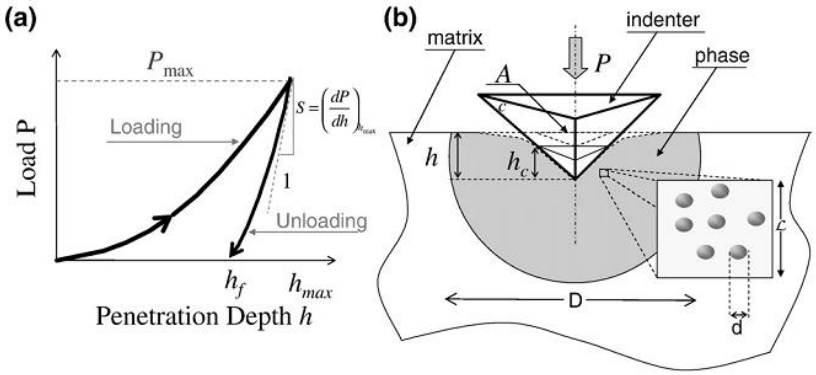

Figure 3.16. a) Typical load-depth curve of a nanoindentation test, b) Schematic representation of a nanoindentation test, adapted from [Sorelli et al., 2008].

Disc-shaped specimens of about 15 mm diameter by about 5 mm thickness were sawed into cement paste samples cured for 90 days in limewater. These specimens were glued on AFM metallic discs and polished with Anamet perforated polishing cloths installed on a Struers automatic polishing machine using diamond oil-based suspensions. A first step of 10 min with a suspension of 15 µm allowed the levelling of the sawed surfaces, which were then polished for 15 min with a 6 µm suspension, followed by two 15 min intervals using a 1 µm suspension. The specimens were cleaned between each step in isopropanol for 3 min using an ultrasonic bath.

For nanoindentation tests, an ultra-nanoindentation meter commercialize by Anton-Paar was used. These tests were developed by William Wilson in Laval University. The indentation tests were performed by controlling the force through a trapezoidal load composed as follows (see figure 3.17a): first loading phase of 30 mN/min, second phase of maintenance of a constant load for 60 seconds and a rapid discharge of 30 mN/Min. The reference contact force was set at 0.2 mN and the indenter contact force was 0.05 mN. The maximum indentation displacement h_{max} was set at 250 nm for constant sampling of micro-volumes in the heterogeneous cement samples.

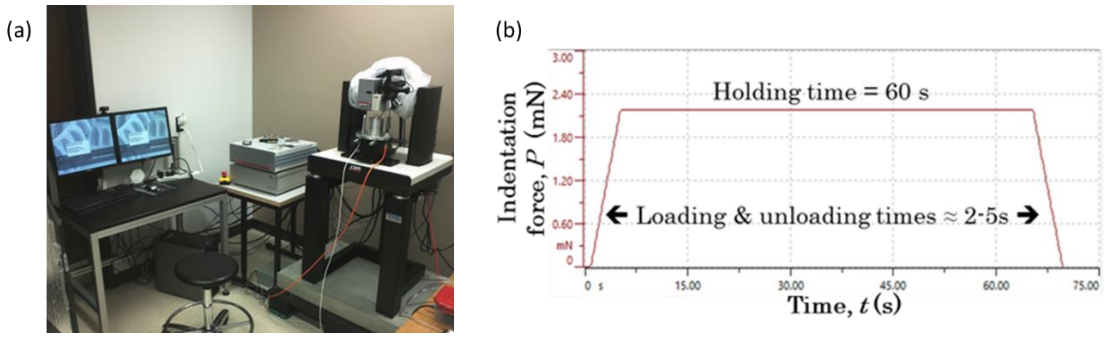

Figure 3.17. a) Appearance of the nanoindentador and accessories and b) controlled force sequence during the test (courtesy of William Wilson).

3.3.4 Stage 3. Concrete fabrication.

3.3.4.1 Fresh state properties.

A conventional concrete mixer with capacity of one sac was used for concrete fabrication. The mixing times were 3 minutes of initial mixing, 3 minutes of rest and 2 minutes of final mixing. At the end of rest period prior to the beginning of the third stage the superplasticizer admixture was added. Following the tests carried out to concrete in fresh and hardened states are presented.

3.3.4.1.1 Slump test.

The slump test was performed immediately upon completion of the concrete mixing, following the procedure described in ASTM C 143.

3.3.4.1.2 Concrete temperature.

During the slump test, concrete temperature was simultaneously measured following the procedure described in ASTM C 1064.

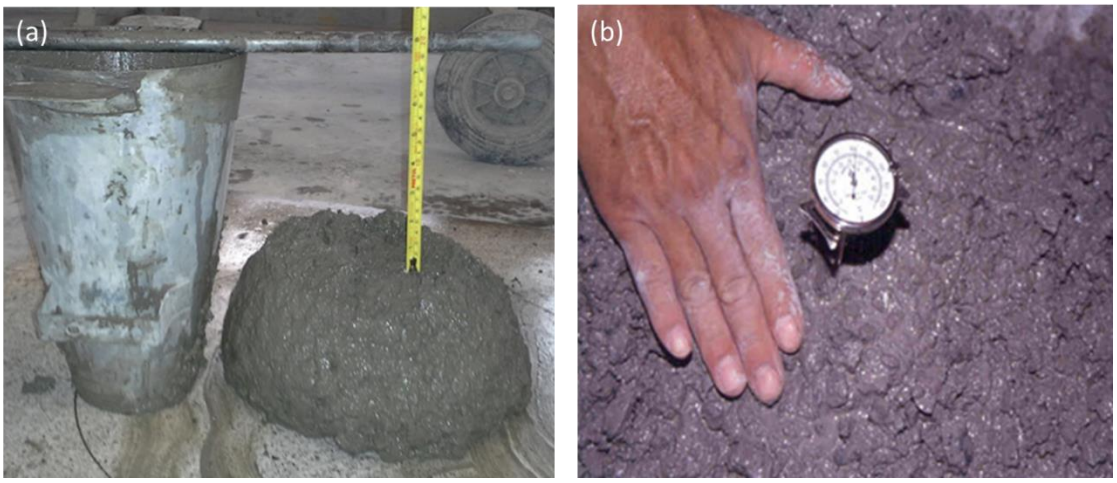

Figure 3.18. a) Slump test and b) measurement of temperature in freshly mixed concrete.

3.3.4.1.3 Air content.

The air content was determined according to Pressure Method Type B according to ASTM C 231. The correction factor for the aggregate with the selected gravel/sand ratios was calculated, resulting in 0.5%. With this value the measurements of the air content for each mixture were corrected.

3.3.4.1.4 Concrete Unit weight.

The unit weight for each mixture was determined following the procedure described in ASTM C 138.

3.3.4.1.5 Setting time.

The setting times of the concretes were determined by penetration resistance according to ASTM C 403 (figure 3.19).

Figure 3.19. Aspect of loading apparatus and penetration needles for setting time tests.

3.3.4.2 Fabrication of specimens and properties of hardened concrete.

For the casting of the specimens, cylindrical steel sheet molds were used according to the procedure described in ASTM C 192. The dimensions of the specimens for the compressive strength and modulus of elasticity tests were 100 mm in diameter by 200 mm in height.

3.3.4.2.1 Compressive strength.

For each mixture, three cylindrical specimens were tested for compression following the procedure outlined in ASTM C 39 at the ages of 3, 7, 28, 56 and 90 days with standard curing until the date of testing as described in ASTM C 511. All specimens were capped according to ASTM C 617. Compressive strength results at 28 and 90 days were taken from the corresponding modulus of elasticity tests.

3.3.4.2.2 Static modulus of elasticity.

For the determination of this property it was followed the established method in ASTM C 469. As well as in the compressive strength tests, all specimens were capped according to ASTM C 617.

Figure 3.20. Compressive strength test (left) and measurement of deformations to determine the modulus of elasticity of concrete (right).

3.3.4.2.3 Chloride migration.

For all mixtures three 100 x 200 mm cylindrical specimens were fabricated in order to determine the migration of chloride ions following the procedure described in the Nordtest NT Build 492 standard. These tests were determined at the ages of 56 and 90 days, during which the specimens received standard curing. For this test a catholyte solution with 10% of NaCl by mass of tap water was prepared (Figure 3.21). The anolyte solution was prepared with 0.3 N NaOH in distilled water (about 12 g NaOH in 1 liter of water). Both solutions were stored in a temperature range of 20 to 25 ºC, and was maintained throughout the test.

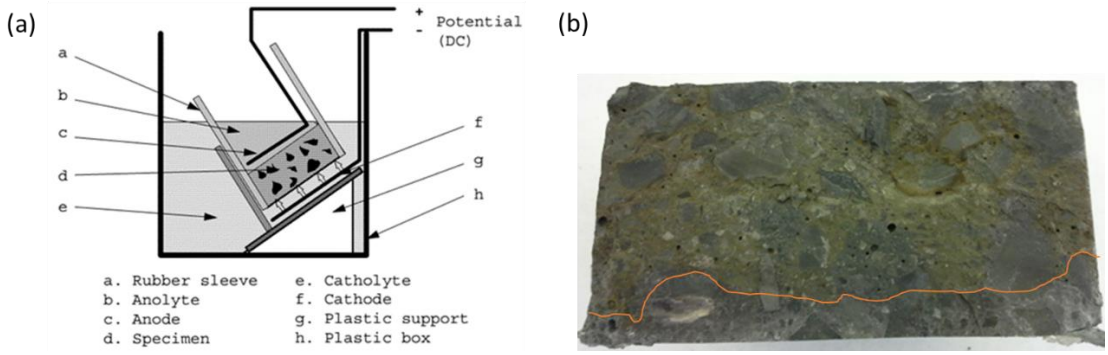

Figure 3.21. a) Proposed arrangement for migration of chlorine ions and b) penetration depth of chlorine ions.

With the following simplified equation proposed in the Nordtest NT Build 492 standard the migration coefficient was calculate:

$$D_{nssm} = \frac{0.0239\,(273+T)L}{(U-2)t}\left(x_d - 0.0238\sqrt{\frac{(273+T)Lx_d}{U-2}}\right)$$

$$D_{nssm} = \frac{0.0239(273+T)L}{(U-2)t}\left(x_d - 0.0238\sqrt{\frac{(273+T)L\,x_d}{U-2}}\right)$$

Where:

D_{nssm}: non-steady-state migration coefficient, $x10^{-12}$ m^2/s;

U: absolute value of the applied voltage, V;

T: average value of the initial and final temperature in the anolyte solution, ºC;

L: thickness of the specimen, mm;

x_d: average value of the penetration depths, mm;

t: test duration, hour.

3.3.4.2.4 Superficial resistivity.

As a durability parameter, the surface electrical resistivity was measured in cylindrical specimens of 100 x 200 mm, for that purpose a PROCEQ Wenner type 4-point resistivity meter was used (Figure 3.22), which has a separation between waves of 38 mm. To perform this test, for each mixture three cylindrical specimens were fabricated and receive a standard curing, the measurement procedure was according to AASHTO TP 95. All measurements were made in the curing room. These results were correlated with chloride ion migration results at 56 and 90 days, additionally, an analysis of their development with respect to the time at the ages of 3, 7, 28, 56 and 90 days was made, during all the measurements the specimens were subject to standard curing.

Figure 3.22. Appearance of PROCEQ Resipod Concrete Resistivity Meter (left) and Surface electrical resistivity measurement (right).

3.3.4.2.5 Carbonation.

For the measurement of the carbonation depth, 50 x 50 x 300 mm prismatic specimens which received standard curing until the age of 56 days were prepared. At the end of curing, the specimens were placed in an accelerated carbonation chamber under the following conditions: temperature of 30 ± 1 ºC, relative humidity of 60 ± 10% and a CO_2 concentration of 10%. The measurements of the carbonation depth were made at 7, 14, 21 and 28 days of CO_2 exposure. For each measurement age, each prism was sectioned to 50 mm in length, the cut was done with the aid of a mallet and a chisel. Later, the sectioned surface was cleaned to remove the dust in it and sprayed with phenolphthalein indicator. Finally, the carbonation depth was recorded as the average of the readings taken on each side of the face to be measured. The rest of the specimen was placed back into the carbonation chamber to continue with the rest of the measurements.

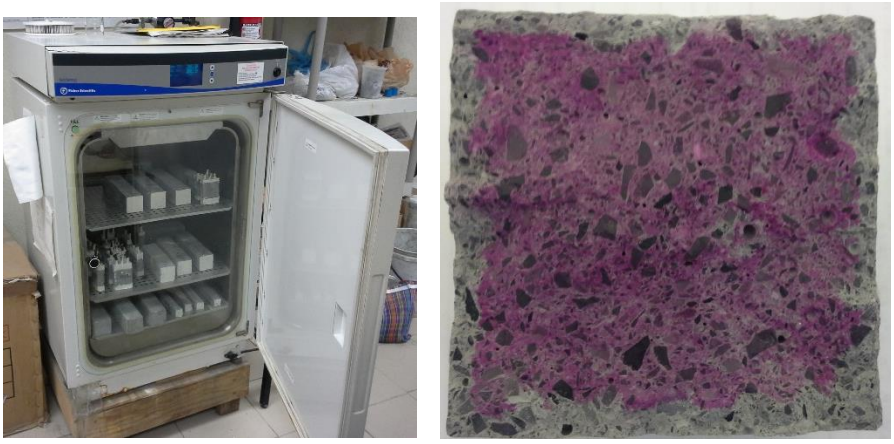

Figure 3.23. Accelerated carbonation chamber (left) and carbonation depth (right).

3.3.4.2.6 Drying shrinkage.

Three prismatic specimens of 75 x 75 x 280 mm were fabricated for each mixture according to ASTM C-157. The initial reading of each specimen was taken one day after its manufacture, later they were put in water saturated with lime until 14 days. At that time their respective readings were taken and placed in the drying and constant evaporation room where readings were taken at 4, 7, 14, 28, 56 and 90 days.

3.3.4.2.7 Percentage of voids in concrete.

Three prismatic specimens of 75 x 75 x 280 mm were fabricated for each mixture and they received standard curing until the age of 90 days as described in ASTM C 511 and the percentage of voids was determined following the procedure described in ASTM C 642.

Chapter 4. Results and discussions.

4.1 Stage 1. Selection of mineral admixtures.

The X-ray diffraction patterns (XRD) of the hydrated pastes are shown in the Figures 4.1 to 4.8. In these figures it can be distinguished the presence of belite (C_2S), Portlandite (CH), calcite ($CaCO_3$), alite (C_3S) and calcium silicate hydrates (C-S-H). Through this technique, the C-S-H compound is difficult to detect because this phase has an amorphous chemical structure (nano-crystalline). However, for this work, its identification was obtained based on previous works [El-Didamony et al., 2014; Abo-El-Enein et al., 2015; Jumate and Manea, 2012]. It is very clear that the peaks of belite and alite decreases with the curing time up to 90 days due to continuous hydration. In the reference pastes with Portland cement, it is evident that the intensity of the portlandite peak increases with the curing time due to the continuous release of portlandite caused by the hydration of alite and belite phases.

The XRD patterns of the pastes with minerals admixtures, exhibit the same hydration products than the reference mixtures, but the intensity of the portlandite peaks tend to decrease because the mineral admixture reacts with the calcium hydroxide and therefore the production of this compound starts to decrease. It can also be seen that as the mineral admixture amount increases, the intensity of the peaks representing the different compounds (belite, portlandita, calcite, alite, and C-S-H) tends to diminish since the clinker is replaced by amorphous cementitious materials, whose reactions are slower.

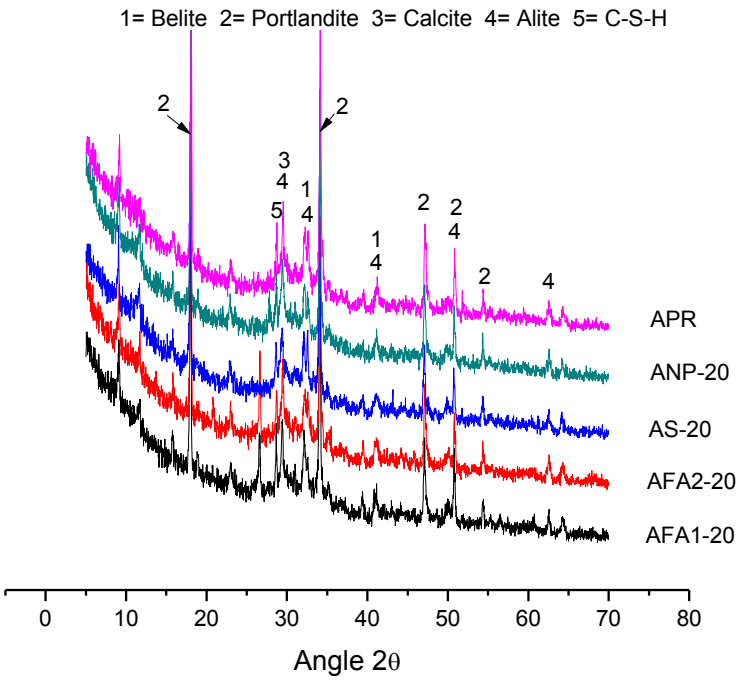

Figure 4.1. XRD patterns of pastes series AP with different Minerals admixtures (dosage 20%) at 28 days.

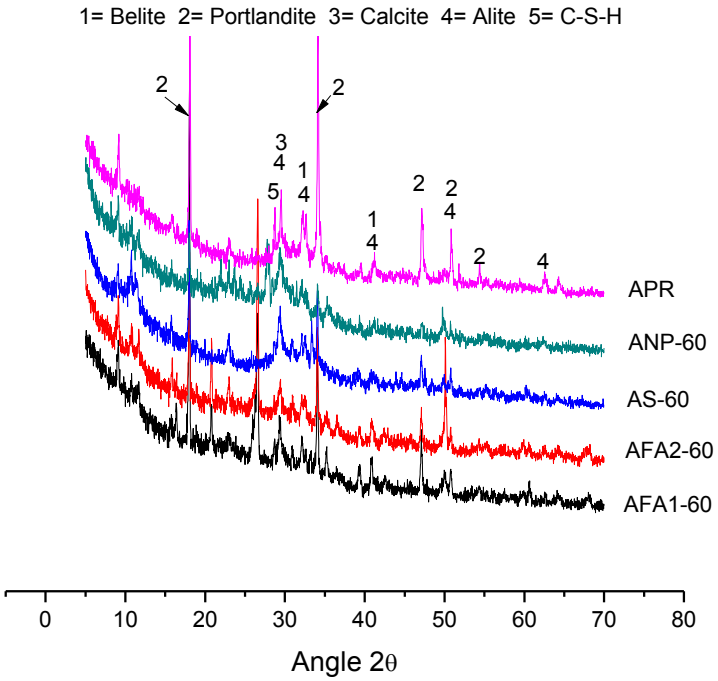

Figure 4.2. XRD patterns of pastes series AP with different Minerals admixtures (dosage 60%) at 28 days.

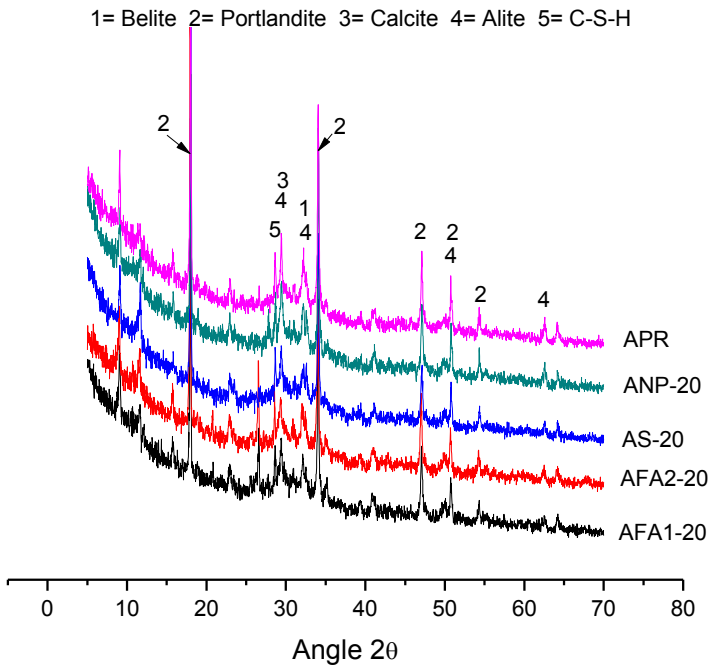

Figure 4.3. XRD patterns of pastes series AP with different Minerals admixtures (dosage 20%) at 90 days.

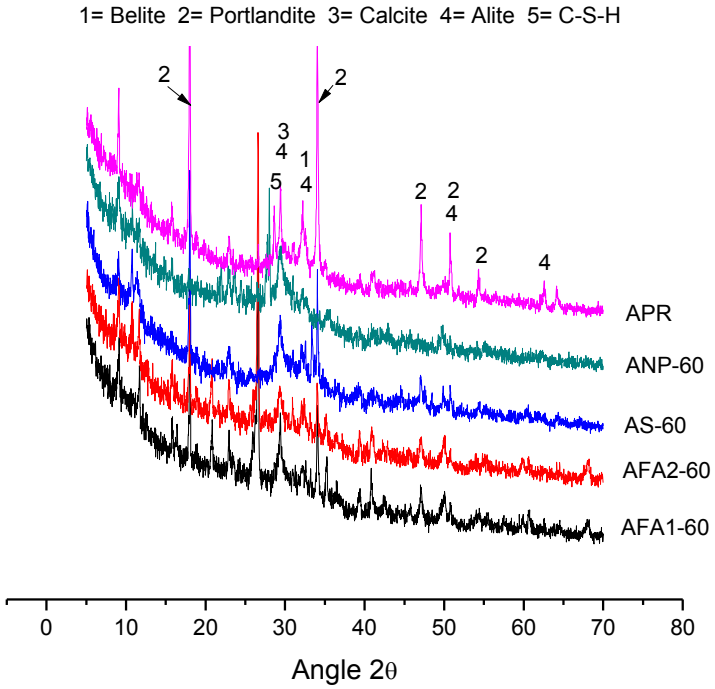

Figure 4.4. XRD patterns of pastes series AP with different Minerals admixtures (dosage 60%) at 90 days.

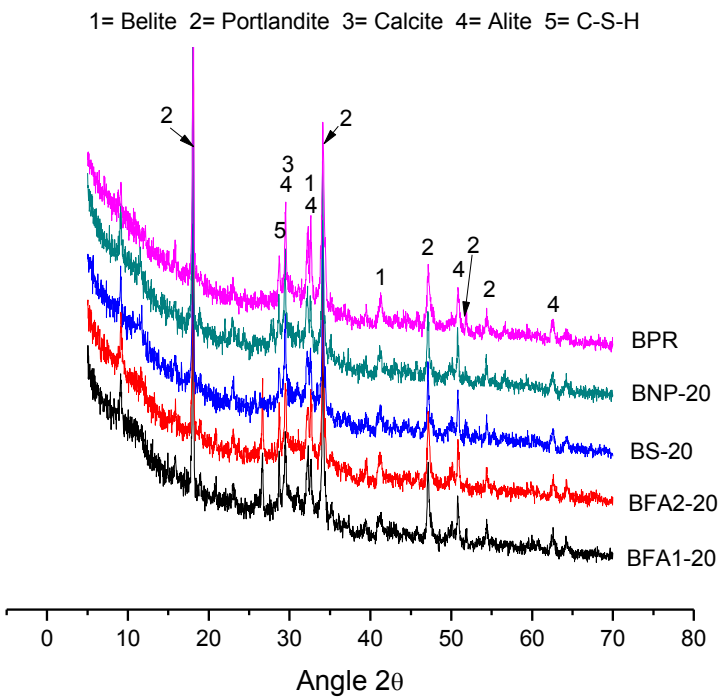

Figure 4.5. XRD patterns of pastes series BP with different Minerals admixtures (dosage 20%) at 28 days.

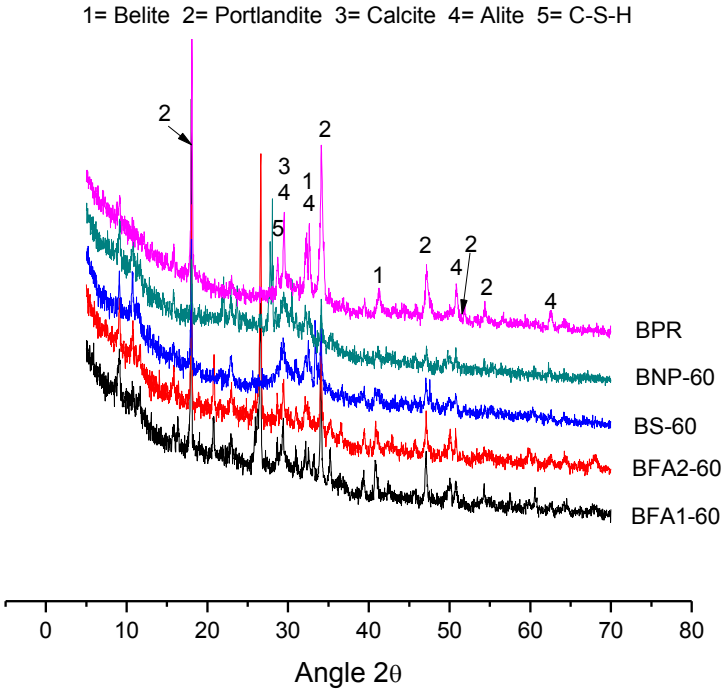

Figure 4.6. XRD patterns of pastes series BP with different Minerals admixtures (dosage 60%) at 28 days.

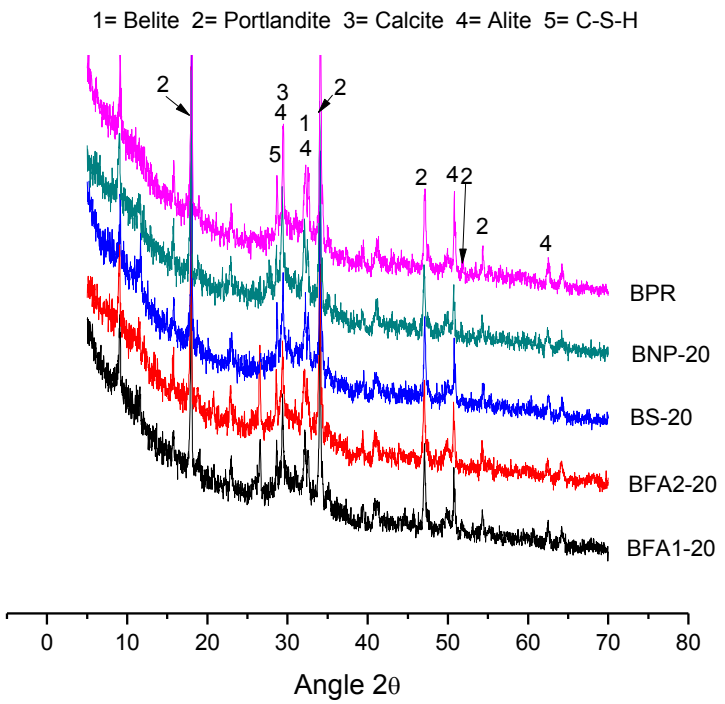

Figure 4.7. XRD patterns of pastes series BP with different Minerals admixtures (dosage 20%) at 90 days.

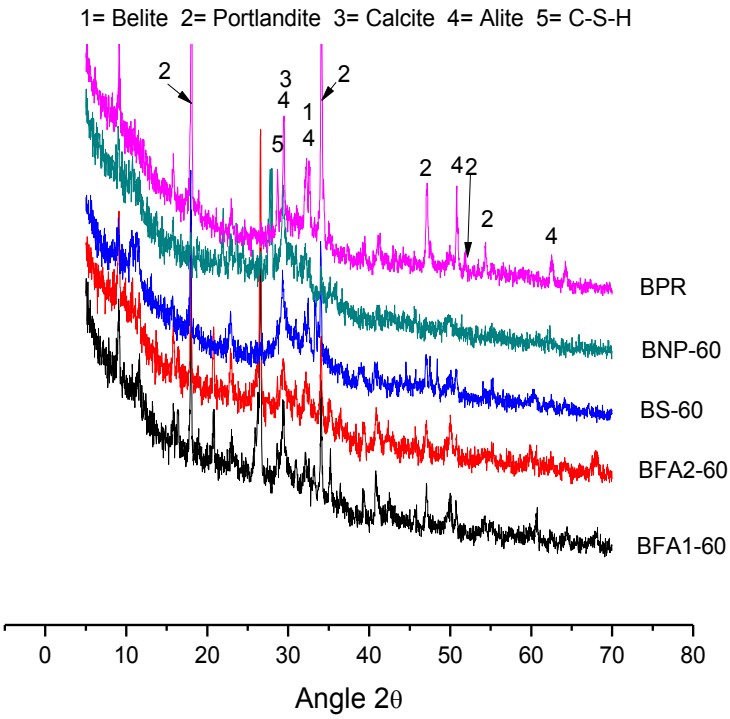

Figure 4.8. XRD patterns of pastes series BP with different Minerals admixtures (dosage 60%) at 90 days.

The CH content in % of the total mass for the pastes produced, was measured by means of a traditional thermogravimetric method. In the Figures 4.9 to 4.12, it can be seen that pastes with mineral additions have a lower portlandite content (CH) than those only consisting of plain cement pastes, and it tends to decrease as the dosage of the mineral admixtures increases, being consistent with their respective diffractograms.

Regarding the influence of the Time (28 to 90 days), in Figures 4.13 to 4.16 it is observed that for the pastes with mineral admixtures of both series (AP and BP), the content of CH decreases with the age of curing due to the pozzolanic effect. For the reference pastes (APR and BPR), the CH content tends to increase with the time, because this hydration product develops as curing progresses.

In Figures 4.17 to 4.20, the effect of W/B ratio can be observed, where it can be seen that as W/B ratio decrease, there is a less CH content, this is because a lower water content reduces the formation of cement hydrates.

Pastes with natural pozzolan resulted with a lower CH content because the fineness of this material contributes to a more efficient heterogeneous nucleation, which improves the hydration rate of cement [Deboucha et al., 2017], in this regard, the rest of mineral admixtures have a particle size distribution similar to Portland cement, which leads to a less efficient nucleation [Berodier and Scrivener, 2014 and Lawrence et al., 2003], where the FA1 pastes (Series AP and BP) resulted with higher CH contents, which reflects a lower reactivity.

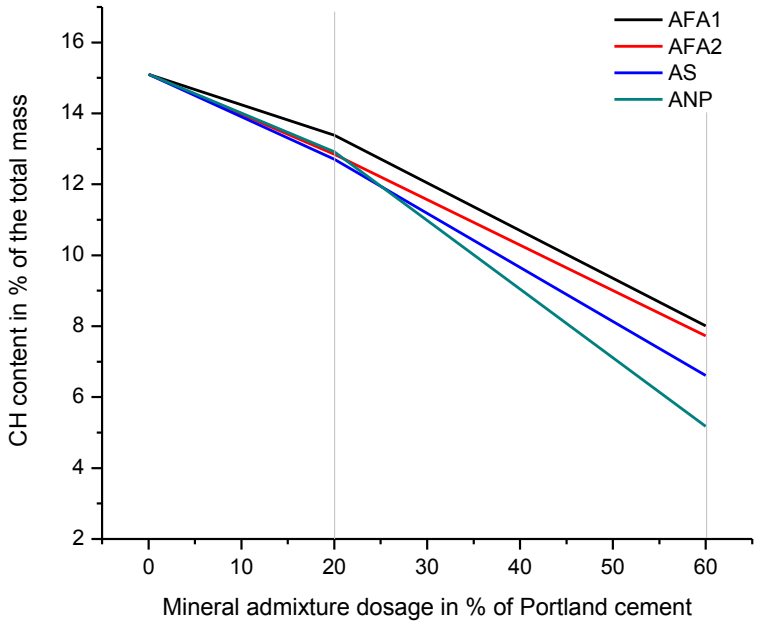

Figure 4.9. Mineral admixture dosage vs. CH content for series AP at 28 days.

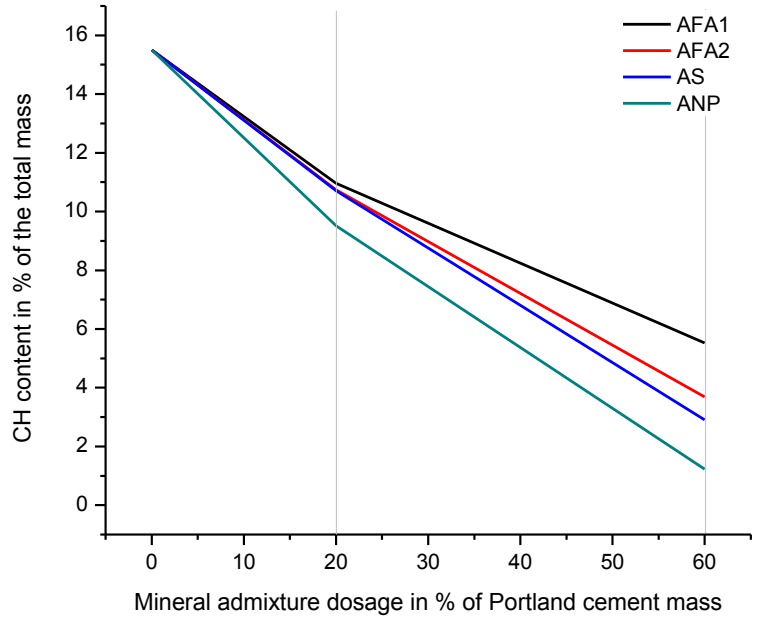

Figure 4.10. Mineral admixture dosage vs. CH content for series AP at 90 days.

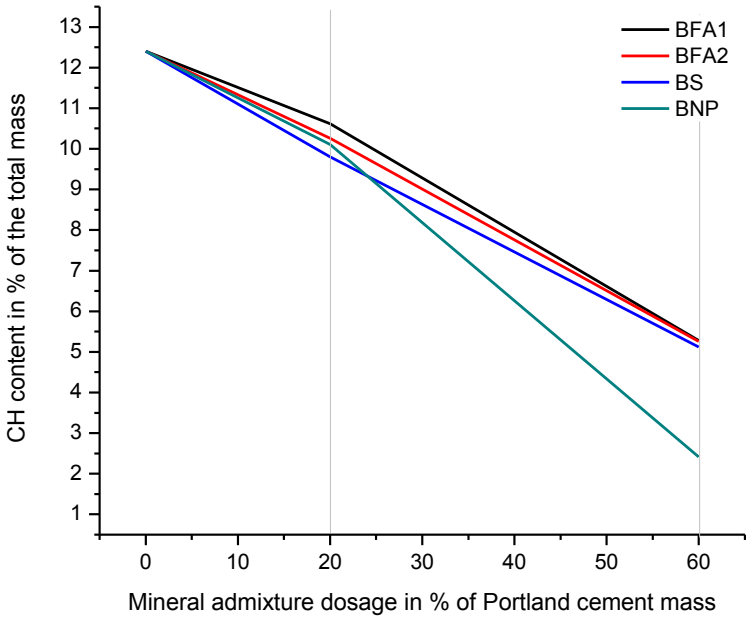

Figure 4.11. Mineral admixture dosage vs. CH content for series BP at 28 days.

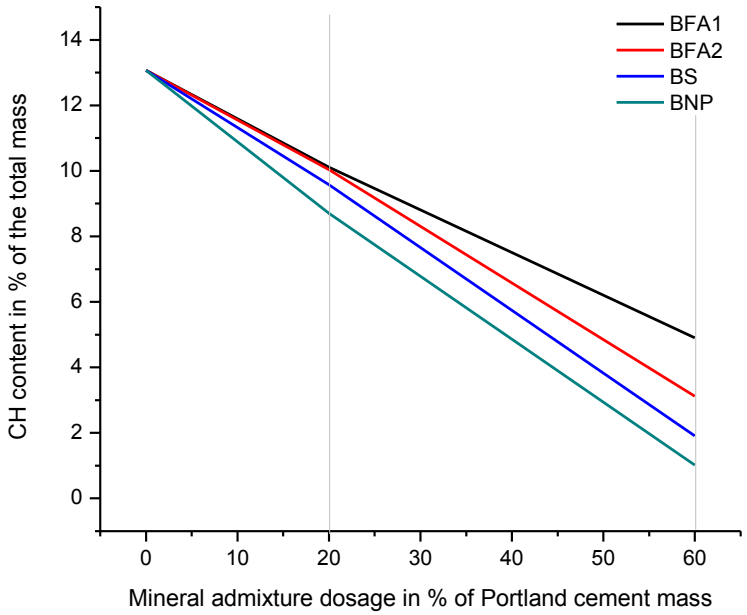

Figure 4.12. Mineral admixture dosage vs. CH content for series BP at 90 days

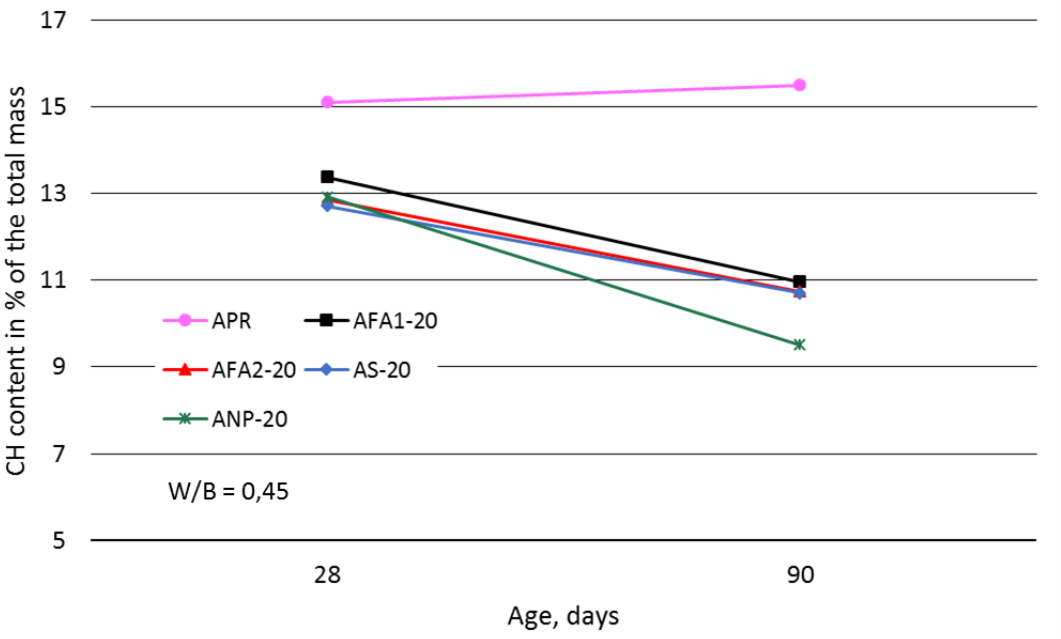

Figure 4.13. Effect of the time on CH content for Series AP with mineral admixtures dosages of 20%.

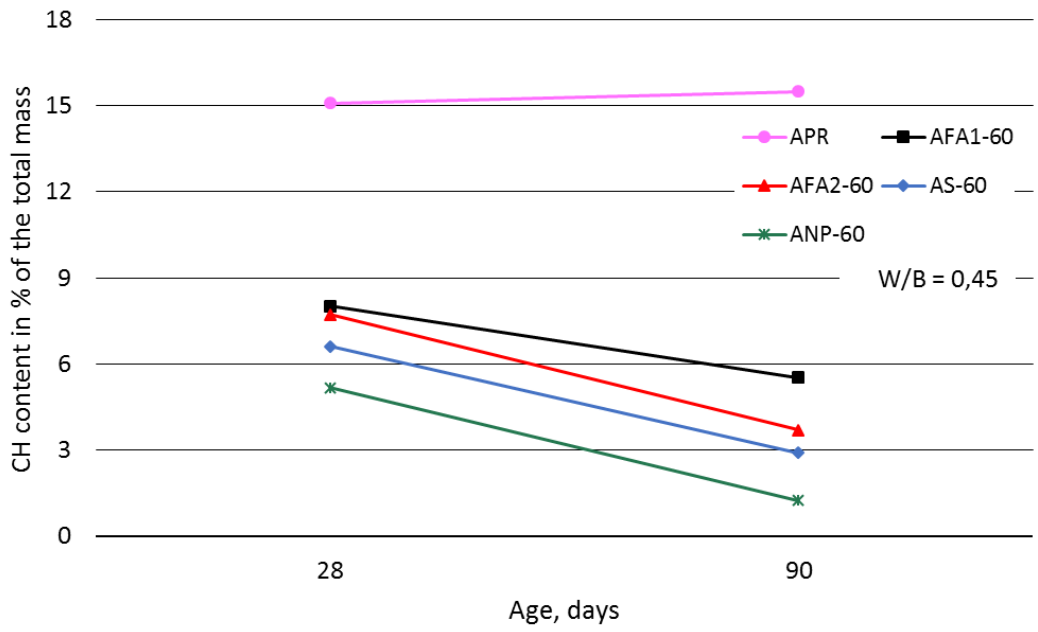

Figure 4.14. Effect of the time on CH content for Series AP with mineral admixtures dosages of 60%.

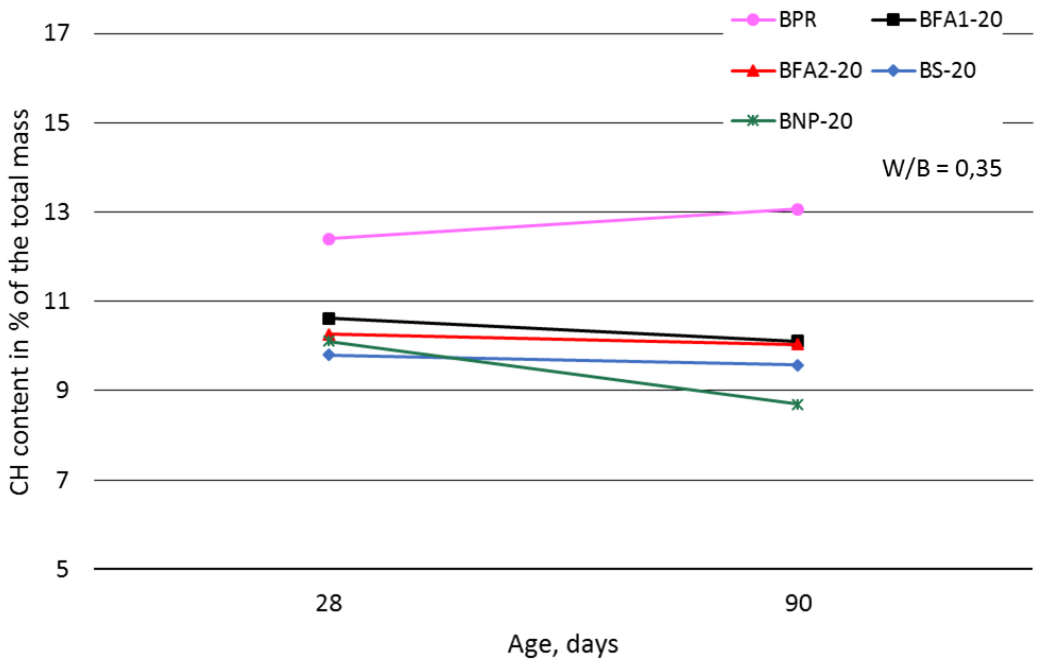

Figure 4.15. Effect of the time on CH content for Series BP with mineral admixtures dosages of 20%.

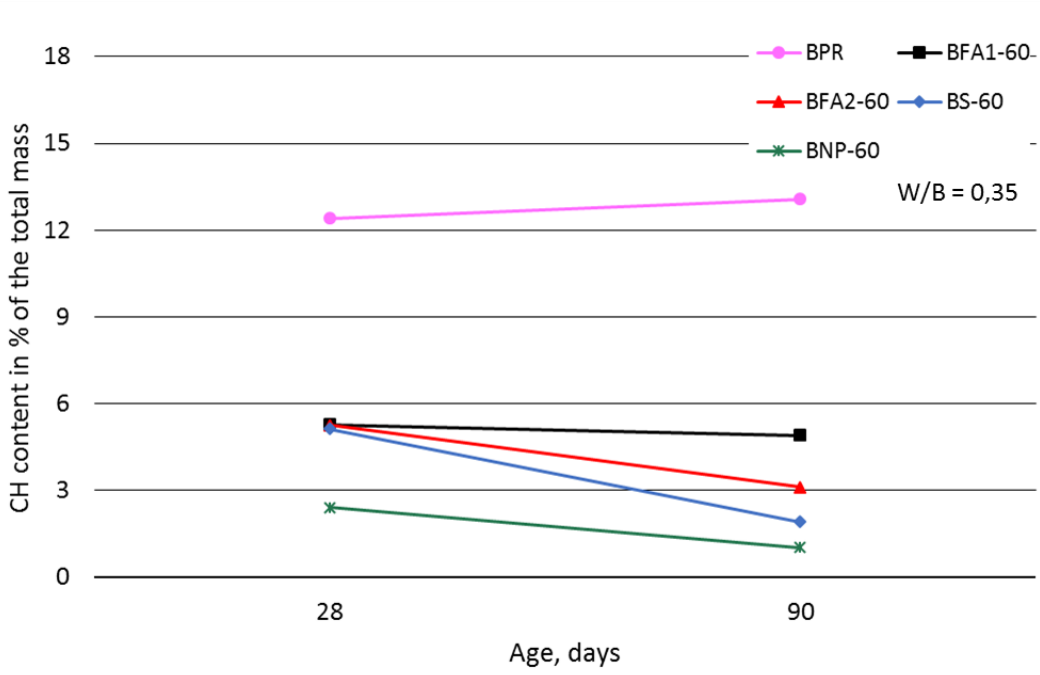

Figure 4.16. Effect of the time on CH content for Series BP with mineral admixtures dosages of 60%.

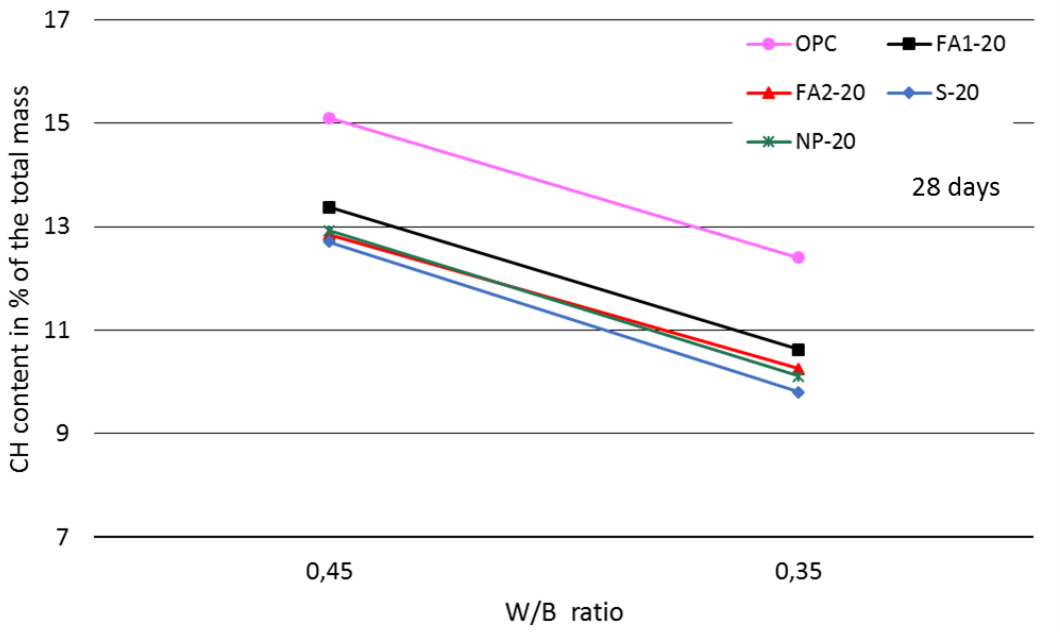

Figure 4.17. Effect of W/B ratio on CH content for pastes with mineral admixtures dosages of 20% (28 days).

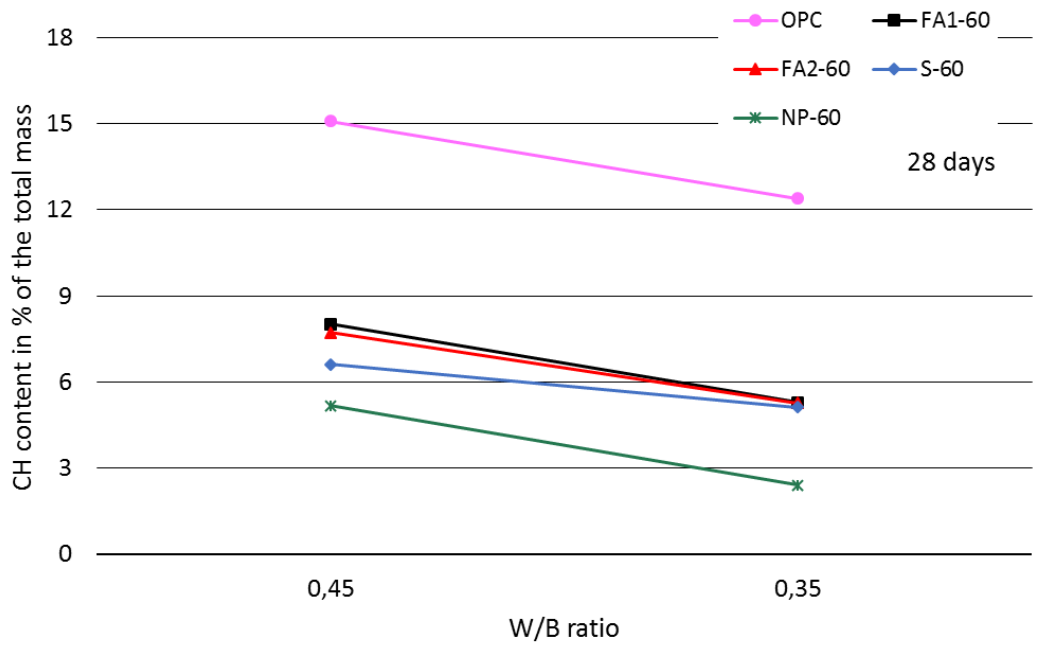

Figure 4.18. Effect of W/B ratio on CH content for pastes with mineral admixtures dosages of 60% (28 days).

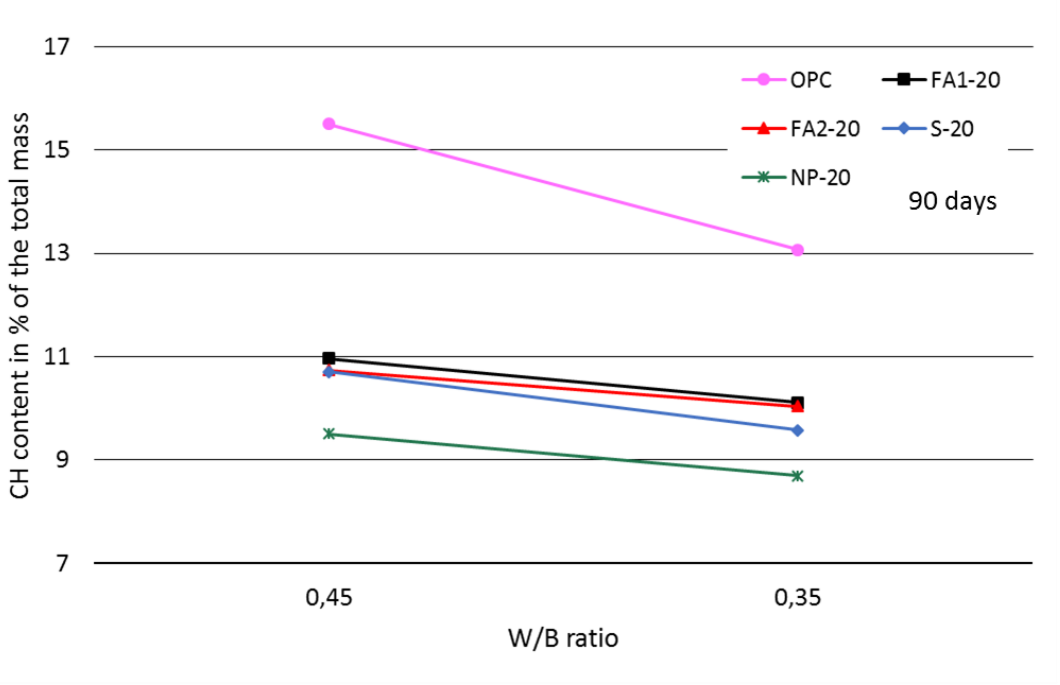

Figure 4.19. Effect of W/B ratio on CH content for pastes with mineral admixtures dosages of 20% (90 days).

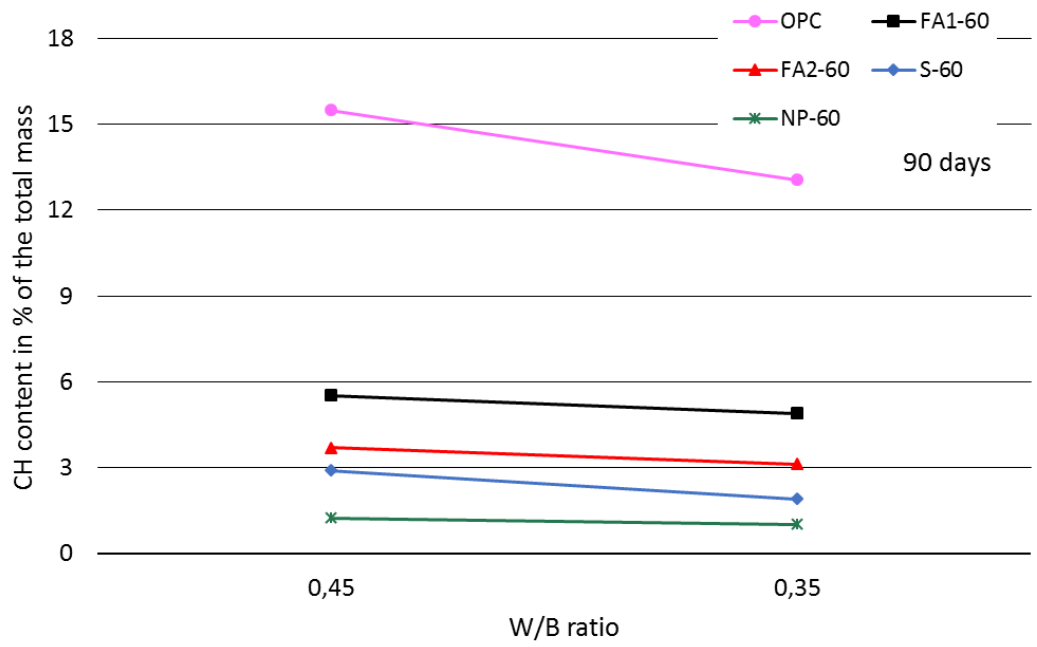

Figure 4.20. Effect of W/B ratio on CH content for pastes with mineral admixtures dosages of 60% (90 days).

In the Tables 4.1 and 4.2 the compressive strengths of the mortars produced in this stage are presented; it can be seen that the mortars containing the natural pozzolan exhibited the highest strengths; having strengths similar to those of their respective references with a content of 20% of NP at 56 days of the W/B = 0,45 and at 28 day for the W/B = 0,35. The mortars containing 60% of the NP in the series AM (W/B ratio = 0,45) obtained strength values of 81% and 86% of the strength of the reference mixture at 56 and 90 days respectively, while mortars of the series BM (W/B ratio = 0,35) obtained strengths of 83% and 92% of the strength of the reference mixture at 56 and 90 days respectively.

Table 4.1. Compressive strength of mortars for series AM (W/B = 0,45)

Mortars ID	Strength, MPa			
	7 days	28 day	56 days	90 days
AMR	42,8	51,7	52,3	53,2
AMFA1-20	34,8	41,1	46,8	50,0
AMFA2-20	30,0	39,2	41,5	45,7
AMS-20	42,9	46,6	49,2	50,7
AMNP-20	33,6	44,0	52,2	53,0
AMFA1-60	9,1	14,5	17,7	21,0
AMFA2-60	9,7	16,3	22,0	25,0
AMS-60	24,2	33,1	36,3	36,9
AMNP-60	17,6	32,2	42,4	45,6

Table 4.2. Compressive strength of mortars for series BM (W/B = 0,35)

Mortars ID	Strength, MPa			
	7 days	28 day	56 days	90 days
BMR	53,7	58,6	69,0	69,9
BMFA1-20	42,4	51,7	56,7	60,3
BMFA2-20	41,7	49,5	57,2	63,9
BMS-20	44,8	58,8	52,6	68,5
BMNP-20	46,1	58,9	63,8	71,1
BMFA1-60	9,5	15,4	21,3	22,5
BMFA2-60	13,4	22,7	31,0	33,4
BMS-60	36,6	48,2	55,6	58,5
BMNP-60	28,2	49,2	57,3	64,4

NP mortars exhibited the highest compressive strength and the mortars which exhibited the lowest compressive strength values were those containing the FA1 and FA2. According to the experimental program described in Chapter 3, the NP and the FA1 will be the mineral admixtures selected to continue with the Stage 2 of the experimental program, which will consist of microstructural analyses, as well as the Stage 3, corresponding to the physical characterization and performance of concrete mixtures produced with the aforementioned selected mineral additions. Further in this document, FA1 will be referred to only as FA, for simplification purposes.

4.2 Stage 2. Microstructural analysis of OPC pastes containing NP.

As mentioned in Chapter 3, the microstructural analysis were performed only on reproduced pastes from concretes BR, B20NP and B60NP with water/binder ratio of 0,35, which were identified as OPC system, B20NP system and B60NP system respectively. The nanoindentation tests were performed at 90 days, during this time the paste specimens were cured in limewater. The results are presented below.

4.2.1 Nanoindentation tests results.

The identifications of the clusters (predominant phases) of the systems OPC, B20NP and B60NP were made based on the micro-mechanical properties reported in previous works (Constantinides and Ulm, 2007 and Abuhaikal, 2011). The results of the statistical analysis of nanoindentations tests corresponding to the OPC system are reported in the Figure 4.21; in this figure, four clusters are distinguished, in which, cluster 1 could correspond to high density (HD) C-S-H phase, in relation to cluster 2, it is thought to be the C-S-H structure called by some authors as ultra-high density (UHD) [Vandamme et al., 2010 and Sorelli et al., 2008] or may it corresponds to nanoindentations performed on the boundaries between C-S-H and clinker or CH, thus may having properties in between these two materials. Cluster 3 appears to correspond to the low density (LD) C-S-H phase and cluster 4 represents anhydrous material.

Referring to the predominant phases detected in the OPC system, the total volume of the C-S-H phase could be around 87%, in which, 30% corresponds to HD C-S-H, 57% to LD C-S-H and 13% to UHD C-S-H.

Cluster	ID	μ_H (GPa)	μ_M (GPa)	π (%)
1	HD C-S-H?	1.2	36.8	26
2	Mix	2.2	53.9	11
3	LD C-S-H?	0.8	27.7	50
4	Anhydrous Part.	7.8	113.7	13

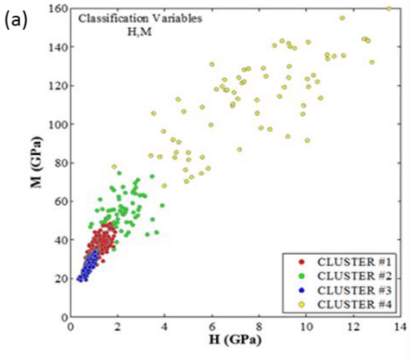

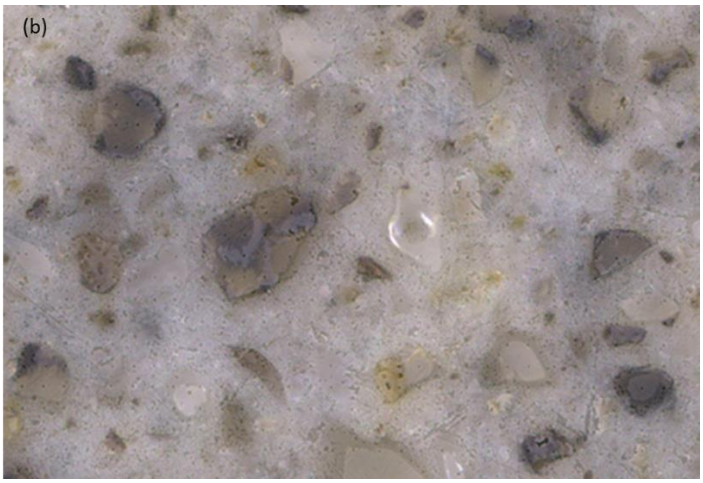

Figure 4.21. Results of statistical nanoindentation tests for OPC system: average indentation hardness (μ_H), modulus (μ_M) and volume fraction (π). a) Cluster repartitions in the representation of indentation hardness (H) vs. indentation modulus (M) and b) Optical micrograph.

For the system B20NP, Four clusters were also detected (see Figure 4.22); where, cluster 1 corresponds to the anhydrous material, cluster 2 could correspond to the structure UHD C-S-H or a mixture of results of the structure C-S-H and clinker or CH, cluster 3 it is suggested to be the LD C-S-H structure and HD C-S-H for the cluster 4. The detected volume fraction of the C-S-H structure could be around 90%, corresponding to 11% to UHD C-S-H, 63% of LD C-S-H and 26% of HD C-S-H.

Furthermore; in the Figure 4.22a, it is distinguishes a tendency to decrease the indentation values of modulus and hardness and, on the other hand, an increase in the formation of C-S-H with respect to the OPC system seems.

Cluster	ID	μ_H (GPa)	μ_M (GPa)	π (%)
1	Anhydrous Pat.	7.8	83.8	11
2	Mix	2.7	55.4	10
3	LD C-S-H?	0.7	25.9	57
4	HD C-S-H?	1.2	24.2	23

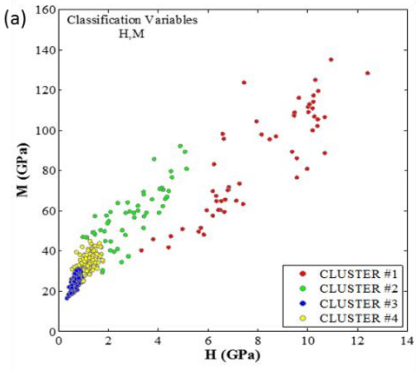

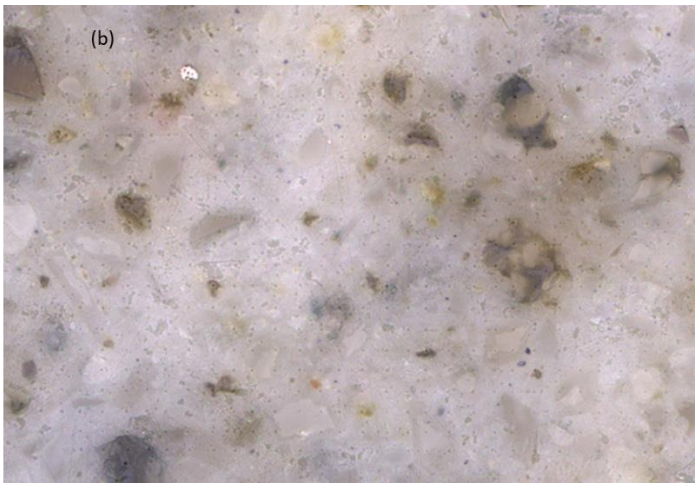

Figure 4.22 Results of statistical nanoindentation tests for B20NP system: average indentation hardness (μ_H), modulus (μ_M) and volume fraction (π). a) Cluster repartitions in the representation of indentation hardness (H) vs. indentation modulus (M) and b) Optical micrograph.

With respect to the statistical analysis of the nanoindentation tests carried out in the B60NP system, the results are presented in Figure 4.23 and reveal the formation of six clusters, this suggests that there is a significant change in the microstructure of cementitious matrix due to the large dosage of natural pozzolan, which is greater than Portland cement. Cluster 1 is identified as LD C-S-H, cluster 2 could be a mixture of micro-mechanical properties of C-S-H and particles of NP. Likewise, the cluster 3 could correspond to the HD C-S-H phase, cluster 4

may correspond to clinker or a mixture of clinker and NP, cluster 5 is identified as NP particles and cluster 6 corresponds to clinker.

For this system, the volume fraction of C-S-H is around 73%, corresponding to 11% of UHD C-S-H structure, 60% of LD C-S-H and 29% of HD C-S-H. This indicates that the products of hydration tend to decrease when increasing the dosage of NP, on the other hand for this system there is an increase of anhydrous material because not all the NP reacts. Because the indentation values of modulus and hardness of the NP particles are greater than those shown by the C-S-H structure, this suggests that could be the reason that the concrete with high NP contents does not present a significant detriment in their mechanical properties regarding plain Portland cement concrete.

Cluster	ID	μ_H (GPa)	μ_M (GPa)	π (%)
1	LD C-S-H?	0.6	22.9	44
2	Mix	1.7	36.8	15
3	HD C-S-H?	0.9	28.2	21
4	Clinker	3.1	70.3	3
5	Pozzolan Part.	5.4	52.8	16
6	Clinker	10.8	126.0	2

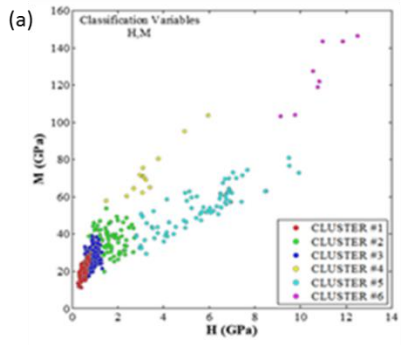

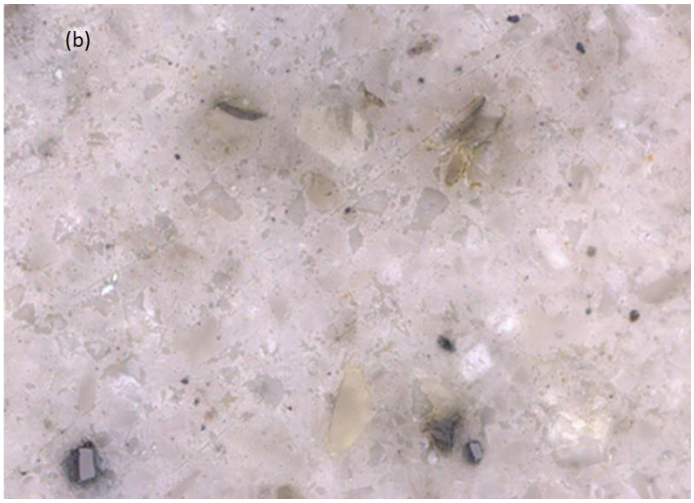

Figure 4.23. Results of statistical nanoindentation tests for B60NP system: average indentation hardness (μ_H), modulus (μ_M) and volume fraction (π). a) Cluster repartitions in the representation of indentation hardness (H) vs. indentation modulus (M) and b) Optical micrograph.

The results presented in figure 4.23 shows that the indentation values of modulus and hardness tend to decrease even more than the 20NP and OPC systems. Large quantities of natural pozzolan bring large amounts of aluminum, so this affects the type of hydration products that are formed. This suggests that aluminum could influence the decrease of the performances of the micro-mechanical properties of the cementitious matrix. So the interpretation of HD and

LD C-S-H should be considered carefully (as other hydrates may be included in the clusters 1 and 3). Now the nanoindentation results are analyzed in combination with chemical analysis (EDS). This analysis was carried out by William Wilson under the supervision of the Professors Luca Sorelli and Arezki Tagnit-Hamou.

4.2.2 Chemical-mechanical statistical analysis.

The chemical composition of the indents of the three cementitious systems (OPC, B20NP and B60NP) were analyzed by using energy dispersive spectroscopy coupled with scanning electron microscopy (SEM-EDS). From the elementary chemical maps of Silicon (Si), Calcium (Ca) and Aluminum (Al), the composite chemical maps of each system were obtained and then proceed to obtain the qualitative chemistry of each indent. The statistical analysis of the nanoindentation tests in conjunction with the chemical analysis of composite maps (SNI-EDS), allows the study of the mechanical properties of the identified phases including their chemical compositions, relative contents and distribution in the cementitious matrix. Next, the analysis of the plain Portland cement paste (OPC system) and the pastes with incorporations of 20% and 60% of NP (systems B20NP and B60NP respectively) are presented. The results presented here, are a part of the results from the paper "*The micromechanical signature of high-volume natural pozzolan concrete by combined statistical nanoindentation and SEM-EDS analyses"* [91 (2017) 1-12] published in Cement and Concrete Research Journal.

4.2.2.1 Plain Portland cement paste (OPC system).

The results of the SNI-EDS analysis of the OPC system are shown in Figures 4.24 and Table 4.11 detecting 8 clusters. Figure 4.24a shows the representation of the results in the dimensions of I_{Ca} vs. I_{Si}, and the Figure 4.24b shows the results of indentations modulus vs. indentation hardness. The predominant phases of each detected cluster are described below.

Cluster 1 contains the largest fraction of data points representing the C-S-H phase. Cluster 4 represents a mixture of C-S-H and CH (I_{Si} = 0, I_{Ca} = 0.8); this suggests that there is intermix between these two phases. Such intermixing between phases occurs when the volume tested by a single indent is not in a single phase but includes more than one phase. In the same way, the clusters 3 and 5 is a mix of C-S-H, AFm+AFt and calcium carbonate (CC) phases respectively. Cluster 2 includes C-S-H and CH. Cluster 6 represents intermixes of clinker and

C-S-H. Finally, the clusters 7 and 8 represent non-hydrated phases, which consist of silicates (C_3S and C_2S) and aluminous phases (C_3A and C_4AF), respectively. Probably the aluminous phases of the clinker are intermixed with silicates.

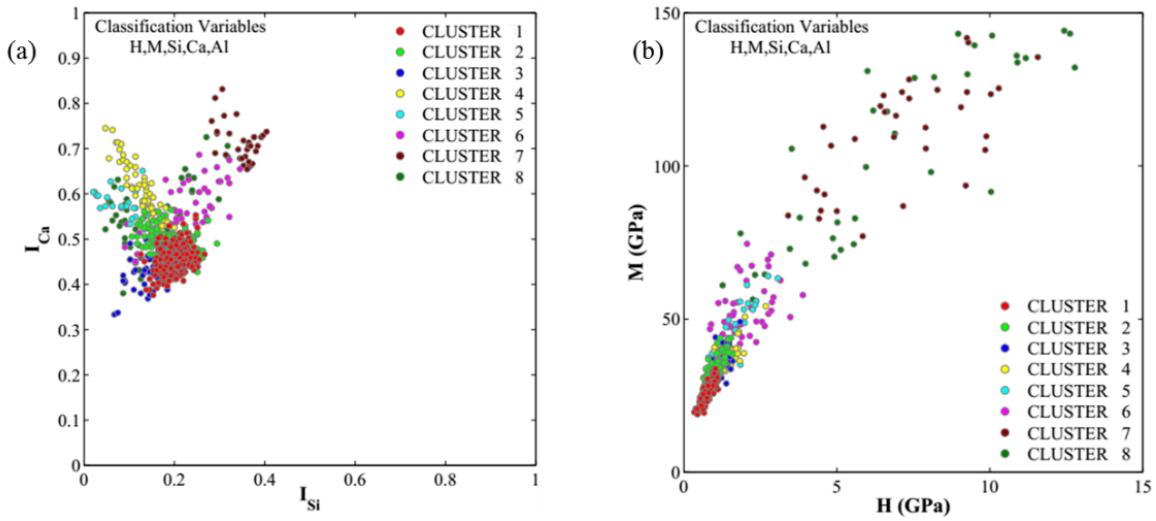

Figure 4.24. a) Representation of relative intensities of calcium (I_{Ca}) and silicon (I_{Si}) for data points of OPC system after SNI-EDS analyses. b) Results of SNI-EDS analyses for system OPC represented by indentations modulus (M) vs. indentation hardness (H).

The mechanical properties of the clusters identified in Figure 4.24b are reported in Table 4.3. The values of μ_M and μ_H of cluster 1 correspond to the structure of C-S-H, which are consistent with the average values reported in previous studies between C-S-H low-density ($\mu_M \approx 21{,}4$ GPa and $\mu_H \approx 0{,}7$ GPa) and C-S-H high-density ($\mu_M \approx 31{,}4$ GPa and $\mu_H \approx 1{,}2$ GPa) [Constantinides and Ulm, 2007; Krakowiak et al., 2015; Chen et al., 2010; Ulm et al., 2007; Davydov et al., 2011; Zhu et al., 2007]. However, the chemo-mechanical clustering of the information obtained from the points tested does not allow distinguishing these two types of C-S-H. Nonetheless, the predominant phases of clusters 2, 3 and 4 showed values of $\mu_M \approx 34 \pm 6$ GPa and $\mu_H \approx 1{,}1 \pm 0{,}3$ GPa. Similarly, the predominant phases of clusters 5 and 6 are similar to the values of C-S-H ultra-high-density reported by Vandamme et al. (2010). Finally, clusters 7 and 8 presented the highest values of modulus and hardness ($\mu_M \approx 106 \pm 40$ GPa and $\mu_H \approx 7{,}1 \pm 4$ GPa). These results are consistent with the values reported by Vélez et al. (2001) corresponding to pure clinker phases. Generally, values greater than 65 GPa for modulus and

greater than 3 GPa for hardness are considered to come from micro-volumes composed in their great majority of clinker phases. [Abuhaikal, 2011; Pellenq et al, 2009 and Ulm et al, 2010].

Table 4.3 provides the average chemical intensities (I_{Si}, I_{Ca} and I_{Al}) along with an estimate of the volume fraction (π) for each cluster. Because a cluster may consist of more than one phase, the volume estimation of each phase was carried out using a simple first-order method; where the points of intermix in the clusters were distributed equally between their predominant phases (e.g. cluster #2 is separated into 10% C-S-H and 10% CH). This assumption leads to an approximate composition of the microstructure for OPC system: around 61% C-S-H, 17% clinker particles, 15% Portlandite and 7% AFm+AFt and calcite.

Table 4.3. Results of SNI-EDS analyses of the OPC system: average indentation hardness (μ_H), modulus (μ_M) and volume fractions (π) for clusters of datapoints attributed to their predominant phases.

Cluster	Predominant Phase(s)	μ_H (GPa)	μ_M (GPa)	I_{Si}	I_{Ca}	I_{Al}	π (%)
1	C-S-H	0,8 ± 0,1	27 ± 3	0,20 ± 0,03	0,46 ± 0,03	0,13 ± 0,02	35
2	C-S-H + CH	1,0 ± 0,2	33 ± 4	0,19 ± 0,04	0,49 ± 0,03	0,13 ± 0,02	20
3	AFm+AFt + C-S-H	1,1 ± 0,3	34 ± 6	0,15 ± 0,04	0,44 ± 0,04	0,22 ± 0,06	9
4	CH + C-S-H	1,2 ± 0,4	35 ± 6	0,13 ± 0,04	0,60 ± 0,06	0,10 ± 0,01	10
5	CC + C-S-H	1,6 ± 0,6	44 ± 11	0,10 ± 0,04	0,57 ± 0,03	0,10 ± 0,03	5
6	Clinker + C-S-H	2,0 ± 0,7	53 ± 9	0,23 ± 0,07	0,57 ± 0,06	0,16 ± 0,05	8
7	Clinker (silicates)	7,1 ± 2,2	110 ± 18	0,35 ± 0,03	0,71 ± 0,04	0,13 ± 0,02	6
8	Clinker (Al-rich)	7,1 ± 4,0	106 ± 40	0,14 ± 0,07	0,55 ± 0,08	0,46 ± 0,19	8

4.2.2.2 Paste with 20% Portland cement replacement by natural pozzolan (B20NP system).

The replacement of 20% of Portland cement by NP has a significant effect on the SNI-EDS results because this material has high content of Aluminum and Silicon content as shown in Figure 4.25, and Table 4.4, where, cluster 1 contains the largest fraction of data points belonging to the C-S-H and C-A-S-H phases, which are represented by the acronym C-(A)-S-H. Clusters 2 is composed of AFm+AFt and C-A-S-H intermix, cluster 3 includes Portlandite, C-(A)-S-H and NP particles. In relation cluster 4, Figures 4.25a and 4.25b Illustrate the presence of NP particles, since an important dispersion is observed due to the different types of NP detected. Finally, the predominant phases of clusters 5 and 6 are constituted by clinker composed by aluminum and silicates respectively.

The mechanical properties of B20NP system are presented in Figure 4.25 and Table 4.4; in which, the modulus and hardness of cluster 1 exhibited lower values than C-S-H phase (OPC system), this suggest that the inclusion of aluminum in the C-S-H structure [Lothenbach et al, 2011 L'Hôpital et al, 2015 and L'Hôpital, 2016] weakness these properties. On the other hand, the AFm+AFt phases and NP particles, which are intermixed in the predominant phase C-(A)-S-H (Clusters 2, 3 and 4), as well as the clinker particles (clusters 5 and 6) contribute to the mechanical properties of the paste (B20NP system). Following the same assumption of the OPC system, the analysis of the results in Table 4.4 provides the following approximative repartition of phases in B20NP system: around 56% C-(A)-S-H, 14% Portlandite, 12% clinker particles and 8% AFm+AFt.

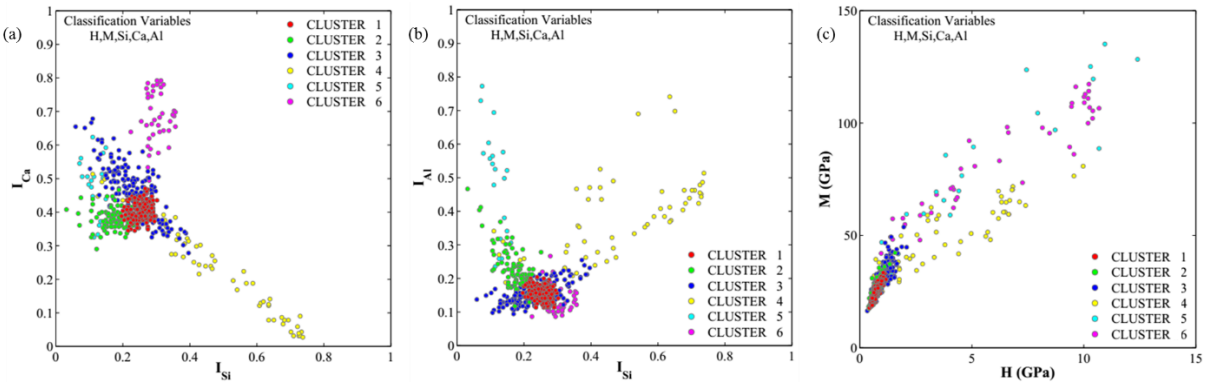

Figure 4.25. Results of SNI-EDS analyses for B20NP system, as represented into three different axes: a) I_{Ca}, vs. I_{Si}, b) I_{Al} vs. I_{Si} and c) M vs. H.

Table 4.4. Results of SNI-EDS analyses of the B20NP system: average indentation hardness (μ_H), modulus (μ_M) and volume fractions (π) for clusters of datapoints attributed to their predominant phases.

Cluster	Predominant Phase(s)	μ_H (GPa)	μ_M (GPa)	I_{Si}	I_{Ca}	I_{Al}	π (%)
1	C-(A)-S-H	0,7 ± 0,2	25 ± 3	0,25 ± 0,02	0,40 ± 0,03	0,15 ± 0,02	29
2	AFm+AFt + C-(A)-S-H	0,8 ± 0,2	27 ± 4	0,17 ± 0,04	0,38 ± 0,03	0,23 ± 0,06	16
3	CH + C-(A)-S-H + NP	1,0 ± 0,3	31 ± 6	0,23 ± 0,06	0,46 ± 0,08	0,15 ± 0,03	33
4	NP + C-(A)-S-H	3,7 ± 2,5	48 ± 15	0,48 ± 0,18	0,23 ± 0,14	0,38 ± 0,12	10
5	Clinker (Al-rich)	5,5 ± 3,6	80 ± 31	0,12 ± 0,03	0,47 ± 0,08	0,46 ± 0,17	4
6	Clinker (silicates)	6,3 ± 3,3	82 ± 24	0,30 ± 0,03	0,68 ± 0,09	0,13 ± 0,04	8

4.2.2.3 Paste with 60% Portland cement replacement by natural pozzolan (B60NP system).

According to the results presented in Table 4.5 and Figure 4.26, B60NP system presents a quite different microstructure compared with the OPC system. For this system, portlandite is not detected, due to the high level of Portland cement replacement by NP, which results in an increase in Si and Al contents for C-(A)-S-H (cluster 1), causing a decrease in Ca/(Si+Al) ratio. The increase of the NP content allows to differentiate three types of NP particles; Type 1, corresponding to cluster 5 with high Al/Si ratio and type 2, corresponding to group 6 with low Al/Si ratio. Cluster 7 seems to contain clinker grains and NP particles type 3 resulting in Al/Si ratio of about 1, this balance of Si and Al amounts seems to favor the increase in the micro-mechanical properties of this cluster. Clusters 2, 3 and 4 correspond to C-(A)-S-H intermixed with AFm+AFt, NP particles and siliceous clinker phases, respectively.

Another important aspect that can be appreciated of Table 4.13 it is that the mechanical properties of the C-(A)-S-H (Cluster 1) are lower than cluster 1 from B20NP system. Following the same criteria of the previous systems (OPC and B20NP), the analysis of the results of Table 4.5 indicates an increase of about 240% in the anhydrous material with respect to the OPC system, corresponding to 8% of clinker and 33% of NP particles. This increase causes a decrease in the hydrate content, so the content of the C-(A)-S-H phase would be around 51% and 8% for AFm+AFt.

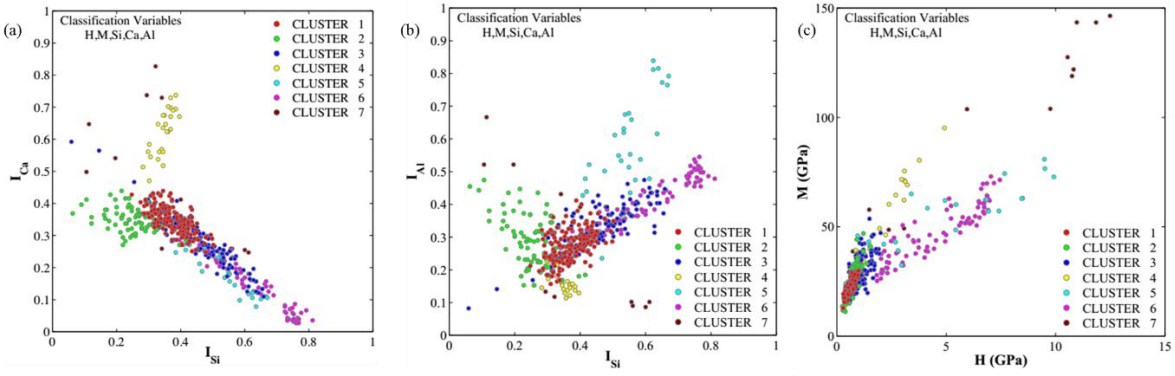

Figure 4.26. Results of SIN-EDS analyses for B60NP system: a) I_{Ca} vs. I_{Si}, b) I_{Al} vs. I_{Si} and c) M vs H.

Table 4.5. Results of SNI-EDS analyses of the B60NP system: average indentation hardness (μ_H), modulus (μ_M) and volume fractions (π) for clusters of datapoints attributed to their predominant phases.

Cluster	Predominant Phase(s)	μ_H (GPa)	μ_M (GPa)	I_{Si}	I_{Ca}	I_{Al}	π (%)
1	C-(A)-S-H	0,6 ± 0,2	23 ± 4	0,37 ± 0,06	0,35 ± 0,04	0,28 ± 0.05	34
2	AFm+AFt + C-(A)-S-H	0,7 ± 0,2	25 ± 7	0,25 ± 0,07	0,35 ± 0,04	0,29 ± 0.08	15
3	C-(A)-S-H + NP	1,1 ± 0,4	31 ± 8	0,46 ± 0,10	0,28 ± 0,09	0,33 ± 0.07	21
4	Clinker (silicates)	2,7 ± 2,5	55 ± 27	0,34 ± 0,03	0,64 ± 0,08	0,16 ± 0.04	6
5	NP (1) + C-(A)-S-H	3,2 ± 3,0	56 ± 28	0,30 ± 0,18	0,40 ± 0,21	0,44 ± 0.16	2
6	NP (2) + C-(A)-S-H	4,2 ± 2,0	46 ± 13	0,60 ± 0,13	0,17 ± 0,10	0,41 ± 0.08	18
7	Other anhydrous	6,1 ± 4,0	67 ± 36	0,56 ± 0,07	0,20 ± 0,06	0,55 ± 0.23	5

4.2.2.4 Effect of the transformation of the hydrated predominant phases and anhydrous inclusions by the incorporation of NP.

Figure 4.27 shows the chemical maps of systems OPC, B20NP and B60NP; in which, the color blue identifies the Portlandite, the dark green identifies AFm+AFt, C-S-H is represented by the purple, brown identifies C-A-S-H and nonhydrated particles are represented by the color white. Through the images of Figure 4.27 it is possible to see how the representation of the different hydrated phases changes as the NP content increases, from large extensions of C-S-H and CH for the OPC system to small areas intermixed with C-A-S-H for the B60NP system. In turn, we can see how the content of hydrates are reduced, as well as, the number of non-hydrated particles increases, furthermore, the pozzolanic consumption of the portlandite is ratified. Figure 4.27d presents a magnification of Figure 4.27c, which exhibits the presence of C-S-H around clinker particles intermixed with C-A-S-H, showing the coexistence of C-(A)-S-H with different Ca/(Si+Al) ratio for the B60NP system.

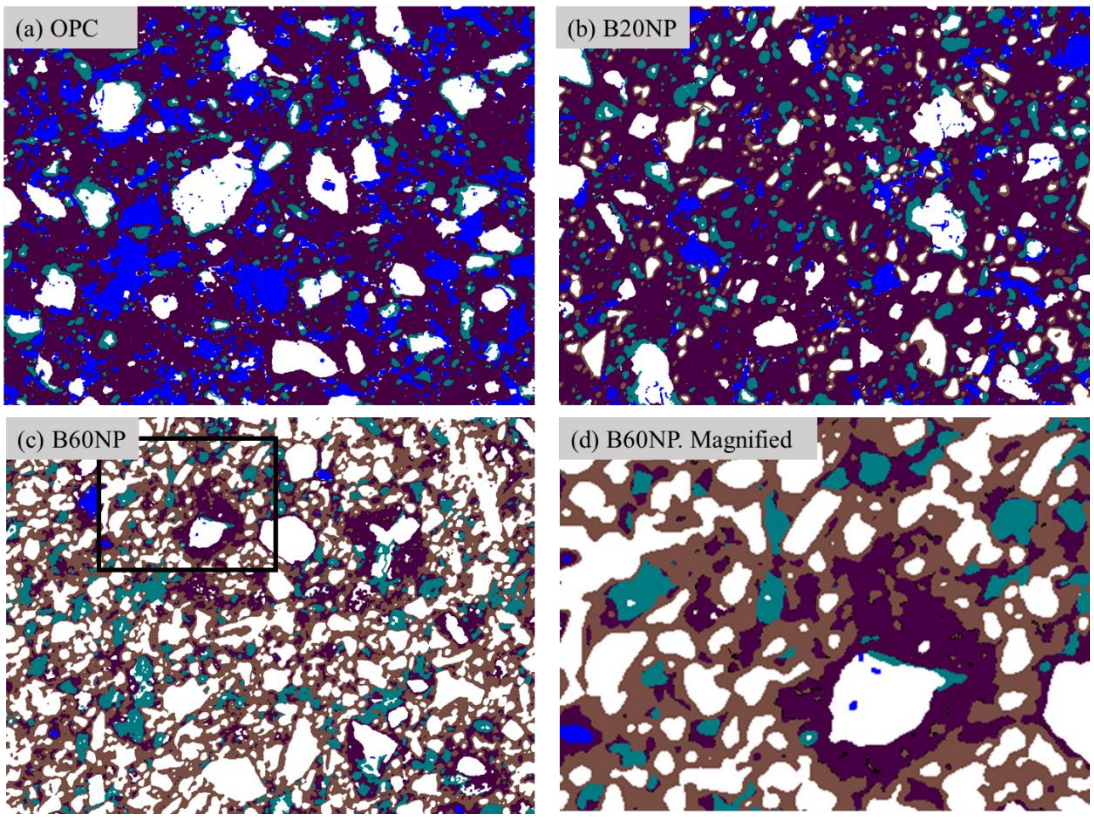

Figure 4.27. Distribution of hydrates obtained by chemical maps of the systems studied: a) OPC, b) B20NP, c) B60NP and d) represents the magnified view of the rectangle in c).

The analysis of the cluster 1 for each studied system (OPC, B20NP and B60NP), Show that the Ca/Si and Ca/Al ratios of this cluster (C-S-H and C-(A)-S-H) tends to decrease as the NP content increases (See Figures 4.28), making it evident that there is a transformation from predominant C-S-H phase for the OPC system to predominant C-(A)-S-H phase for the B60NP system. This change in the structure results in a reduction of the average indentation modulus from 27 ± 3 to 23 ± 4 GPa and the average indentation hardness of 0,8 ± 0,1 to 0,6 ± 0,2 GPa. Therefore, this suggests that the pozzolanic reaction between the NP and Portlandite does not produce a stronger binding in the predominant C-(A)-S-H phase, so the good performance of the mechanical properties of B60NP concrete is not attributed to this hydration process.

On the other hand, as NP content increases, the number of Al-bearing phases also increases and because of the mechanical properties of the intermixed clusters containing AFm+AFt were found to be greater than the predominant C-(A)-S-H phase (Table 4.3, 4.4 and 4.5), it is attributed that an increase in the Al-bearing phases in the systems B20NP and B60NP may contribute positively to the performance of their engineering properties (concrete B20NP and B60NP).

Figure 4.29 shows the anhydrous particles and their distribution in the three studied systems. These particles are clinker phases consisting of silicates (identified in purple), clinker phases formed by aluminates and ferrite (represented in cyan) and the three types of NP (type 1 in lemon yellow, type 2 in beige and type 3 in reddish brown).

The analysis of the images presented in figure 4.29 reveal the following findings: It is detected that the average size of the NP particles are approximately 40% smaller than the clinker particles, corresponding to approximately 10,6 μm of average diameter for the NP particles and 17,5 μm for the clinker particles. Another important finding is that by increasing the NP dosage there is a tendency to decrease hydrate formation and at the same time a tendency to increase the anhydrous particle content corresponding approximately to 130% for the B20NP system and 230% for the B60NP system with respect to the OPC system, being consistent with increases detected in Tables 4.3, 4.4 and 4.5 (135% and 240% for systems B20NP and B60NP respectively). This indicates that the incomplete reaction of clinker and NP favors the formation of a cementitious matrix with small hard inclusions that apparently have an optimal distribution. This optimal distribution of anhydrous inclusions may be another important factor that contributes to the good performance of the mechanical properties of concrete with high level of Portland cement replacement by NP (B60NP concrete). in fact under stress, the heterogeneity formed by these inclusions causes that the fracture planes are deviated (crack deflection), leading to a decrease crack tip stress [Wiederhorn, 1984] thus helping to increase the toughness of the cementitious matrix up to five times due to combined effects of crack trapping and bridging, depending on the particles toughness and size [Bower and Ortiz, 1991].

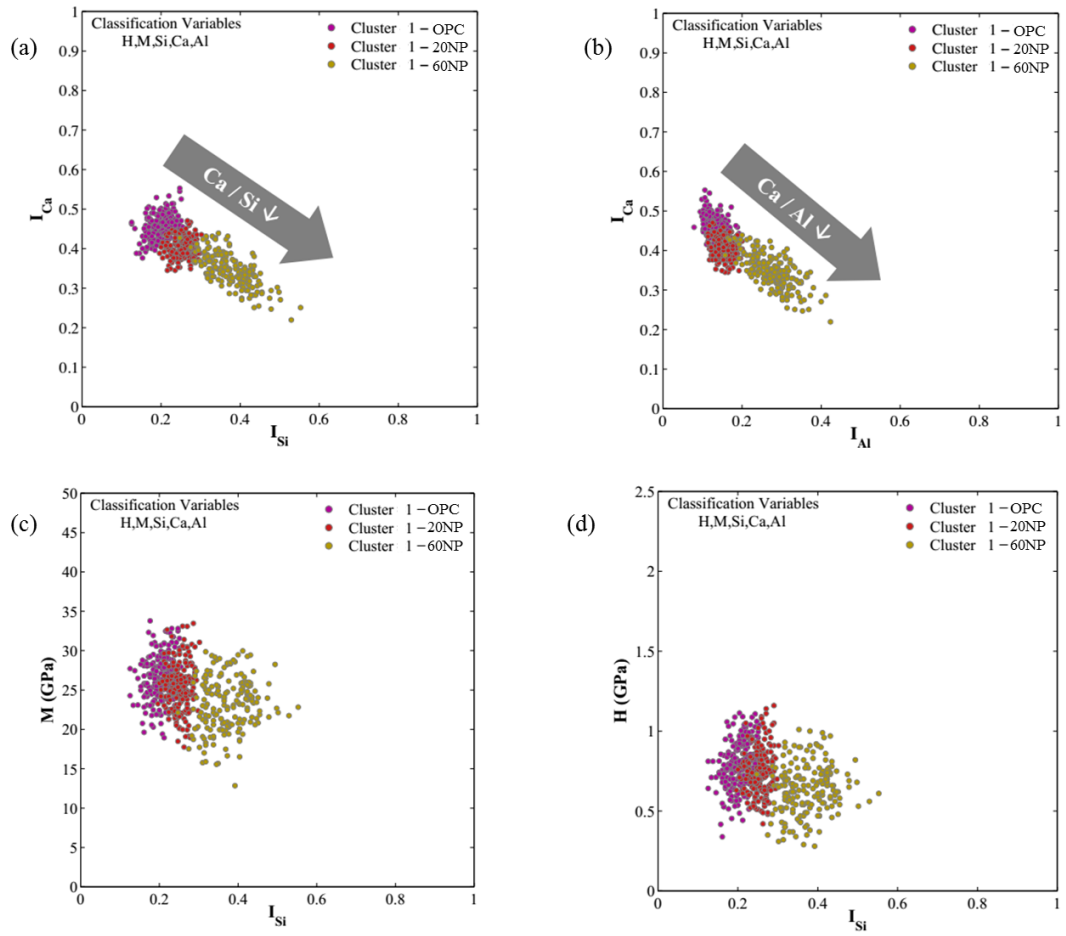

Figure 4.28. Variations in the properties of cluster 1 (C-S-H, C-(A)-S-H) for the systems OPC, B20NP and B60NP represented for the following variables: a) I_{Ca} vs I_{Si}, b) I_{Ca} vs I_{Al}, c) M vs. I_{Si} and d) H vs. I_{Si}.

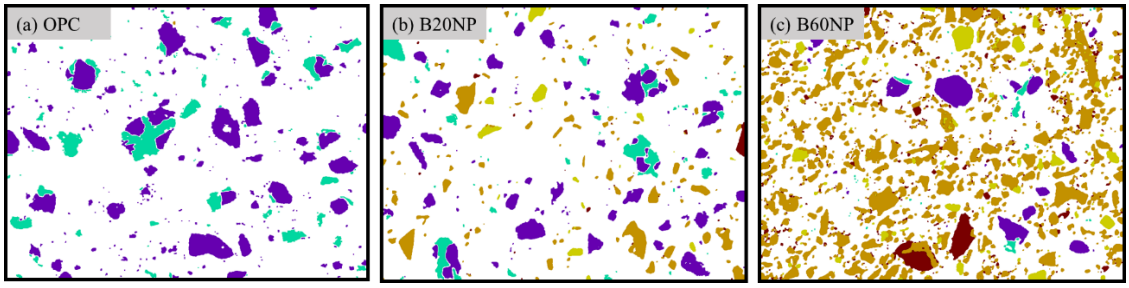

Figure 4.29. Distribution of anhydrous particles on the analyzed surfaces as obtained by chemical maps of the systems studied: a) OPC, b) B20NP and c) B60NP.

Although fracture toughness measurements were not contemplated in this study, the effect of non-hydrated particles (hard inclusions) in the failure process of a heterogeneous material subjected to compression may explain the high strength obtained in the concrete B60NP mixture at 90 days.

Although there is a tendency to decrease the values of the micro-mechanical properties by increasing the NP dosage in the studied systems (Tables 4.3, 4.4 and 4.5), the engineering properties of the B20NP mixture are not affected at 90 days; in contrast, the B60NP mixture shows slight decreases about 11% in the compressive strength and 10% in the modulus of elasticity compared to the reference mixture.

The good performance of concrete mixtures with dosages of 20% and 60% NP is attributed to a combination of mechanisms that occur at microstructural level, of which the reactivity of the NP appears to be the most important, since contributes to forming a dense cementitious matrix, due to the formation of hydrates with hard inclusions (anhydrous particles). On one hand, the formation of the predominant phase C-(A)-S-H is not reduced impressively even with Portland cement replacements of 60% (61% to 52%), furthermore, there is an additional formation of AFm+AFt with good performance in their micro-mechanical properties. On the other hand, it is considered that the presence of smaller non-hydrated particles with a good distribution in the cementitious matrix contribute both to the development of the mechanical properties and to the resistance to chloride ingress since these hard inclusions provide an increase the segmentation of the porous network.

4.3 Stage 3. Concrete.

4.3.1 Fresh properties.

As it was mentioned in the section 3.1, the slump was set as a target parameter for all the mixtures (200 ± 20 mm). The rest of the evaluated properties are shown in the table 4.1.

Table 4.6 Fresh concretes properties.

Series	W/B	Mixture ID	Slump, cm	Unit weight, kg/m^3	Temperature, ^{o}C	Air, %
A	0.45	AR	19,5	2374	24,4	2,6
		A20NP	22,0	2336	25,1	2,2
		A60NP	18,0	2306	24,0	2,0
		A20FA	18,0	2315	24,0	2,0
		A60FA	22,0	2234	24,0	2,2
B	0.35	BR	18,0	2424	20,7	2,1
		B20NP	18,5	2358	23,7	1,9
		B60NP	21,5	2329	22,8	1,4
		B20FA	22,0	2339	24,8	2,0
		B60FA	21,5	2270	25,0	2,2

4.3.1.1 Slump.

The workability of concrete mixtures containing supplementary cementitious materials depends on the shape, size distribution and surface texture of its particles. [Malhotra and Mehta, 2002]. In this topic it has been reported that for concretes with the same consistency, the incorporation of fly ash (FA) usually improves the workability, even with high volumes of this material [PCA, 2008; Bentz et al., 2012; Malhotra and Mehta, 2012; Hemalatha and Ramaswan, 2017]. On the other hand, the angular shape and the high porosity of the natural pozzolans (NP) increase the surface area of its particles leading to an increase in the water and/or superplasticizer admixture requirement in order to maintain a determined consistency. [Uzal et al., 2007; Najimi et al., 2012; Markiv et al., 2016]. In order to achieve the objective slump, the mixtures with only Portland cement of the series A and B, required 1,2 l/m^3 and 2,3 l/m^3 of superplasticizer admixture respectively (Table 3.4). In spite of the pumice having a high porosity (macro scale), the concretes with NP maintained constant the superplasticizer dosage compared to the reference mixtures (mixtures AR and BR); except for the mixture with greater replacement

of Portland cement by NP of the Series B (mixture B60NP), has a slightly higher superplasticizer demand from 2,3 l/m^3 to 2,5 l/m^3 (Table 3.4), which can be considered insignificant, this can be attributed to the absence of porosity at the scale of the pulverized pumice, as it can be seen in the Figure 4.30.

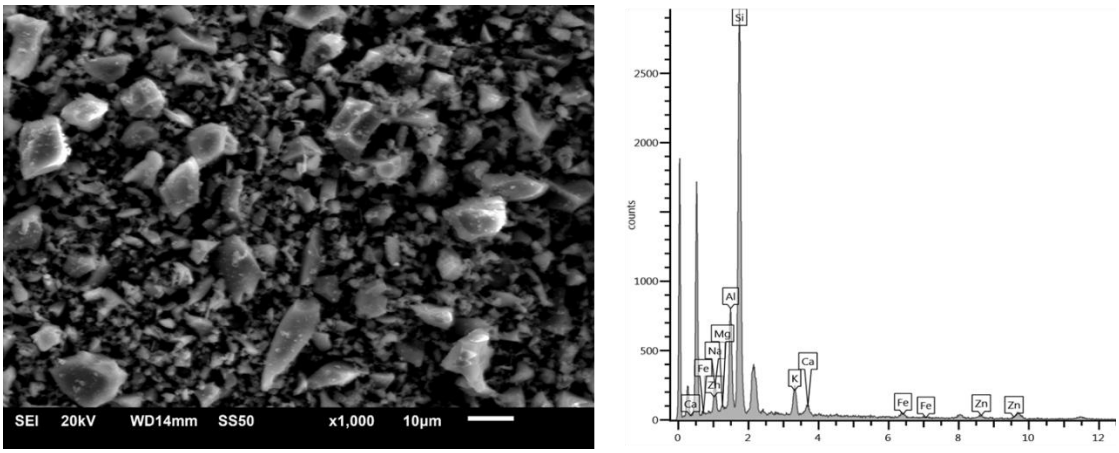

Figure 4.30. SEM image and EDS analyses of natural pozzolan particles.

With the exception of the mixture A60FA; which required a slight reduction in the superplasticizer dosage from 1,2 l/m^3 to 1,00/m^3 (see Table 3.4) in order to achieve the objective slump, the rest of the mixtures with FA required the same superplasticizer dosages than the mixtures with natural pozzolan.

4.3.1.2 Concrete Unit weight.

In the Table 4.6 it can be seen that the unit weights decreased as the Portland cement was substituted for NP and/or FA; this was expected because of the difference in the densities of the supplementary cementitious materials when compared to Portland cement.

4.3.1.3 Air content and temperature of the concrete.

In Table 4.6, it can be seen that the mixtures with FA tend to maintain the entrained air similar to their references, and the mixtures with natural pozzolan show a tendency to decrease the air content as the dosage of NP increased. This trend is consistent with the results of packing density measured by wet packing method when NP is added (Table 4.10). In this same Table

4.6, it can also be seen that the temperature values of the concrete mixtures were within a narrow range of 20,7 to 25,1 ºC.

4.3.1.4 Setting times.

In previous works it has been reported that the natural pozzolans accelerate the setting times due to the combined action of a self-dessecation and the high specific surface typical of a porous microstructure [Uzal et al., 2007; Uzal and Turnali, 2012]. As shown in the Table 4.7, the mixtures with a 20% replacement of Portland cement by NP (mixtures A20NP and B20NP) exhibited shorter setting times. The mixture A20NP exhibited reductions in its initial and final setting times of 39 minutes, while the reductions in the setting times of the mixture B20NP where of 80 and 49 minutes for the initial and final setting times respectively. In contrast, the mixtures with high contents of natural pozzolan (mixtures A60NP and B60NP) exhibited setting times similar to the references mixtures (mixtures AR and BR respectively). Since this pozzolan doesn't have a high porosity (Figure 4.30); this effect can be attributed to the combined action of its high fineness and considerable alkali content (see Table 3.1), which can act as an alkaline accelerator, where the ions of this compounds react rapidly with the ions Ca^{2+} and SO_4^{2-} to create ettringite and monosulfate, which leads to a high heat release [Salvador et al., 2016].

As expected, the high content of fly ash led to important delays in the setting times [Malhotra and Mehta, 2012; Bentz et al., 2010], in this matter, the mixture A60FA exhibited delays in its initial and final setting times of 2,0 and 3,5 hours, while in the mixture B60FA those delays where of 1,5 and 2,5 h respectively. The replacement of 20% of Portland cement by fly ash led to setting times similar to the mixtures with only Portland cement.

Table 4.7. Setting times of the concretes.

Series	Mixture ID	Setting Times	
		initial	Final
A	AR	265 minutes	360 minutes
	A20NP	226 minutes	321 minutes
	A60NP	297 minutes	501 minutes
	A20CV	257 minutes	384 minutes
	A60CV	399 minutes	582 minutes

Series	Mixture ID	Setting times	
		Initial	Final
B	BR	251 minutes	349 minutes
	B20NP	171 minutes	300 minutes
	B60NP	260 minutes	389 minutes
	B20CV	240 minutes	332 minutes
	B60CV	340 minutes	499 minutes

4.3.2 Hardened properties.

4.3.2.1 Compressive strength.

The compressive strength of concrete is an important mechanical property that determines its quality as a building material and is usually used in calculations to design bridges, buildings and general infrastructure. It can be defined as the maximum axial load applied to concrete specimens until failure divided by its transversal area. This property is usually reported at the age of 28 days and is expressed in kilograms per square centimeter (kg/cm^2), mega-pascals (MPa) or in pounds per square inch (psi).

The development of the compressive strength of the concrete mixtures of the series A and B was monitored at the ages of 3, 7, 28, 56 and 90 days and its results are shown in the Table 4.8, Figures 4.31 and 4.32; where it can be seen that the lowest values of early age strength (3, 7 and 28 days) where obtained by the concretes with a higher replacement of Portland Cement for NP and/or FA, which is a typical performance of concretes with a high content of cementitious materials [Poon et al., 2000; Lam et al., 2000 and Celik et al., 2014] due to the lower reactivity of this materials and to the important reduction in the cement content (which is the most reactive material), causing an increase in the effective water/cement ratio, which leads to a delay in the formation of Portlandite, and once this compound is formed, the hydration of the cementitious materials may begin. However, the concretes with FA where those who showed

a lower strength partly because the fineness of this material is lower than that of the NP, so the filler effect triggered by this material (NP), leads to a higher acceleration in the clinker hydration, [Gutteridge and Dalziel, 1990; Berodier and Scrivener, 2014 and Rossen, 2014] and also, because the reaction of the FA at ordinary temperatures is generally slow, and begins to react usually after the first week or later [Hanehara et al., 2001 and Snyder et al., 2009].

Table 4.8. Compressive strength of Series A and B concretes.

Series	W/B	Mixture ID	Strength, MPa									
			3 days	V (%)	7 days	V (%)	28 days	V (%)	56 days	V (%)	90 days	V (%)
A	0,45	AR	28,5	6,5	35,4	7,0	42.0	1,7	44,3	0,5	46,0	4,4
		A20NP	25,4	3,4	28,7	0,9	34.8	5,8	41,4	2,7	45,4	2,3
		A60NP	10,6	3,8	14,5	3,2	28.0	4,5	32,3	7,3	35,1	0,6
		A20FA	23,4	5,4	26,4	7,0	31.3	3,1	36,7	1,6	41,4	0,8
		A60FA	7,9	4,7	11,9	9,8	22.0	5,6	26,5	5,8	29,7	4,8
B	0,35	BR	39,7	3,2	47,4	0,8	55.1	2,0	55,8	1,9	61,3	4,5
		B20NP	37,9	9,7	40,5	5,6	49.5	8,4	56,9	2,5	61,7	2,1
		B60NP	19,7	6,4	26,2	3,2	41.0	3,8	49,5	1,5	54,8	2,6
		B20FA	36,9	4,0	38,8	9,1	44.9	0,4	50,7	3,3	52,8	4,5
		B60FA	17,8	4,1	21,0	1,3	33.7	3,0	37,6	1,2	44,3	7,7

V.- Range of variation from the average of three specimens.

In the Figures 4.31 and 4.32 it can be seen also that as the curing age increases, the ratio of increase in the strength of the concretes with cementitious materials (NP and/or FA) is greater than their respective reference mixtures, and so the gap between the strengths of these mixtures tends to reduce with time, because after 28 days, the hydration process of the cementitious materials tends to be more stable [Taylor, 1984]. In this matter, at early ages (between 56 and 90 days) the concretes with NP also exhibited a better strength performance than the concretes with FA, which indicates that the pozzolanic reaction of the NP is greater than that of the FA, being consistent with the results of the TGA analysis shown in Section 4.1, where the paste mixtures with NP exhibited a greater Portlandite consumption than the paste mixtures with FA, due to its high amorphous behavior (see Figures 4.11 and 4.12).

Additionally, it can also be seen that the concretes with the cementitious materials of the Series B (W/B ratio of 0,35) showed a better strength performance than the concretes of the series A (W/B ratio of 0,45). In particular, the mixture B20NP had slightly higher values than

the reference mixture at 56 and 90 days, additionally, the mixture with the greatest substitution of cement by NP (mixture B60NP), has strength values of 49.5 MPa and 54.8 MPa at 56 and 90 days respectively, representing a strength reduction in the range of 11,0% for both ages. At 90 days, compressive strength of this concrete is higher than the one of mixture B20FA.

With the exception of the mixture B60FA, all the mixtures of the B Series can be classified as high strength and high performance concretes, because at the age of 28 days they showed strengths higher than 40,0 MPa and the water/cementitious material ratio was less than 0,45 [ACI 363R; Aïtcin, 1998]. The good performance of concretes from series B with incorporations of mineral admixtures (lower water/binder ratio) is attributable to a shorter distance between the particles of the cementitious materials due to the lesser amount of water, causing a more efficient nucleation [Berodier and Scrivener, 2014].

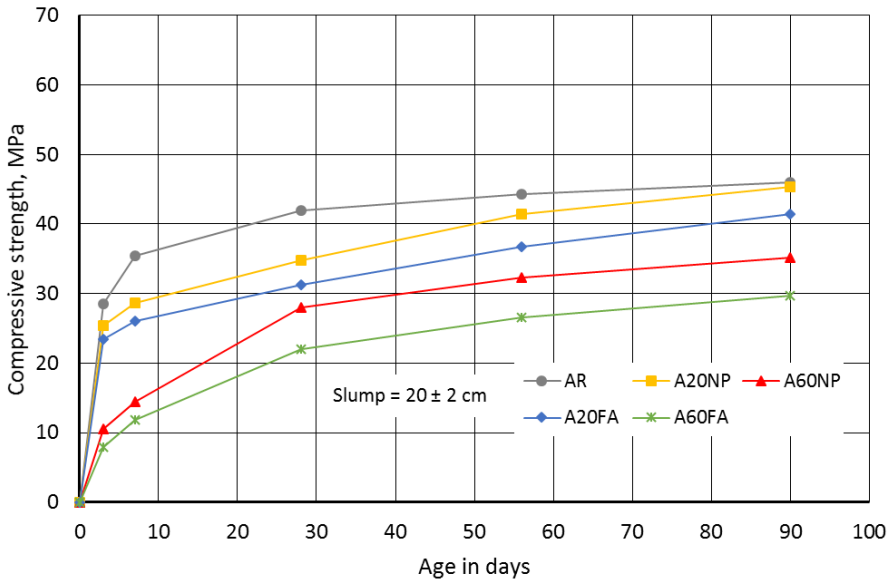

Figure 4.31. Compressive strength development for series A concretes (W/B = 0,45).

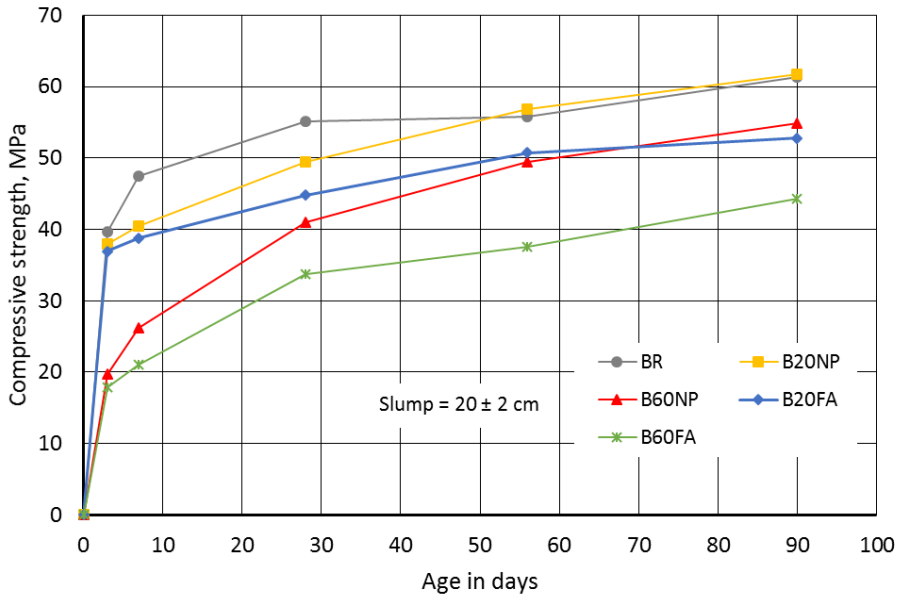

Figure 4.32. Compressive strength development for series B concretes (W/B= 0,35).

4.3.2.2 Modulus of elasticity.

Concrete such as many materials has a certain degree of elasticity, which means that the elastic properties of this material are a measure of its stiffness. The static modulus of elasticity is defined as the slope of the stress-strain curve of the concrete in the elastic range [PCA, 2008]. This mechanical property is very useful for both the design of simple elements and elaborated structures under loads that induce stresses, moments and deflections. For normal mass concrete, this property ranges from 14 GPa to 41 GPa (140,000 to 420,000 kg/cm^2), depending on the strength level and type of aggregate [PCA, 2008].

The modulus of elasticity of the concretes studied was determined at the ages of 28 and 90 days and their results are shown in Table 4.9, Figure 4.33 and 4.34. For both Series (A and B), the value of modulus of elasticity of plain Portland cement mixtures remained practically constant between 28 and 90 days, indicating that the curing time in these concretes does not improve this property. In contrast, the mixtures with mineral admixtures, presented significant increases of modulus of elasticity, due to the pozzolanic effect of the NP and FA.

Since the modulus of elasticity is related to the strength level that the concrete develops [Durán et al., 2011; Saridemir, 2013 and Shariq et al., 2013], the concretes' performance in

terms of this property was equivalent to their attained strengths, which were already discussed in the section 4.3.2.1. The modulus of elasticity of the concretes with mineral admixtures also depends in the amount of the cementitious materials, their reactivity, fineness, water/binder ratio, and curing.

Table 4.9. Static modulus of elasticity for Series A and B concretes.

Series	Mixture ID	Modulus of elasticity, GPa			
		28 days	V (%)	90 days	V (%)
A	AR	34,5	10,7	34,7	8,6
	20NP	32,1	3,6	35,1	3,4
	60NP	26,3	3,4	30,3	4,5
	20FA	29,0	1,6	33,9	0,2
	60FA	24,3	0,6	29,5	3,1

Series	Mixture ID	Modulus of elasticity, GPa			
		28 days	V (%)	90 days	V (%)
B	BR	39,1	5,3	39,6	10,6
	20NP	36,7	6,0	39,7	0,7
	60NP	33,7	1,5	35,7	5,3
	20FA	35,9	3,3	39,0	2,6
	60FA	27,1	9,5	32,6	8,0

V.- Range of variation from the average of three specimens.

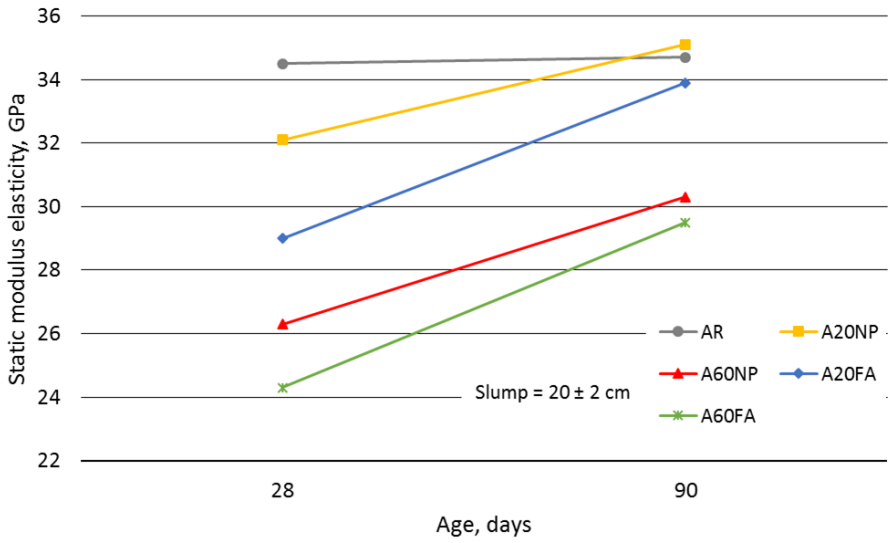

Figure 4.33. Static modulus of elasticity for series A concretes (W/B = 0,45).

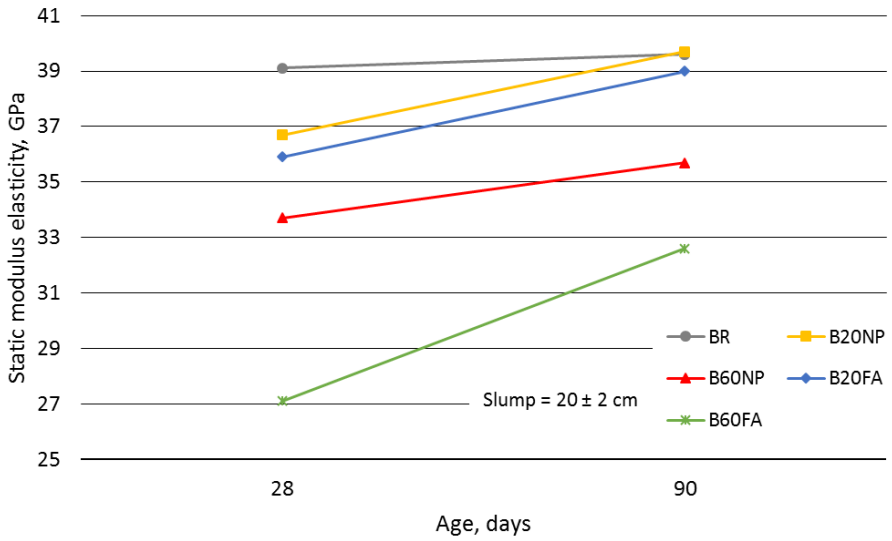

Figure 4.34. Static modulus of elasticity for series B concretes (W/B = 0,35).

4.3.3 Durability tests.

4.3.3.1 Non-steady chloride migration coefficient.

The chloride migration coefficient (D_{nssm}) determined by the Nordtest method is a parameter that reflects the resistance that the concrete offers to the chlorides ingress. This measurements were made at the ages of 56 and 90 days, and their results are shown in the Figures 4.35 and 4.36; where it can be seen that the reference mixtures of both concrete series (A and B) exhibited values of D_{nssm} practically constant at these ages (56 and 90 days), which indicates that the time of curing in these concretes doesn't reduces the ingress of chlorides. In contrast, in the concretes with mineral admixtures, the curing time is of high importance, since these concretes showed important reductions in the values of the D_{nssm} from 56 to 90 days, which indicates that the pozzolanic effect took place more efficiently due to the curing. In this sense, the packing density seems to be a not very important factor that influences the chloride ingress, since the mixtures with FA turned out to be less compact (Table 4.10). This indicates that the particles of NP and FA act as fine granulates, that after hydration, they partially obstruct the pores, improving their refinement, what seems to depend on the tortuosity of the capillary pores (mainly mixtures with FA) [Massazza, 1998].

In figures 4.35 and 4.36, it can also be see that as the Portland cement replacement by supplementary cementitious materials increases, the ingress of chlorides tends to decrease. This being consistent with results reported by Zunino and Lopez (2016), Duan et al., (2013), Baroughel-Bouny et al. (2011), Badogiannis et al. (2015) and Hossain et al., (2007). Additionally, it can also be seen that the substitution of Portland cement by NP and/or FA is a factor more significant than the reduction in the water/cement ratio.

The presence of NP and FA in the concrete mixtures lead to a reduction in the portlandite (CH) content, due to the pozzolanic reaction of these materials, which generates new hydration products (C-S-H) that are smaller in size and in the case of NP, more irregular [Massazza, 1998], and that increases the resistance to chloride ions penetration (see Figure 4.37). Other studies by Hossain (2008) show that the addition of natural pozzolans, even in different cement types, reduces the content of CH, increasing the resistance to chloride penetration. At 56 days, concretes with NP are considered to have extremely high resistance to chloride ingress (see Table 4.11).

Table 4.10. Packing densities of cementitious materials (pastes reproduced from the concretes studied) measured by wet packing method.

Pastes ID	Packing density
OPC	0,568
20NP	0,587
60NP	0,610
20FA	0,569
60FA	0,530

OPC.- Ordinary Portland cement, NP.- Natural pozzolan, FA.- fly ash

Table 4.11 Resistance to chloride ingress based on non-steady state migration method [Nilsson, L. et al., 1998].

Chloride Diffusivity $m^2/s \times 10^{-12}$	**Resistance to Chloride ingress**
> 15	Low
10 – 15	Moderate
5 – 10	High
2.5 – 5	Very high
< 2.5	Extremely high

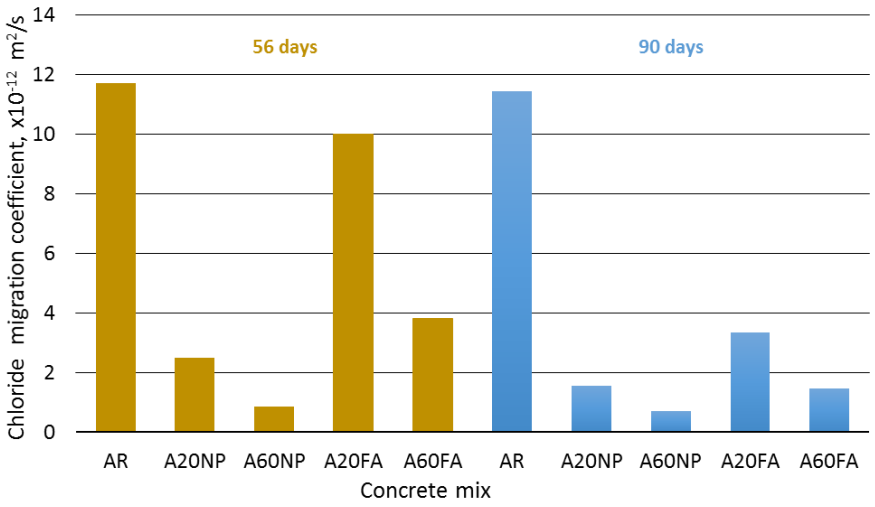

Figure 4.35. Chloride migration coefficient (D_{nssm}) for series A concretes at 56 and 90 days (W/B = 0,45).

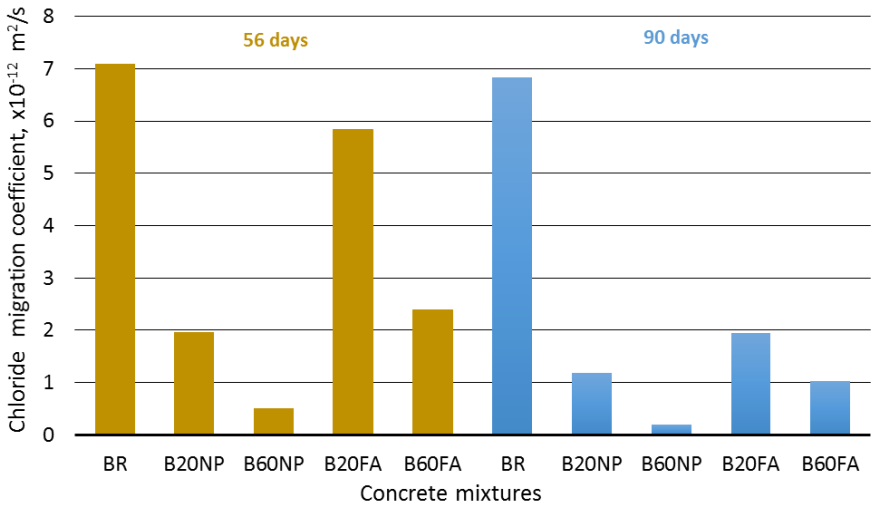

Figure 4.36. Chloride migration coefficient (D_{nssm}) for series B concretes at 56 and 90 days (W/B = 0,35).

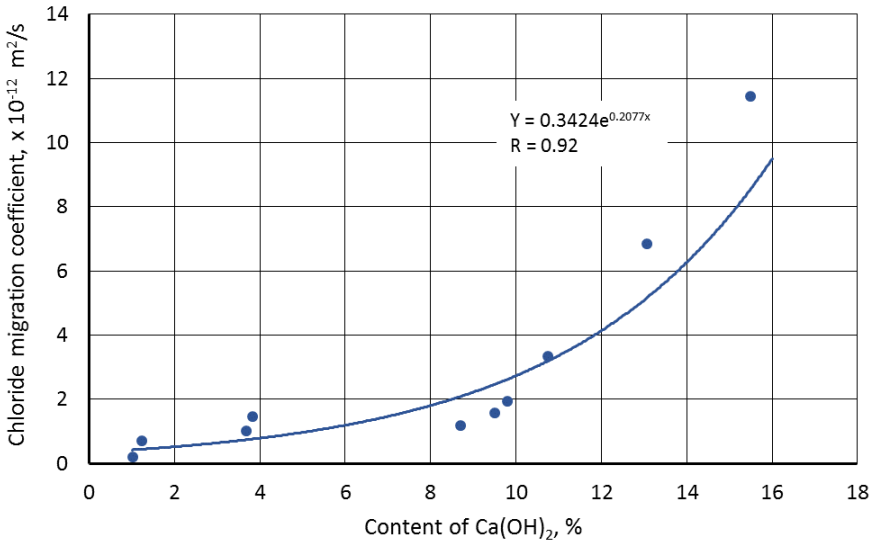

Figure 4.37. Relationship between the content of Portlandite ($Ca(OH)_2$) and the chloride migration coefficient of the reproduced pastes from series A and B concretes.

4.3.3.2 Surface resistivity.

The surface resistivity (SR) is a non-destructive laboratory test method that measures the electrical resistivity of water-saturated concrete and provide an indication of its permeability. The performance in terms of this parameter was monitored at the ages of 3, 7, 28, 56 and 90 days and its results are shown in the figures 4.38 and 4.39.

Since the electrical resistivity of the concrete represents the movement of ions (such as chloride ions) in the pore solution [Ramezanianpour, et al., 2011]; the SR results of both concrete series (A and B) showed the same trend than the values of chloride diffusion discussed in the previous section (section 4.3.3.1), where once again the concretes with NP showed the best performance.

The permeability of concrete with mineral admixtures depends mainly on three factors: Portland cement hydration, filler effect of mineral additions and pozzolanic reaction [Rivera et al., 2015]. In that regard, although cement hydration is slower at early ages (cement replacement by mineral admixtures), somehow, the filler effect of these additions compensates the reduction of hydration products. After 7 days, the mixtures with NP improve their electrical resistivity compared to the reference mixture; and for mixtures with FA, this improvement is presented

after 12 days (figures 4.38 and 4.39). This can be attributed to the start of the pozzolanic reaction combined with the filler effect from each material.

In order to know the correlation among the values of SR and D_{nssm}, the results of all the concrete mixtures in both series (A and B) were considered, and shown in the Figure 4.40. The value of R was of 0.95, which indicates a good correlation, being consistent with results reported by Ramezanianpour, et al. (2011), Sengul, (2014) and Kessler et al., (2008). This suggests that the chlorides fixation by the cementitious materials doesn't affect importantly in the low penetration of these ions, because the surface resistivity test doesn't involve them. Also, studies performed by Thomas et al. (2012), showed that for low water/binder ratios (W/B = 0,30), the ability to bind chlorides diminishes, even with cementitious materials high in alumina.

According to the values of resistivity proposed by AASHTO TP 95-11 (Table 4.12), the mixtures A60NP and B60NP showed a chloride ion penetration very low at 28 days.

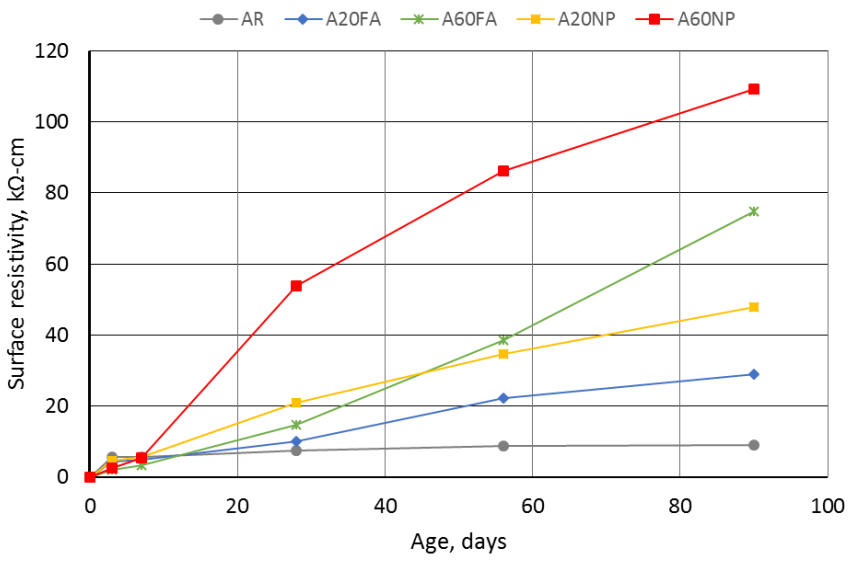

Figure 4.38. Surface resistivity development for series A concretes, (W/B = 0,45).

Table 4.12. Chloride ion penetration adopted from AASHTO TP 95-11.

Chloride ion penetration	**Surface resistivity test** 100 mm x 200 mm Cylinder (kilohm-cm) a = 38 mm
High	< 12
Moderate	12 – 21
Low	21 – 37
Very low	37 – 254
Negligible	> 254

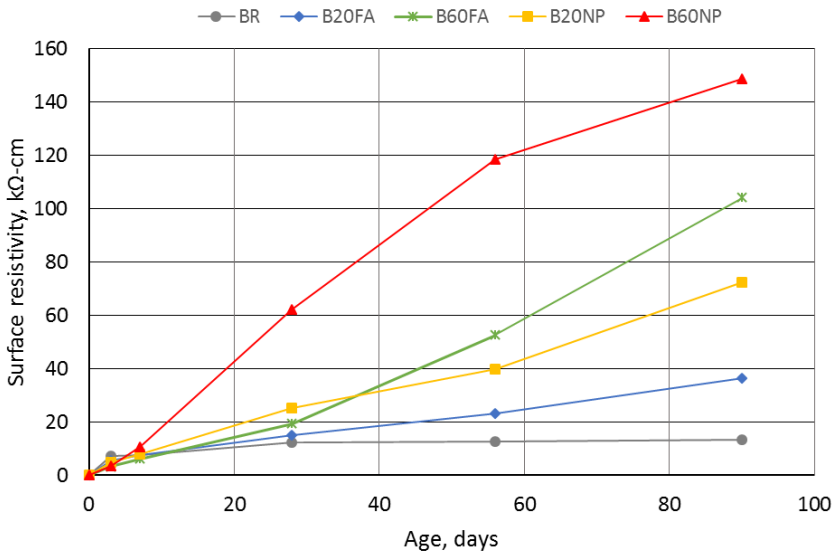

Figure 4.39. Surface resistivity development for series B concretes, (W/B = 0,35).

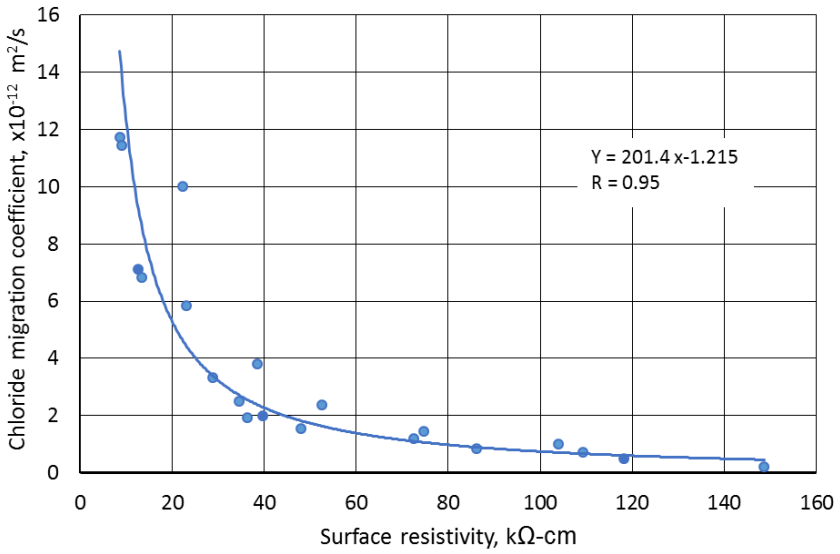

Figure 4.40. Relationship between surface resistivity and Chlorine migration coefficient for all concretes mixtures (Series A and B).

4.3.3.3 Carbonation.

Carbonation is the reaction of the atmospheric gaseous CO2 with the concrete phases that contain calcium, which produces chemo-mechanical changes in its microstructure [Savija and Lukovic, 2016]. This reaction causes a decrease of the alkalinity of the pore solution of the concrete, thereby promoting the corrosion of the reinforcing steel [Andrade and Buják, 2013]. Usually, the carbon dioxide diffuses through the coatings of concrete following a square root in relation to time, resulting in a front of carbonation [Pappadakis et al 1991, Castellote et al 2008].

The Table 4.13 and the Figures 4.41 and 4.42 present the depth of the carbonation. Just as expected, the concretes with mineral admixtures showed the greatest carbonation progress measured by the phenolphthalein test in agreement with the results reported by Andrade and Buják (2013) and Borges et al (2010), which worked with combined mixtures with slag and fly ash. In the figures 4.41 and 4.42, it is observed that as the content of both the natural pozzolan and the fly ash increases, the resistance to the advance of carbonation progress tends to be lower. On the other hand, it can also be noticed that the concretes from the series B presented lesser depths of penetration, where the mixtures B60NP and B60FA showed a decrease of the order of 47% and 36%; while the mixtures BR, B20NP and B20FA did not present any advance through the phenolphthalein test (Figure 4.42).

Table 4.13. Carbonation depths of Series A and B concretes.

Series	Mixture	Depths, mm			
		7 days	14 days	21 days	28 days
A	AR	0.48	0.90	1.40	1.78
	20NP	0.55	1.38	1.79	2.25
	60NP	5.64	9.83	11.19	12.35
	20FA	0.50	0.95	1.51	1.98
	60FA	3.93	6.88	8.88	9.12

Series	Mixture	Depths, mm			
		7 days	14 days	21 days	28 days
B	BR	0	0	0	0
	20NP	0	0	0	0
	60NP	3.44	4.56	5.19	6.52
	20FA	0	0	0	0
	60FA	3.10	4.12	4.89	5.81

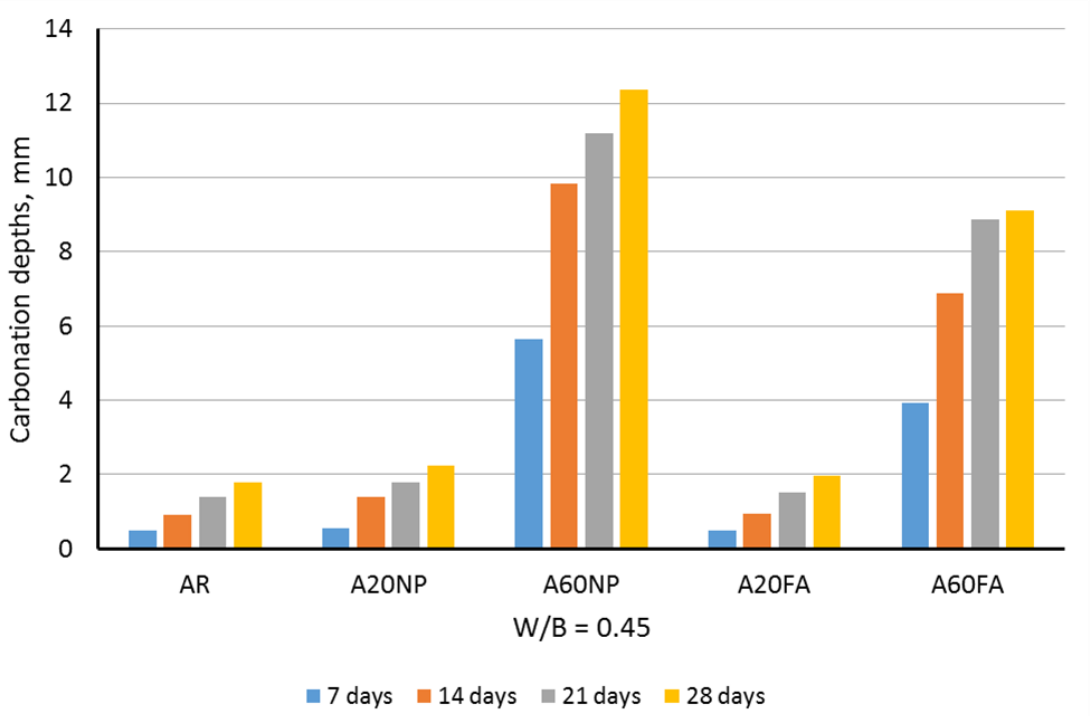

Figure 4.41. Carbonation depths for Series A concretes.

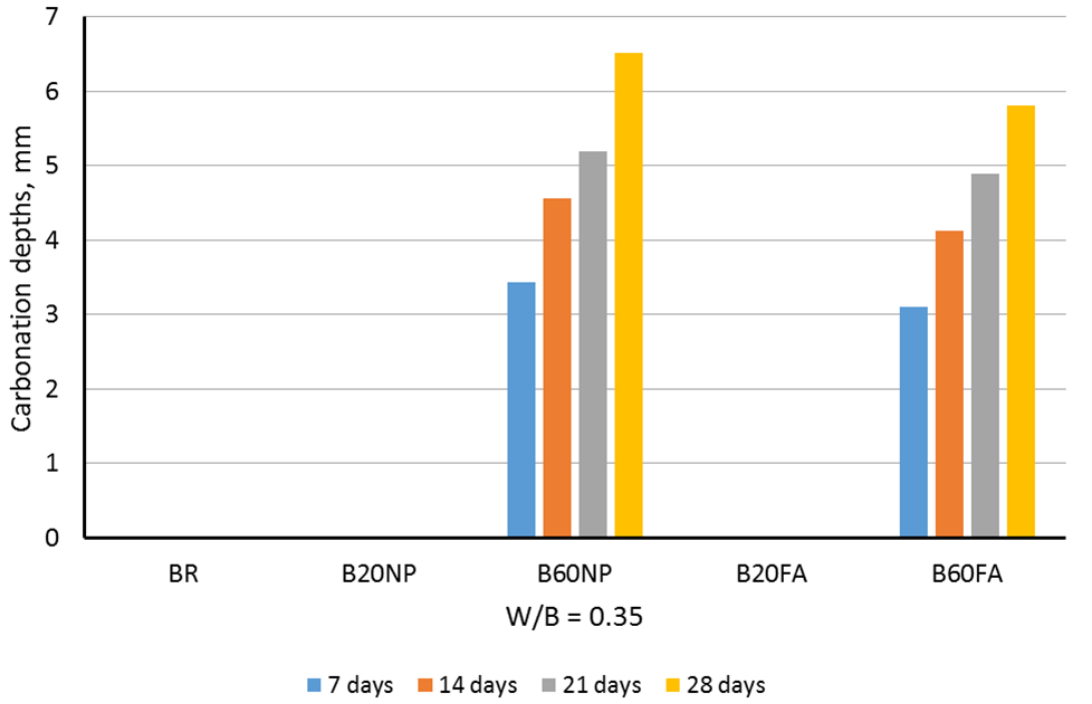

Figure 4.42. Carbonation depths for Series B concretes.

For both concrete series (A and B), the mixtures with natural pozzolan showed higher depths of penetration, being attributable to the high reactivity of this material, which leads to a greater decrease of the content of portlandite. In this sense, although some mineral additions can provide high contents of soluble alkali in the pore solution, the reaction of the portlandite with the phases of the addition can absorb these alkalis as well [Jawed et al 1978, Glasser et al 1985]. Once the portlandite is consumed, the C-S-H structure contributes to the buffering capacity when it is decalcified, but the process is not effective enough to stop the pH decrease resulting in a highly silicious amorphous decomposition [Sevelsted and Skibsted, 2015].

4.3.3.4 Drying shrinkage.

The drying shrinkage is the change in volume of the concrete in long term caused by the loss of humidity over time in its hardened state. The combination of drying shrinkage and the restrictions of the concrete cause tensile stresses, when these stresses exceed the tensile strength of the concrete, the cracking takes place, being denominated cracks by drying shrinkage.

To carry out the measurements of the dryings shrinkage strain, firstly, all specimens where cured at standard temperature for a period of 14 days since the curing time between 7 and 28 days does not have a significant effect in the development of these deformations [Zhang et al 2015].]. Subsequently, the specimens were placed in a dry room at constant temperature to measure the shrinkage strain at ages of 4, 7, 14, 28, 56 and 90 days.

Figures 4.43 and 4.44 show the drying shrinkage evolutions of the concrete mixtures of the series A and B, where it is able to notice that the concretes with a ratio water/binder of 0,45 (Series A) presented greatest strains, which was expected, due to the highest amount of available water to evaporate.

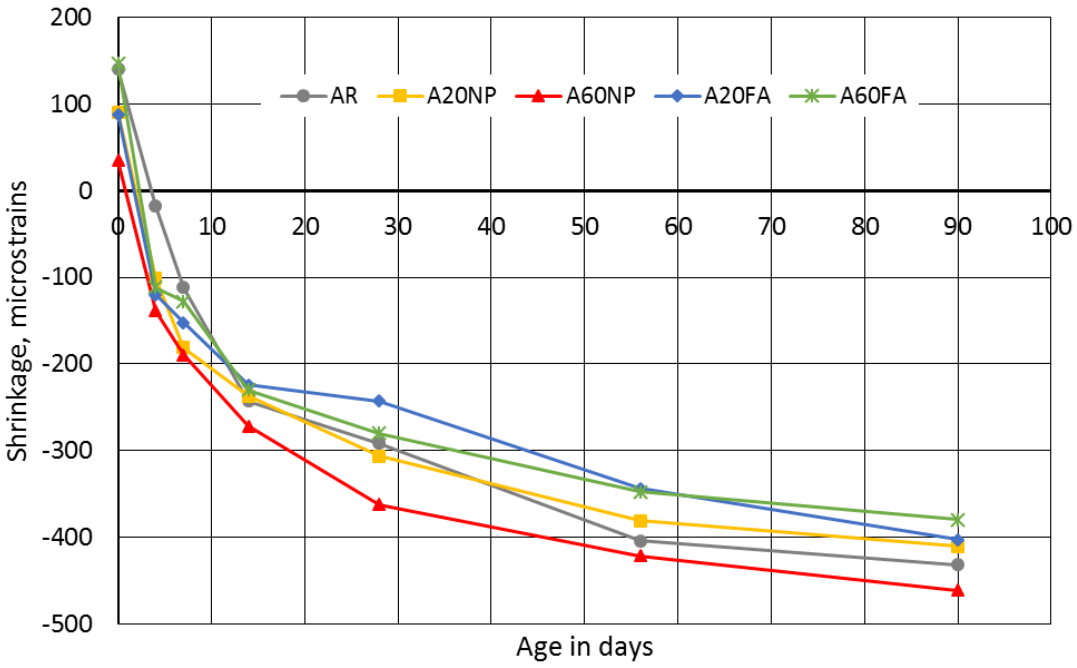

Figures 4.43. Drying shrinkage of Series A concretes.

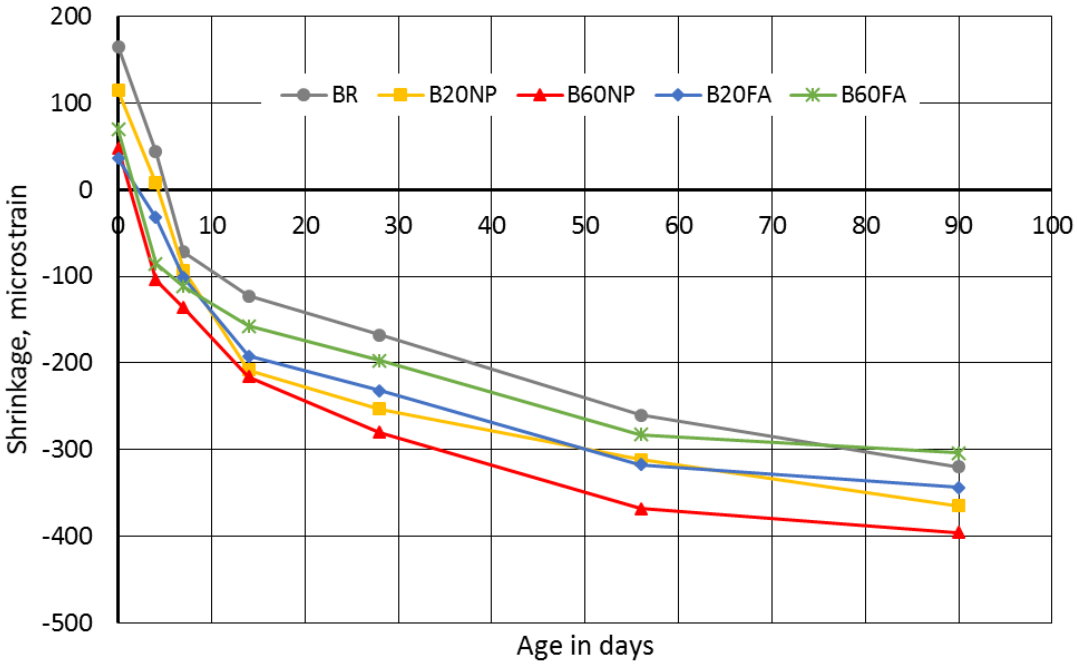

Figure 4.44. Drying shrinkage of Series B concretes.

For both series of concrete, the mixtures with higher amount of natural pozzolan showed greater shrinkage. being attributable in the first place to the greater fineness that this material presents, since the finer particles have a greater surface exposed to be carried out the pozzolanic reaction at a faster rate [Güneyisi et al 2010, Wongkeo et al 2012], which leads to a higher densification of the cementitious matrix with a greater volume of mesopores [Collins et al 2000, Jiang et al 2005]. In this sense, the B60NP and A60NP mixtures have the highest volume of permeable pore space (see 4.3.3.5), which suggests that most of the volume of these pores present sizes of capillary diameter less than 50 nm. On the other hand, finer particles with a rough texture can also absorb more water, thus causing a greater capillary pore pressure due to the lower amount of free water for self-drying [Shariq et al 2016]. Another important aspect that can influence in the drying shrinkage increase is the greater volume of cementitious paste produced due to the replacement of natural pozzolan by the Portland cement on a base of equal weight [Chern and Chan, 1989].

4.3.3.5 Percentage of voids.

Concrete is a porous material, where its porous volume (or porosity) is determined by the voids contained or caused by the aggregates, by the porosity of the hydrated cementitious paste and by the presence of trapped air bubbles. Porosity is an important characteristic of concrete that influences both its mechanical properties and its durability [Song et al 2007; Winslow, et al 1990]. Therefore, is vitally important that the volume of the permeable voids is limited in order to obtain concretes that are resistant and durable.

Table 4.14 and Figures 4.45 and 4.46 shown the determined volume of permeable voids according to ASTMC C 642, where it can be noticed that the concretes with greater ratio water/binder (Series A) exhibit a higher percentage of voids. Another important aspect that can be seen is that for both series (A and B), the concrete mixtures that incorporate mineral admixtures are the ones that contain greater content of voids than the reference concretes. This increases in the porosity of these concretes are perfectly correlated with the compression resistance performance, mainly at an early age. In this sense, it can be observed how the compression resistance tends to decrease as the percentage of voids increases (See 4.3.2.1), which is consistent with the results reported by Yundenfreund et al 1972, Pantazopoulou et al 1995 and Chen et al 2013.

Table 4.14. Permeable void content of Series A and B concretes.

Series	Mixture	Voids, %
A	AR	11.88
	20NP	12.13
	60NP	15.37
	20FA	13.25
	60FA	14.29

Series	Mixture	Voids, %
B	BR	10.92
	20NP	11.19
	60NP	12.53
	20FA	11.35
	60FA	11.72

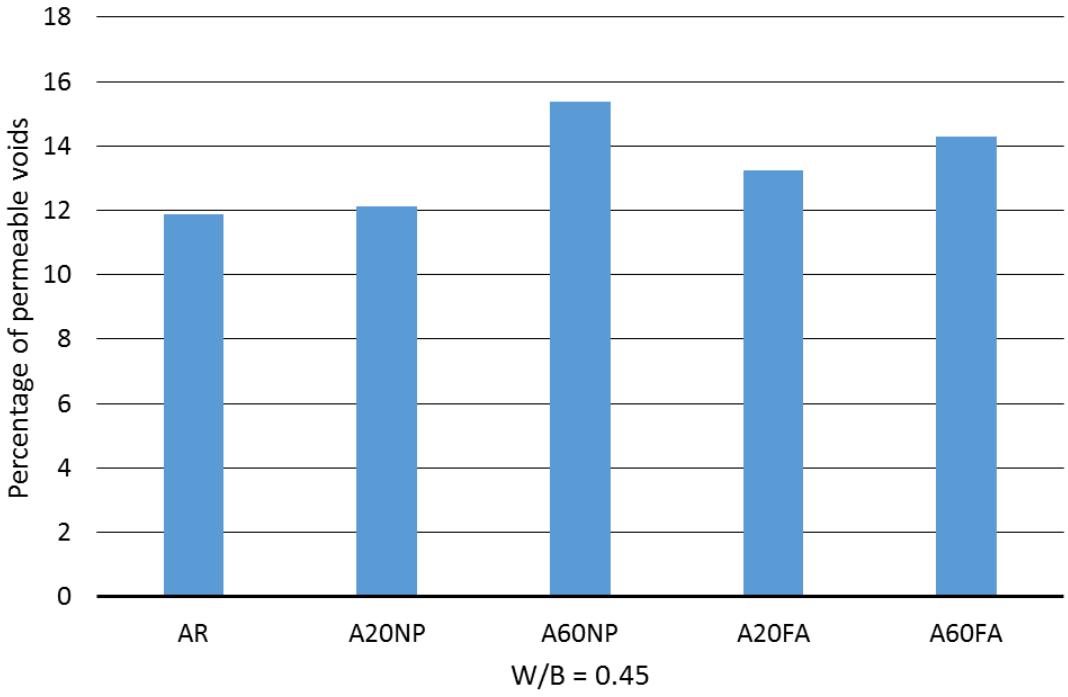

Figure 4.45. Percentage of voids, Series A concretes at 90 days.

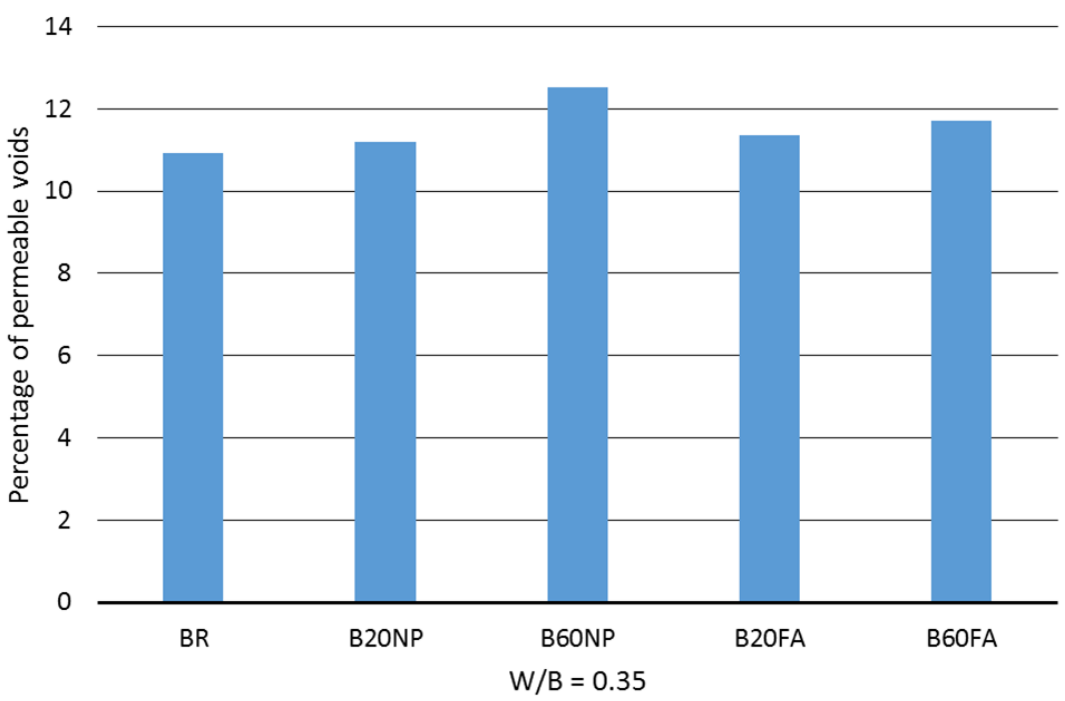

Figure 4.46 Percentage of voids, Series B concretes at 90 days.

On the other hand, the chloride migration coefficient as a function of the void volume presented in Figure 4.47 and 4.48 exhibits a high chloride penetration with the increase of the void percentage in the reference mixtures, while in the mixtures that incorporate mineral admixtures, the relationship is not clear. It is likely that several mechanisms of action are involved in this behavior, particularly the filler effect and the pozzolanic effect. According to Petrov (1998), the pores with a radius greater to 50 nm are those that control the concrete permeability; meaning that the incorporation of mineral admixtures causes a densification in the cementitious matrix with a finer porosity (less than 50 nm) characterized by a greatest segmentation and pore tortuosity. Furthermore, any physical-chemical interaction between the chloride ions and the cementitious matrix affects the chloride ions movability, also favoring its low penetration in concretes with mineral admixtures.

Due to the aforementioned, the low penetrability of the chloride ions in the concrete mixtures that incorporate mineral admixtures, despite the relatively higher porosities than those of the reference mixtures, provides information on the pores interconnectivity. These results suggest that cementitious matrices of the reference concrete are essentially composed of big

interconnected pores, while those of concretes with mineral admixtures are composed by relatively poorly connected smaller pores. In addition, the volume of pores penetrated in ASTM C642 test, represent only the pores in the first layer, near to the surface of the concrete, so the water is not penetrating deeper.

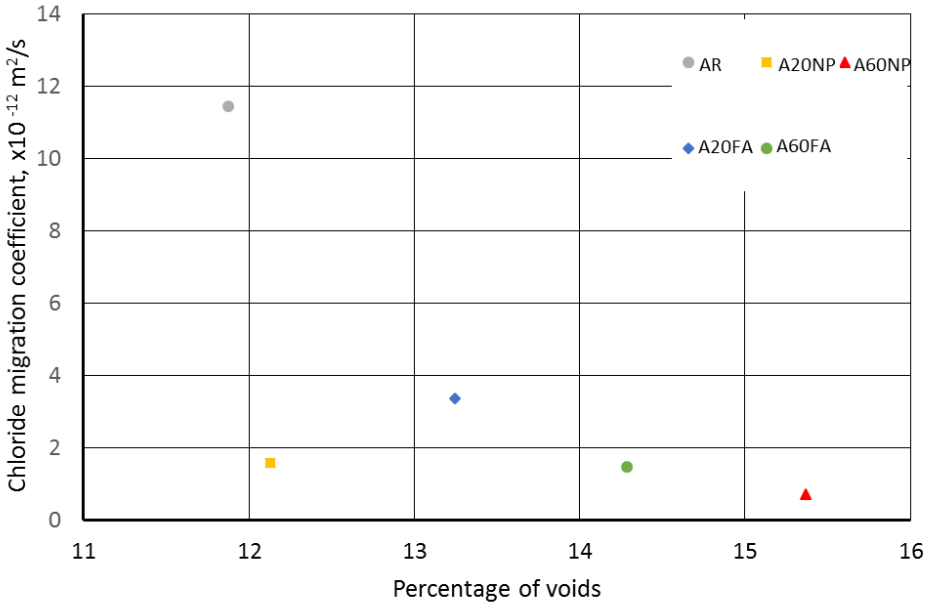

Figure 4.47. Variation of the chloride migration coefficient according to the percentage of voids of Series A concrete at 90 days.

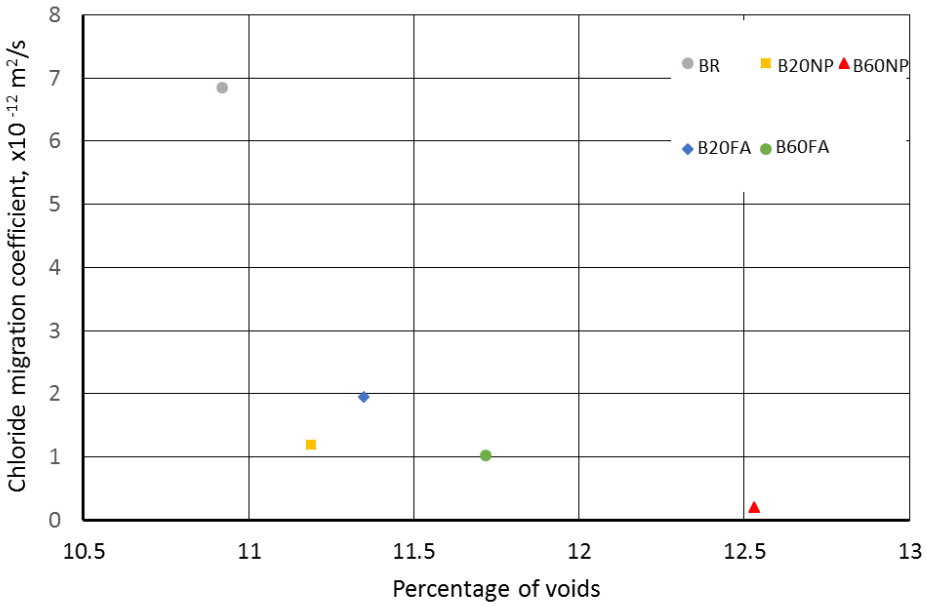

Figures 4.48. Variation of the chloride migration coefficient according to the percentage of voids of Series B concrete at 90 days.

Chapter 5. Conclusions and suggestions.

5.1 Conclusions.

Based on the analysis and discussion of the results from this research, the following remarks are made:

a) Selection of mineral admixture.

- The strength activity index are in agreement with the thermogravimetric results, indicating that the NP is more reactive than FA. Thermogravimetric analysis also show that the portlandite consumption increases as the W/B ratio decreases.

b) The chemo-mechanical clustering of nanoindentation tests did not allow distinguishing the two types of C-S-H (low and high density), so it was not possible to determine if the NP influence the increase in the formation of high density; however, the results obtained illustrate the effects of natural pozzolan on the microstructure of cement pastes, as well as their distribution, where the following findings are highlighted:

- The incorporation of NP led to a change from the typical C-S-H structure to a C-A-S-H structure with lower micro-mechanical properties. So, the pozzolanic reaction between the Portlandite and the natural pozzolan does not produce a stronger binding in this structure.

- By increasing the NP content, the Ca/Si and Ca/Al ratios reduce, causing that the values for the indentation modulus and hardness tend to decrease as well.

- The presence of NP leads to an increase in the formation of AFm+AFt with greater micro-mechanical properties than the C-(A)-S-H, positively contributing to the mechanical performance of concrete.

- The incomplete reaction of the NP favors the formation of a cementitious matrix with small hard inclusions distributed optimally. This heterogeneity increases the mechanical properties of concrete and contributes to reduce pore interconnectivity.

- It is suggested that the dosages of 60% of NP favor an optimal combination of hydrated and anhydrous products (59% hydrates, 33% NP particles and 8% clinker particles) that influence the optimal mechanical performance of the concrete. So the SNI-EDS results of the pastes showed that although the compressive strength and modulus of elasticity in plain Portland cement concretes depend mainly on the density of the C-S-H (calcium-silicate-hydrate), the mechanical properties of concretes with NP rather originate from an optimal combination of hard anhydrous particles, aluminum bearing hydrates and C-(A)-S-H.

- The mechanical properties of the mineral admixture particles, the level of reaction and the size distribution are key considerations that must be taken into account for the concrete mixture design with low Portland cement dosages, considering that the particles of this mineral admixtures contribute to reinforce the cementitious matrix improving the strength as well as the durability of the concrete.

c) Fresh state properties.

- The unconventional absence of porosity of the NP did not affect negatively the concrete's consistency and workability. This is an advantageous feature, because the superplasticizer dosage can remain constant.

- Results of packing density calculated through the wet packing method indicate that the densification of the cementitious matrix is improved by the substitution of Portland cement by NP. As the Portland cement substitution by NP increases, the air content tends to diminish, confirming the results of the calculations for the packing density.

- The presence of NP accelerates the setting times. This is attributed to the higher alkali content that accelerates the hydration process.

d) Hardened state properties.

- At the age of 90 days, the concretes with high contents of NP of the series B (W/B ratio of 0.35) exhibit slightly lower values in compressive strength as well as in modulus of elasticity (11% and 10% respectively) than the concrete mixtures only

with Portland cement. At the same age, concretes with high contents of FA showed significant reductions in the aforementioned properties (28% for compressive strength and 18% in modulus of elasticity).

- In both concrete series (W/B of 0.35 and 0.45), the incorporation of NP led to a higher impermeability to the chloride ingress, being consistent with the packaging density induced by this material.
- The Portland cement replacements by NP (20% and 60%) led to significant reductions of the chloride migration coefficient, originating concretes with extremely high resistances to the chloride ingress.
- A very good correlation between the surface resistivity and the chloride ion migration coefficient, with a correlation coefficient (R) of 0.95.
- The surface resistivity results indicate that the Portland cement substitutions by NP (20% and 60% in mass) leads to a very low probability of chloride ion penetration. Even though the FA also causes a similar benefit, the NP induces it at earlier ages.
- For both series of concrete (A and B), mixtures with natural pozzolan showed greater carbonation depths, being attributable to the high reactivity of this material, which leads to a faster decrease in the portlandite content. Although natural pozzolan can provide high contents of soluble alkalis in the pore solution, it is suggested that the reaction of this addition with portlandite can also fixe these alkalis.
- The concrete mixtures with higher contents of mineral admixtures show higher percentages of voids and higher drying shrinkage, which suggests that the voids volume of these concretes is mainly composed of mesopores due to the pozzolanic effect. Another aspect that can contribute to greater shrinkage strains is that the finer particles with rough texture can absorb more capillary water causing a greater pressure of the capillary pore due to the low amount of free water for self-drying.

- The concrete mixtures with the highest water / cement ratio (Series A) exhibited a higher percentage of voids, being attributable to the greater amount of free water.
- The concrete mixtures with incorporations of mineral admixtures exhibited a higher percentage of voids than the control mixtures, however, these mixtures showed greater resistance to chloride ion penetration, mainly due to the filler effect and the pozzolanic effect, causing a densification of the cement matrix with less interconnectivity between pores and greater tortuosity.

5.2 Suggestions.

This co-tutoring work was proposed to investigate the effect of the physical and mechanical properties of concretes with incorporations of a natural pozzolan and a fly ash based on the C-S-H formation and its microstructural morphology. In this regards, the findings from this study reveal that the performance of concretes with NP, is due to an optimal combination of hydrated and anhydrous products that mainly involve its level of reactivity, mechanical properties of the anhydrous particles and its size distribution.

Therefore, in order to complement the results of this work it is suggested to:

- Carry on with other research studies that involve different mineral admixture dosages as well as different water/binder ratios with the objective of evaluating the quantitative thresholds for these optimal combinations of hydrated and anhydrous products considering the size and mechanical properties of the anhydrous inclusions in the cementitious matrix.
- Evaluate the benefit of the NP in concretes with lower water/binder ratios, even those used in the production of reactive powder concretes or ultra-high performance concretes.
- Evaluate the performance of the NP with greater finesse (13000 m^2/kg) in cementitious systems for concretes with plastic or fluid consistencies.

References

AASHTO. *Standard Method of Test for Surface Resistivity Indication of Concrete's Ability to Resist Chloride Ion Penetration*. 10 p. (AASHTO TP 95-11).

Abo-El-Enein, S.A, El-Kady, G., El-Sokkary, T.M. and Gharieb M. (2015). Physico-mechanical properties of composite cement pastes containing silica fume and fly ash. *HBRC, 11*, p. 7-15.

Abuhaikal, M. (2011). Nano-ChemoMechanical Assessment of Rice Husk Ash Cement by Wavelength Dispersive Spectroscopy and Nanoindentation. *Masters Thesis Massachusetts Institute of Technology, Department of Civil and Environmental Engineering, Cambridge, MA.*

ACI Manual of Practice Concrete (2004). *State of the art report on high-strength concrete*. 55 p. (Committee 363R).

Acker, P. (2001). Micromechanical analysis of creep and shrinkage mechanisms, *in: F.J. Ulm, Z.B. and F. Wittmann (Eds), Creep, Shrinkage Durab. Mech. Concr. Other Quasi-Brittle Materials, Elsevier, Oxford. UK.*

Adrade, C. and Buják, R. (2013). Effects of some mineral additions to Portland cement on reinforcement corrosion. *Cement and Concrete Research*, 53, p. 59-67.

Ahmaruzzaman, M. (2010). A review on the utilization of fly ash. *Progress in Energy and Combustion Science, 36*, p. 327-363.

Aïtcin, P.C. (1998). High-Performance Concrete. *E & FN Spon*.

Andarde, C. and D'Andrea, R. (2011). La resistividad eléctrica como parámetro de control del hormigón y de su durabilidad. *Revista ALCONPAT*, Volumen 1, Numero 2, p. 90-98.

ASTM International (2004). *Standard Test method for measurement of rate of absorption of water by hydraulic-cement concretes,* 6 p. (Standard ASTM C1585).

ASTM International (2010). *Standard Practice for Capping Cylindrical Concrete Specimens*. 6 p. (Standard ASTM C617).

ASTM International (2010). *Standard Practice for Making and Curing Concrete Test Specimens in the Laboratory*. 8 p. (Standard ASTM C192).

ASTM International (2010). *Standard Specification for Chemical Admixtures for Concrete*. 10 p. (Standard ASTM C494).

ASTM International (2010). *Standard Specification for Concrete Aggregates*. 11 p. (Standard ASTM C33).

ASTM International (2010). *Standard Specification for Mixing Rooms, Moist Cabinets, Moist Rooms, and Water Storage Tanks Used in the Testing of Hydraulic Cements and Concrete*. 3 p. (Standard ASTM C511).

ASTM International (2010). *Standard Test Method for Air Content of Freshly Mixed Concrete by the Pressure Method*. 10 p. (Standard ASTM C231).

ASTM International (2010). *Standard Test Method for Air Density (Unit Weight), Yield, and Air Content (Gravimetric) of Concrete*. 4 p. (Standard ASTM C138).

ASTM International (2010). *Standard Test Method for Density of Hydraulic Cement*. 3 p. (Standard ASTM C188).

ASTM International (2010). *Standard Test Method for Density, Relative Density (Specific Gravity), and Absorption of Coarse Aggregate*. 6 p. (Standard ASTM C127).

ASTM International (2010). *Standard Test Method for Density, Relative Density (Specific Gravity), and Absorption of Fine Aggregate*. 7 p. (Standard ASTM C128).

ASTM International (2010). *Standard Test Method for Sieve analysis of Fine and Coarse Aggregates*. 5 p. (Standard ASTM C136).

ASTM International (2010). *Standard Test Method for Slump of Hydraulic-Cement Concrete*. 4 p. (Standard ASTM C143).

ASTM International (2010). *Standard Test Method for Static Modulus of Elasticity and Poisson's Ratio of Concrete*. 5 p. (Standard ASTM C469).

ASTM International (2010). *Standard Test Method for Temperature of Freshly Mixed Hydraulic-Cement Concrete*. 3 p. (Standard ASTM C1064).

ASTM International (2010). *Standard Test Method for Time of Setting of Concrete Mixtres by Penetration Resistance*. 7 p. (Standard ASTM C403).

ASTM International (2010). *Standard Test Methods for Compressive Strength of Cylindrical Concrete Specimens*. 7 p. (Standard ASTM C39).

ASTM International (2010). *Standard Test Methods for Fineness of Hidraulic Cement by Air-Permeability Apparatus*. 9 p. (Standard ASTM C204).

ASTM International (2010). *Standard Test Methods for Sampling and Testing Fly Ash or Natural Pozzolan for Use in Portland-Cement Concrete*. 10 p. (Standard ASTM C311).

ASTM International (2012). *Standard Specification for Coal Fly Ash and Raw or Calcined Natural Pozzolan for Use in Concrete*. 5 p. (Standard ASTM C618).

ASTM International (2014). *Standard Practice for High-Shear Mixing of Hydraulic Cement Pastes*. 3 p. (Standard ASTM C1738).

ASTM International (2014). *Standard Specification for Slag Cement for Use in Concrete and Mortars*. 8 p. (Standard ASTM C989).

ASTM International (2014). *Standard Test Method for Compressive Strength of Hydraulic Cement Mortars (Using 2-in or [50 mm] Cube Specimens)*. 10 p. (Standard ASTM C109).

ASTM STP 169D (2006). Significance of tests and properties of concrete and concrete-making materials. USA.

Badogiannis, E., Aggeli, E., Papadakis, V.G. and Tsivilis, S. (2015). Evaluation of chloride-penetration resistance of metakaolin concrete by means a diffusion – Binding model and of the k-value concept. *Cement and –concrete Composites, 63*, p. 1-7.

Bagheri, A.R., Zanganesh, M.M. and Moalemi, M.M. (2012). Mechanical and durability properties of ternary concretes containing silica fume and low reactivity blast furnace slag. *Cement and Concrete Composites, 34*, p. 663-670.

Baroghel-Bouny, V., Kinomura, K., Thiery, M. and Moscardelli, S. (2011). Easy assessment of durability indicators for service life prediction or quality control of concretes with high volumes of supplementary cementitious materials. *Cement and Concrete Composites, 33*, p. 832-847.

Bentz, D.P., Ehlen, M.A., Ferraris, F. and Garboczi, E.J. (2001). Sorptivity-based service life predictions for concrete pavements. *Proceedings of the 7th International Conference on Concrete Pavements*, p. 181-193.

Bentz, D.P., Ferraris, F., De la Varga, I., Peltz, M.A. and Winpigler, J.A. (2010). Mixture proportions options for improving High Volume fly ash concretes. *International journal of Pavement Research and Technology, 3*, p. 234-240.

Bentz, D.P., Ferraris, F., Galler, F.A., Hansen, A.S. and Guynn, J.M. (2012). Influence of particle size distribution on yield stress and viscosity of cement-fly ash pastes. *Cement and Concrete Research, 42*, p. 404-409.

Berodier, E. and Scrivener, K. (2014). Understanding the filler effect on the nucleation and growth of C-S-H. *Journal of the American Ceramic Society, 97*, p. 3764-3773.

Borges, P.H.R., Costa, J.O., Milestone, N.B., Lynsdale, C.J. and Streatfield, R.E. (2010). Carbonation of CH and C-S-H in composite cement pastes containing high amounts of BFS. *Cement and Concrete Research*, 40, p. 284-292.

Bouzoubaâ, N., Zhang, M.H. and Malhotra, V.M. (2000). Mechanical properties and durability of concrete made with high-volume fly ash blended cements using a coarse fly ash. *Cement and Concrete Research, 31*, p. 1393-1402.

Bower, A.F. and Ortiz, M. (1991). A three-dimensional analysis of crack trapping and bridging by tough particles. *Journal of Mechanics and Physics of Solids, 39*, p. 815-858.

Castellote, M. and Andrade, C. (2008). Modelling the carbonation of cementitious matrixes by means of the unreacted-core model, UR-CORE. *Cement and Concrete Research*, 38, p. 1374-1384.

Celik, K., Jackson, M.D., Mancio, M. Meral, C. Emwas, A.H. Mehta, P.K. and Monterio, P.J.M. (2014). High-volume natural volcanic pozzolan and limestone powder as partial replacements for Portland cement in self-compacting and sustainable concrete. *Cement and Concrete Composite, 45*, p. 136-147.

Chen, X., Wu, S. and Zhou, J. (2013). Influence or porosity on compressive and tensile strength of cement mortar. *Construction and Building Materials*, 40, p. 869-874.

Chern, J.C. and Chan, Y.W. (1989). Deformations of concretes made with blast-furnace slag cement and ordinary Portland cement. *ACI Materials Journal*, 86, p. 372-382.

Collins, F.G. and Sanjayan, J.G. (2000). Effect of pore size distribution on drying shrinkage of alkali-activated slag concrete. *Cement and Concrete Research*, 30, p. 1401-1406.

Constantinides, G. (2013). Nanoscience and nanoengineering of cement-based materials, *in: F.Pacheco-Torgal, M.V. Diamanti, A.N. and C.G. Granqvist. (Eds.), Nanotechnology Eco-Efficient Construction.* Woodhead Publishing, p. 9-37.

Constantinides, G. and Ulm, F.J. (2004). The effect of two types of C-S-H on the elasticity of cement-based materials: Results from nanoindentation and micromechanical modeling. *Cement and Concrete Research, 34*, p. 67-80.

Constantinides, G. and Van Vliet, K. (2003). On the use of nanoindentation for cementitious materials. *Cement and Concrete Research, 36*, p. 191-196.

Constantinides, G., and Ulm, F.J. (2007). The nanogranular nature of C-S-H. *Journal of the Mechanical and Physcics of solids, 55*, p. 64-90.

Corr, D. and Shaha, S.P. (2005). Concrete materials science at the nanoscale, Aplications of nanotechnology in concrete design, *in: Proc. Int. Conf. University Dundee,* Scotl. UK., p. 1-12.

Damtoft, J.S., Lukasik, J., Herfort, D., Sorrentino, D. and Gartner, E.M. (2008). Sustainable development and climate initiatives. *Cement and Concrete Research, 38*, p. 115-127.

Davydov, D., Jirásek, M. and Kopecký. (2011). Critical aspects of nano-indentation technique in application to hardened cement paste. *Cement and Concrete Research, 41*, p. 20-29.

Deboucha, W., Leklou, N., Khelidj, A. and Oudjit, M. N. (2017). Hydration development of mineral additives blended cement using thermogravimetric analysis (TGA): Methodology of calculating the degree of hydration. *Construction and Building Materials, 146*, p. 687-701.

DeJong, M.J. and Ulm F.J. (2007). The nanogranular behavior of C-S-H at elevated temperatures (up to 700^{o}C). *Cement and Concrete Research, 37*, p. 1-12.

Dempster, A.P., Larid, N.M. and Rubin, D.B. (1977). Maximum Likelihood from incomplete data via the EM algoritm. *Journal of the Royal Statistical Society, Series B, 39*, p. 1-38.

Diamon, S. and Bonen D. (1993). Microstructure of hardened cement paste – A new interpretation. *Journal of the American Ceramic Society, 76*, p. 2992-2999.

Duan, P., Shui, Z., Chen, W. and Shen C. Enhancing microstructure and durability of concrete from ground granulated blast furnance slag and metakaolin as cement replacement materials. *Journal of Materials Research and _Technology, 2*, p. 52-59.

Durán-Herrea, A., Juárez. C.A., Valdez, P. and Bentz, D.P. (2011). Evaluation of sustainable high-volume fly ash concretes. *Cement and Concretes Composites, 33*, p. 39-45.

Elahi, A., Basheer, P.A.M. and Nanukuttan, S.V. (2010). Mechanical and durability properties of high-érforance concretes containing supplementary cementitious materials. *Cosntruction and Building materials, 24*, p. 292-299.

El-Didamony, H., Khalil, K.A., and Heikal, M. (2014). Physico-chemical and surface characteristics of some granulated slag-fried drinking water sludge composite cement pastes. *HBRC journal, 10*, p. 73-81.

Feldman, R.F. and Sereda P.J. (1970). A new model for hydrated Portland cement paste and its practical implications, *Eng. J. Can.*, p. 53-59.

Feldman, R.F. and Sereda, P.J. (1968). A model for hydrated Portland cement paste as deduced from sorption-length change and mechanical properties. *Matériaux Construction.*, p. 509-520.

Foley, E.M., Kim, J.J. and Reda Taha, M.M. (2012). Synthesis and nano-mechanical characterization of calcium-silicate-hydrate (C-S-H) made with 1.5 CaO/SiO_2 mixture. *Cement and Concrete Research, 42*, p. 1225-1232.

Fraley, C. and Raftery, A.E. (2002). Model-based clustering, discrimination analysis and density estimation. *Journal of the American Statistical Association, 97*, p. 611-631.

Ganseh Babu, K. and Sree Rama Kumar, V. (2000). Efficiency of GGBS in concrete. *Cement and Concrete Research, 30*, p. 1031-1036.

Gjorv, O.E. (2014). Durability design of concrete structures in severe environments. Second Edition, Taylor and Francis Group, U.S.A.

Glasser, F.P. and Mart, J. (1985). The alkali binding potential of OPC and blended cements. Part II: Effects, II cement, 2, p. 85-94.

Groves, G. (1987). TEM studies of cement hydration, *in: Materials Research Society Symposium Proceedings,* p. 3-12.

Güneyisi, E., Gesoglu, M. and Ozbay, E. (2010). Strength and drying shrinkage properties of self-compacting concretes incorporating multi-system blended mineral admixtures. *Costruction and Buildinig Materials,* 24, p. 1878-1887.

Gutteridge, W.A. and Dalziel, J.A. (1990). Filler cement: the effect of the secondary component on the hydration of Portland cement: part I. A fine non-hydraulic filler. *Cement and Concrete Research, 20,* p. 778-782.

Gutteridge, W.A. and Dalziel, J.A. (1990). Filler cement: the effect of the secondary component on the hydration of Portland cement: part II. Fine hydraulic binders. *Cement and Concrete Research, 20,* p. 853-861.

Hanehara, S. Tomosawa, F., Kobayakawa M. and Hwang, K.R. (2001). Effects of water/powder ratio, mixing ratio of fly ash, and curing temperature on pozzolanic reaction of fly ash in cement paste. *Cement and Concrete Research, 31,* p. 19-31.

Hemalatha, T. and Ramaswan A. (2017). A review on fly ash characteristics- Towards promoting high volume utilization in developing sustainable concrete. *Journal of Cleaner Production, Accepted manuscript.*

Herts, K. (1992). Investigations on silica fume concretes at elevated temperatures. *ACI Materials Journal, 89,* p. 345-357.

Holt, E. (2001). Early age autogenous shrinkage of concrete. *VTT Building Transport, Technical Research Centre of Finland,* Finland, 197 p.

Hossain, K.M.A. (2008). Pumice based blended cement concretes exposed to marine environment: Effects of mix composition and curing conditions. *Cement and Concretes Composites, 30,* p. 97-105.

Hu, C. (2014). Microstructure and Mechanical properties of fly ash blended cement pastes. *Construction and Building Materials, 73*. P. 618-625.

Hu, C. and Li Z. (2014). Micromechanical investigation of Portland cement paste. *Constructions and Buildings Materials, 71,* p. 44-52.

Hu, C. and Li, Z. (2015). Property investigation of individual phases in cementitious composites containing silica fume and fly ash. *Cement and Concrete Composites, 57,* p. 17-26.

Hu, C., Han, Y., Gao, Y., Zhang, Y., and Li, Z. (2014). Property investigation of calcium-silicate- hydrate (C-S-H) gel in cementitious composites. *Materials Characterization, 95,* p. 129-139.

Janz, M. (2000). Moisture transport and fixation in porous materials at high moisture levels. Doctoral dissertation, Report TVBM-1018, Lound Institute of Technology, Lound Suecia, 33 p.

Jawed, I. and Skalny J. (1978). Alkalis in cement: a review. Part II: Effects of alkalis on hydration and performance of Portland cement. *Cement and Concrete Research,* 8, p. 37-52.

Jennings, H.M. (2000). A model for the microstructure of calcium silicate hydrate in cement paste. *Cement and Concrete Research, 30*, p. 101-116.

Jennings, H.M. (2003). Colloid model of C-S-H and implications to the problem of creep and shrinkage. *Materials Structure, 37*, p. 59-70.

Jennings, H.M. (2008). Refinements to colloid model of C-S-H in cement: CM-II. *Cement and Concrete Research, 38*, p. 275-289.

Jiang, Z, Sun, Z. and Wang, P. (2005). Autogenous relative humidity change an autogenous shrinkage of high-performance cement pastes. *Cement and concrete Research*, 35, p. 1539-1545.

Jumate E. and Manea D.L. (2012). Application of X-Ray diffraction (XRD) ans scanning electron microscopy (SEM) methods to the Portland cement hydration processes. *Journal of Applied Engineering Sciences, University of Oradea, 2*, p. 35-42.

Kessler, R.J., Powers, R.G., Vivas, E., Paredes, M.A. and Virmani, Y.P. (2008). Surface resistivity as an indicator of concrete chloride penetration resistance. *Concrete Bridge Conference.*

Krakowiak, K.J., Wilson, W., Musso, S. and Ulm, F.J. (2015). Interference of the phase-to-mechanical property link via coupled X-Ray spectrometry and indentation analysis: Aplication to cement-based materials. *Cement and Concrete Research, 67,* 271-285.

Lawrence, P. and Cyr, M. (2003). Mineral admixtures in mortars effect on inert materials on short-term hydration. *Cement and Concrete Research, 33*, p. 1939-1947.

L'Hôpital, E., Lothenbach, B., Kulik, D.A. and Scrivener, K. (2016). Influence of calcium to silica ratio on aluminum uptake in calcium silicate hydrate. *Cement and Concrete Research, 85*, p. 111-121.

L'Hôpital, E., Lothenbach, B., Le Saout, G., Kulik, D. and Scrivener, K. (2015). Incorporation of aluminum in calcium-silicate-hydrates. *Cement and Concrete Research, 75*, p. 91-103.

Lam, L., Wong, Y.L. and Poon, C. (2000). Degree of hydration and gel/space ratio of high-volume fly ash/cement systems. *Cement and concrete Research, 30*, p. 747-756.

Lee, C.L., Huang, R., Lin, W.T. and Weng, T.L. (2012). Establishment of the durability indices for cement –based composite containing supplementary cementitious materials. *Materials and Design, 37*, p. 28-39.

Liu, R., Han, F. and Yan, P. (2013). Characteristics of two types of C-S-H gel in hardened complex binder pastes blended with slag. *Science China Technology Sciences. 56*, p. 1395-1402.

Lothenbach, B., Scrivener, K. and Hooton, R.D. (2011). Supplementary cementitious materials. *Cement and Concrete Research, 41*, p. 1244-1232.

Malhotra, V. M. and Mehta, P.K. (2002). High-performance high-volume fly ash concrete: materials, mixture proporting, properties, construction practice and case histories. *Supplementary Cementing Materials for sustainable Development Inc., Ottawa, Canada*.

Malhotra, V.M. and Mehta, P.K. (2012). High-performance, high-volume fly ash concrete for building durable and sustainable structures. *Supplementary Cementing Materials for sustainable Development Inc., Ottawa, Canada*.

Malhotra, V.M., Zhang, M.H., Read, P.H. and Ryell, J. (2000). Long-term mechanical properties and durability characteristics of high-strength concrete incorporating supplementary cementing materials under outdoor exposure conditions. *ACI Metrials Journals, 97*, p. 518-525.

Markiv, T., Sobol, K., Franus, M. and Franus, W. (2016). Mechanical and durability properties of concretes incorporating zeolite. *Archives of Civil and Mechanical Engineering, 16*, p. 554-562.

Massazza, F. (1998). Pozzolan and pozzolanic cements. *Lea's Chemistry of Cement and Concrete, Fourth edition*, edited by Hewlett, P. C., p. 471-631.

Mehta, P.K., Monteiro, P.J. (2006). *Microstructure, Properties and Materials.* 3rd edition, Mc Graw-Hill Companies Inc., New York.

Mendoza, O., Giraldo, C., Camargo, S.S. and Tobón, J.I. (2015). Structural and nano-mechanical properties of calcium silicate hydrate (C-S-H) formed alite hydration in the presence of sodium and potassium hydroxide. *Cement and Concrete Research, 74*, p. 88-94.

Mindess, S. and Young, J.F. (2007). Concrete, Printece-Hall, Montreal Canada.

Mondal, P., Shah, S.P. and Marks, L. (2007). A reliable technique to determine the local mechanical properties at the nanoscale for cementitious materials. *Cement and Concrete research, 37*, p. 1440-1444.

Najimi, M., Sobhani, J., Ahmadi, B. and Shekarchi, M. (2012). An experimental study on durability properties of concrete containing zeolite. *Constrction and building Materials, 35*, p. 1023-1033.

Neithalath, N. (2006). Analysis of moisture transport in mortars and concrete using sorption-diffusion approach. *ACI Materials Journal, 103*, p. 209-218.

Němeček, J. (2009). Creep effects in nanoindentation of hydrated phases of cement pastes. *Materials Characterization, 60*, p. 1028-1034.

Nilsson, L., Ngo, M.H., and Gjørv, O.E. (1998). High-Performance Repair Materials for Concrete Structures in the Port of Gothenburg. In *Proceedings, Second International Conference on Concrete under Severe Conditions—Environment and Loading*, vol. 2, ed. O.E. Gjørv, K. Sakai, and N. Banthia. E & FN Spon, London, p. 1193–1198.

Nordtest Method. *Concrete, Mortar and Cement-Based Repair Materials: Chloride migration Coefficient from Non-Steady-State Migration Experiments*. 8 p. (NT BUILD 492).

Oliver, W.C. and Pharr, G.M. (1992). An improved technique for determining hardness and elastic modulus using load and displacement sensing indentation experiments. *Journal of Materials Research, 7*, p. 1564-1583.

Oliver, W.C. and Pharr, G.M. (2004). Measurement of hardness and elastic modulus by instrumented indentation: advances in understanding and refinements to methodology. *Journal of Materials Research, 19*, p. 3-20.

Pantazopoulou, S.J. and Mills, R.H. (1995). Microstructural asects of the mechanical response of plain concrete. *ACI Materials Journal*, 92, p. 605-616.

Papadakis, V.G. (2000). Effect of supplementary cementing materials on concrete resistance against carbonation and chloride ingress. *Cement and Concrete Research, 30*, p. 291-299.

Pappadakis, V.G., Vayenas, C.G. and Fardis, M.N. (1991). Experimental investigations and mathematical modeling of concrete carbonation problem. *Chemical Engineering Science*, 46, p. 1333-1338.

PCA, (2008). Design and control of Concrete Mixtures. *Portland cement Association, USA*.

Pellenq, R.J.M., Kushima, A., Shahsavari, R., Van Vliet, K.J., Buehler, M.J., Yip, S. and Ulm, F.J. (2010). A realistic molecular model of cement hydrates. *Proceedings of the National Academy of Science of the United States of America, 106*, p. 16102-16107.

Petrov, N. (1998). Étude des propriétés d'un béton auto nivelant in situ et de leurs influences sur l'interface-armature. Memoria de Maîtrise es Science appliquée. Sherbrooke, Québec. 158 p.

Poon, C., Azhar, S. Anson, M. and Wong, Y. (2001). Comparison of strength and durability performance of normal and high strength pozzolanic concretes at elevated temperatures. *Cement and Concretes Research, 31*, p. 1291-1300.

Poon, C., Lam. L. and Wong, Y. (200). A study on high strength concrete prepared with large volumes of low calcium fly ash. *Cement and Concrete Research, 30*, p. 447-455.

Raki, L., Beaudoin, R., Alizadeh, R., Makar, J. and Sato, T. (2010). Cement and concrete nanoscience and nanotechnology, *Materials (Basel).* 3 p. 918-942.

Ramezanianpour, A.A., Mousavi, R., Kalhori, M., Sobhani, J. and Najimi, M. (2015). Micro and macro level properties of natural zeolite contained concretes. *Construction and Building Materials, 101*, p. 347-358.

Richardson, I.G. (1999). The nature of C-S-H in hardened cements. *Cement and Concrete Research, 29*, p. 1131-1147.

Richardson, I.G. (2000). Nature of the hydration products in hardened cement pastes, *Cement and Concrete Composites, 22*, p. 91-113.

Richardson, I.G. (2004). Tobermorite/jennite and tobermorite/calcium hydroxide-based models for the structure of C-S-H: Applicability to hardened pastes of tricalcium silicate, dicalcium silicate, Portland cement and blens of Portland cement with blast furnace slag, metakaolin. *Cement and Concrete Research, 34*, p. 1733-1777.

Richardson, I.G. (2008). The calcium silicate hydrates. *Cement and Concrete Research, 38*, p. 137-158.

Rivera, F., Martínez, P., Castro, J. and López M. (2015). Massive volume fly-ash concrete: A more sustainable material with fly ash replacing cement and aggregates. *Cement and Concrete Composites, 63*, p. 104-112.

Rossen, J.E. (2014). Composition and morphology of C-A-S-H in pastes of alite and cement blended with supplementary cementitious materials. *These á la faculté des sciences et techniques de l'ingénieur laboratoire des matériaux de construction. École Polytechnique Fédérale de Lausanne. Programme Doctoral en Science et Génie des Matériaux.*

Sabir, S., Wid, M. and O'Farrell. (1998). A water sorptivity test for mortar and concrete. *Materials and Strctures, 31*, p. 568-574.

Sakulich, A.R. and Li, V.C. (2011). Nanoscale characterization of engineered cementitious composites (ECC). *Cement and Concrete Research, 41*, p. 169-175.

Salvador, R.P., Cavalaro, S.H.P., Segura, I., Figueiredo, D. and Pérez, J. (2016). Early age hydration of cement pastes with alkaline and alkali-free accelerators for sprayed concrete. *Cosntruction and Building materials, 111*, p. 386-398.

Saridemir, M. (2013). Effect of silica fume and ground pumice on compressive strength and modulus of elasticity of high strength concrete. *Construction and Building Materials, 49*, p. 484-489.

Savija, B. and Lukovic, M. (2016). Carbonation of cement paste: Understanding, challenges and opportunities. *Construction and Buildings Materials*, 117, p. 285-301.

Schneider, C.A., Rasband, W.S. and Eliceiri, K.W. (2012). NIH image to ImageJ: 25 years of image analysis. *Nature Methods, 9*, p. 672-675.

Scrivener, K., Patell, H., P.P and Parrot L. (1985). Analysis of phases in cement pastes using backscattered electron images, methanol adsorption and thermogravimetric analysis, *in: Materials Research Society Symposium Proceedings, 85*, p. 67-76.

Seleem, H.E.-D.H., Rashad, A.M. and El-Sabbagh, B.A. (2010). Durability and strength evaluation of high performance concrete in marine structures. *Construction and Building Materials, 24*, p. 878-884.

Sengul, O. (2014). Use of electrical resistivity as an indicator for durability. *Construction and Building Materials, 73*, p. 434-441.

Sengul, O. and Gjorv, O.E. (2008). Electrical resistivity measurement for quality control during concrete construction. *ACI Materials Journal*, 105, p. 541-547.

Sevelsted, T.F. and Skibted, J. (2015). Canbonation of C-S-H and C-A-S-H samples studied by ^{13}C, ^{27}Al and ^{29} Si MAS NMR spectroscopy. *Cement and concrete Research*, 71, p. 56-65.

Shariq, M., Prasad, J. and Abbas H. (2016). Creep and drying shrinkage of concrete containing GGBFS. *Cement and Concrete Composite*, 68, p. 35-45.

Shariq, M., Prasad, J. and Abbas, H. (2013). Effect of GGBFS on age dependent static modulus of elasticity of concrete. *Construction and Building Materials, 41*, p. 411-418.

Snyder, K.A, Stutzman, P.E., Philip, J. and Esh, D. (2009). Hydrated phases in blended cementitious systems for nuclear infrastructure, Longterm Performance of Cementitious Barriers and Reinforced Concrete in Nuclear Power Plants and Waste Management. *NUCPERF, RILEM, Cadarache, France*, p. 91-98.

Song, H.W. and Kwon, S.J. (2007). Permeability characteristics of carbonated concrete considering capillary pore structure. *Cement and Concrete Research*, 37, p. 909-915.

Sorelli, L., Constantinides, G., Ulm, F.J. and Toutlemonde, F. (2008). The nano-mechanical signature of ultra-high performance concrete by statistical nanoindentation techniques. *Cement and Concrete Research, 38*, p. 1447-1456.

Tang, L. and Zhu, W. (2007). Chloride penetration Report 38: Durability of self-compacting concrete. *RILEM TC 205-DSC*: *State of the art report*, p. 77-88.

Taplin, J. (1959). A method for following the hydration reaction in Portland cement paste. *Australian Journal of Applied Science,* p. 329-345.

Taylor, H.F.W. (1984). Studies on the chemistry and microstructure of cement pastes. *Proceedings of the British Ceramic Society, 35*, p. 65-82.

Taylor, H.F.W. (1997). *Cement Chemistry, 2nd. Edition.* Thomas Telford, London.

Tennis, P.D. and Jennings, H.M. (2000). A model for two types of calcium silicate hydrate in the microstructure of Portland cement pastes. *Cement and Concrete Research, 30*, p. 855- 863.

Thomas, J.J. and Jennings H.M. (2006). A colloidal interpretation of chemical aging of the C-S-H gel and its effects on the properties of cement paste. *Cement and Concrete Research, 36*, p. 30-38.

Ulm, F.J., Vandamme, M., Bobko, C. and Ortega, J. (2007). Statistical indentation techniques for hydrated nanocomposites: concrete, bone and shale. *Journal of the American Ceramic Society, 9*, p. 2677-2692.

Ulm, F.J., Vandamme, M., Jennings, H.M., Vanzo, J., Bentivegna, M., Krakowiak, K.J., Constantinides, G., Bobko, C.P. and Van Vliet, K.J. (2010). Does microstructure matter for statistical nanoindentation techniques? *Cement and Concrete Composites, 32*, p. 92-99.

Uysal, M. Yilmaz, K. and Ipek, M. (2012). The effect of mineral admixture on mechanical properties, chloride ion permeability and impermeability of self-compacting concrete. *Construction and Building Materials, 27*, p. 262-270.

Uzal, B. and Turnali, L. (2012). Blended cements containing high volume of natural zeolites: properties, hydration and microstructure. *Cement and Concrete Research, 34*, p. 101-109.

Uzal, B., Turnali, L, and Mehta, P.K. (2007). High-volume natural pozzolan concrete for structural applications. *ACI Materials Journal, 104,* p. 535-538.

Vandamme, M., Ulm, F.J. and Fonollosa, P. (2010). Nanogranular packing of C-S-H at substochiometric conditions. *Cement and Concrete Research, 40*, p. 14-26.

Velez, K., Maximilien, S., Damidot, D., Fantozzi, G. and Sorrentino, F. (2001). Determination by nanoindentation of elastic modulus and hardness of pure constituents of Portland cement clinker. *Cement and Concrete Research, 31*, p. 555-561.

Wiederhorn, S.M. (1984). Brittle fracture and toughening mechanisms in ceramics. *Annual Review of Materials Science, 14*, p. 373-403.

Wilson, W., Rivera-Torres, J.M., Sorelli, L., Durán-Herrera, A. and Tagnit-Hamou. (2017). The micromechanical signature of high-volume natural pozzolan concrete by combined

statistical nanoindentation and SEM-EDS analyses. *Cement and Concrete Research*, 91, p. 1-12.

Winslow, N.N. and Liu, D. (1990). Pore structure of paste in concrete. *Cement and Concrete Research*, 20, p. 227-235.

Wongkeo, W., Thongsanitgarn, P. and Chaipanich, A. (2012). Compressive strength and drying shrinkage of fly ash-bottom ash-silica fume multi-blended cement mortars. *Materials and Design*, 36, p. 655-662.

Xu, J., Corr, D.J., Shah, S.P. (2015). Nanomechanical properties of C-S-H- gel/cement grain interface by using nanoindentation and modulus mapping. *Journal of Zhejiang University-Science, 16*, p. 38-46.

Yundenfreund, M. Hanna, K.M., Skalny, J., Oder, I. and Brunauer S. (1972). Hardened Portland cement paste of low porosity, V: Compressive strength. *Cement and Concrete Research*, 2, p. 731-743.

Zadeh, V.Z. and Bobko, C.P. (2013). Nanoscale mechanical properties of concrete containing blast furnace slag and fly ash before and after thermal damage. *Cement and Concrete Research, 37*, p. 215-221.

Zhang, W., Hama, Y. and Na, S.H. (2015). Drying shrinkage and microstructure characteristics of mortar incorporating ground granulated blast furnace slag and shrinkage reducting admixture. *Construction and Building Maerials*, 93, p. 267-277.

Zhu, W., Hughes, J.J., Bicanic, N. and Pearce, C.J. (2007). Nanoindentation mapping of mechanical properties of cement paste and natural rocks. *Materials Characterization, 58*, p. 1189-1198.

Zunino, F., and Lopez, M. (2016). Decoupling the physical and chemical effects of supplementary cementitious materials on strength and permeability: A multi-level approach. *Cement and Concrete Composites, 65*, p. 19-28.